P 2

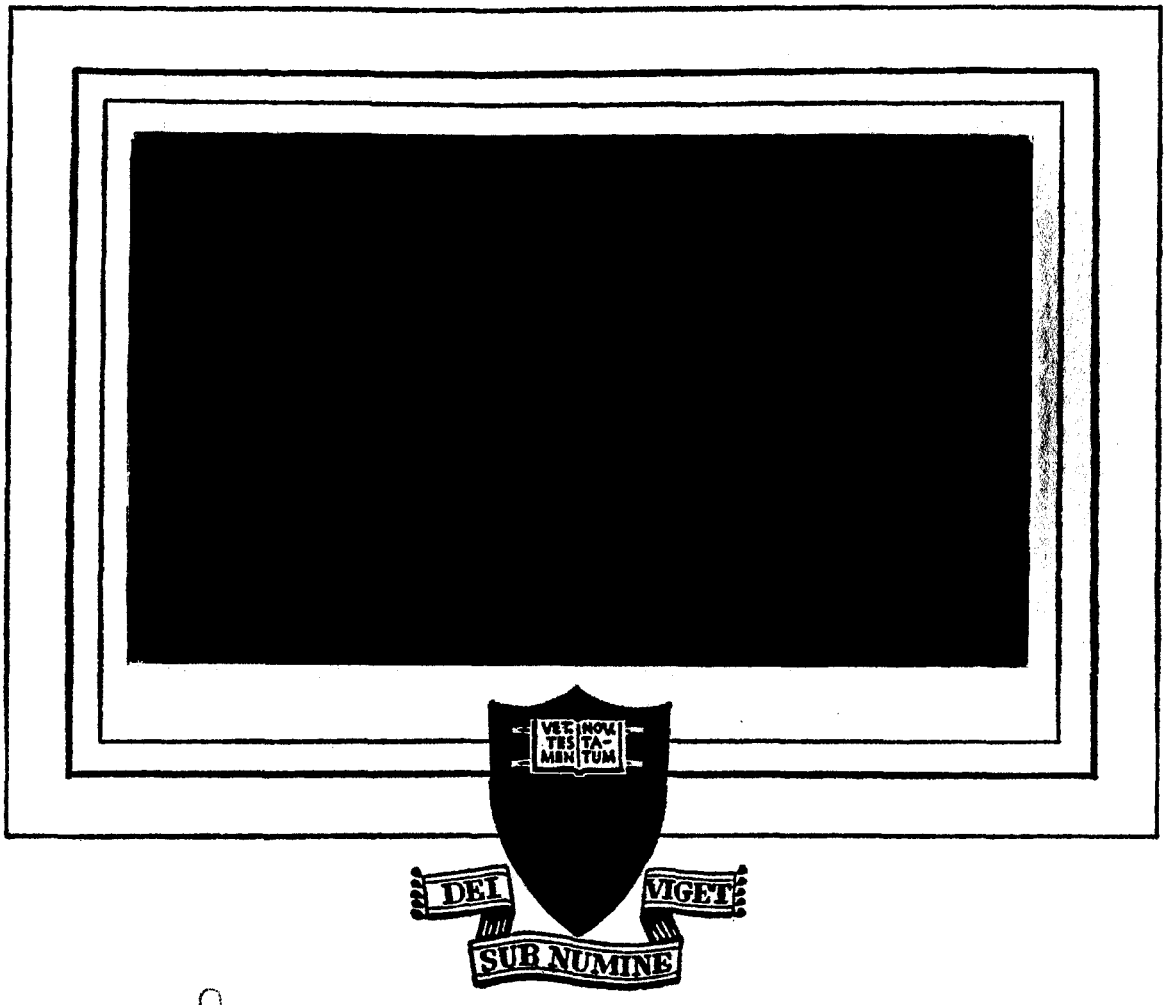

PRINCETON UNIVERSITY

DEPARTMENT OF AEROSPACE AND MECHANICAL SCIENCES

National Aeronautics and Space Administration
NGL 31-001-005

PULSED ELECTROMAGNETIC GAS ACCELERATION

1 July 1972 to 31 December 1972

Semi-annual Report 634t

Prepared by: Robert G. Jahn

Robert G. Jahn
Dean, School of Engineering and
Principal Investigator

and

W. von Jaskowsky

Woldemar F. von Jaskowsky
Sr. Research Engineer and
Lecturer

Kenn E. Clark

Kenn E. Clark
Research Engineer

January 1973

School of Engineering and Applied Science
Department of Aerospace and Mechanical Sciences
Guggenheim Aerospace Propulsion Laboratories
Princeton University
Princeton, N.J.08540

ABSTRACT

Direct measurements of the power deposited in the anode of a multi-megawatt MPD accelerator using thermocouples attached to a thin shell anode reveal a dramatic decrease in the fractional anode power from 50% at 200 kW input power to less than 10% at 20 MW power. The corresponding local power flux peaks at a value of 10,000 W/cm^2 at the lip of the anode exhaust orifice, a distribution traced to a corresponding peak in the local current density at the anode. A comparison of voltage-current characteristics and spectral photographs of the MPD discharge using quartz, boron nitride and Plexiglas insulators with various mass injection configurations has led to the identification of different voltage modes and regions of ablation free operation. The technique of piezoelectric impact pressure measurement in the MPD exhaust flow has been refined to account for the effects due to probe yaw angle.

In the hollow cathode portion of the program, spectral photographs of the discharge with low mass flows through the cathode reveal a radiance of ionized argon inside the cavity which is absent at high flow rates. The possibility that some fraction of the current is attached inside the cathode may also be reflected in the voltage-current characteristic, which shows an abrupt slope change for low mass flow and increasing current. A simple analysis of the balance between gasdynamic and magnetic pressure in the cavity supports this conclusion.

In preparation for development of the MPD arc as a plasmadynamic laser source, axial and radial profiles of the spectral radiance from neutral and ionized argon show that

the recombination process is essentially complete 36 cm downstream of the anode. Initial relative measurements of the optical depth of two ionized argon lines for various operating conditions indicate substantial differences in the total absorption for these transitions.

TABLE OF CONTENTS

LIST OF ILLUSTRATIONS

LIST OF ILLUSTRATIONS

CURRENT STUDENT PARTICIPATION

Student	Period	Degree	Thesis Topic
BOYLE, Michael J.	1968-1969 1971-	B.S.E. Ph.D. Cand.	Velocity and Acceleration Patterns in the MPD Exhaust
CAMPBELL Edward M.	1972-		Plasmadynamic Laser Studies of the Quasi-Steady MPD Discharge
DUTT, Gautam S.	1971-	Ph.D. Cand.	Impact Pressure Measurements in the MPD Exhaust Flow
HIXON, Todd L.	1970-1972	A.B.	Near-Ultraviolet Spectroscopic Studies of a Quasi-Steady MPD Arc
KRISHNAN, M.	1972-	Ph.D. Cand.	The Hollow Cathode Discharge
SABER, Aaron J.	1969-	Ph.D. Cand.	Anode Power Deposition in a Quasi-Steady MPD Accelerator
VILLANI, Daniel D.	1969-	Ph.D. Cand.	Effect of Distribution of Injected Propellant on an MPD Discharge

I. INTRODUCTION

The original research topic of this grant on plasma acceleration has been extended recently to include work on hollow cathode physics and plasmadynamic lasers,[142] and these activities will now provide additional theses projects for our graduate students. This semi-annual report describes the progress over the past six months on each of these three aspects of the research program.

The investigations of the physical processes in the MPD thruster to be reported here include a) anode power dissipation, b) voltage-current characteristics of discharge chambers constructed with boron nitride or quartz backplates, c) injected propellant distributions and d) impact pressure measurement techniques which have been refined considerably. The first three projects are now approaching conclusion, while the piezoelectric pressure measurements will continue for determinations of thruster performance.

Work on hollow cathode discharges has been accelerated by the operation and calibration of apparatus designed and constructed specifically for these studies. Photographs taken through selected spectral filters establish that ionized propellant exists inside the cathode cavity under particular operating conditions. For this discharge mode, the voltage-current characteristics of the hollow cathode have been mapped over a wide range of mass flows and currents. Detailed probing of the distributions of potential and current inside the cavity and in the surrounding flow is now in progress.

In connection with the plasmadynamic laser studies, the recombination and relaxation processes in the plasma flow are being assessed from spectroscopic data on the distribution of ionization levels. Radiation from neutral argon (AI) in the near-infrared region of the spectrum has been studied to supplement earlier spectrographic work on AII and AIII. Photoelectric recordings of the radiation profiles in the argon plasma flow from the discharge in a chamber with a boron nitride backplate provide additional background for the laser studies.

The absorption or amplification of radiation in an active medium manifests itself in the sign and magnitude of the optical depth. Therefore, as the next step in the plasmadynamic laser studies, the relative optical depth for a few spectral lines of the propellant has been determined.

Finally, it is to be mentioned that Mr. David B. Fradkin, a former graduate student of this laboratory, has submitted a dissertation for the Ph.D. degree on "Analysis of Acceleration Mechanisms and Performance of an Applied Field Arcjet."

II. QUASI-STEADY MPD DISCHARGE

II-A. Anode Power Deposition (Saber)

Steady state MPD arcs operating in a power regime up to several hundreds of kilowatts characteristically suffer power fluxes to the anode of up to one-half of the total input power.[A-1] This power loss necessarily limits the power which can be deposited in the propellant, only a portion of which ultimately appears as useful thrust power.

Early experiments in this laboratory, which yielded the floating potential and current density distributions near the anode of a pulsed quasi-steady MPD arc operating at multi-megawatt power levels, revealed that the fraction of the total power deposited into the anode, as indirectly deduced from these local plasma measurements, decreased as the total arc power increased.[113] The expectation is that with a smaller fraction of the power lost to the anode, a greater fraction will appear as directed kinetic energy, i.e. the thrust efficiency will increase as the arc power increases. This exciting possibility led to an experiment designed to measure directly, with thermocouples, the power deposited in the anode. The early results of this study verified the expected trend of the anode power fraction decreasing with arc total power over a limited range of quasi-steady arc powers.[143] This trend has recently been substantiated over an extended range of operating conditions: arc powers from 200 kW to 20 MW with currents from 5.5 kA to 44 kA and argon propellant mass flows of 1 to 48 g/sec. In addition, a complementary program of plasma diagnostic probing near the anode has begun in order to gain insight into the specific mechanisms that produce the anode fractional power drop.

Apparatus

The geometry of the MPD arc used for the anode power deposition study, shown schematically in Fig. 1, has been described in detail previously.[143] Briefly, it differs from the usual MPD configuration by the 1 mm thick aluminum shell anode which is internally fitted with 12 copper-constantan thermocouples: two on the discharge chamber side, six in the region of the lip and four on the downstream face. The current conduction area and the overall thruster dimensions and materials are identical to those in the standard thruster.[141]

Anode Temperature Rise

The local temperature rise in the anode shell was determined by amplifying the signals of the internally mounted thermocouples. Due to the time required for heat to diffuse through the thickness of the shell from the outer surface to the thermocouples, the temperature rise was not measured during the 0.5 to 1 msec quasi-steady operating period, but 20 msec later. Analysis of the temperature profiles has shown that the heat flux along the shell is negligible by comparison during this time, i.e. the temperature data 20 msec after the discharge can still be used to infer the distribution of heat flux into the anode.

The temperature profile along the anode is shown in Fig. 2 for three typical operating conditions. The abscissa represents a linearly rolled-out anode; it traces a line of constant azimuth along the anode surface from the chamber insulator, around the lip (with the anode midplane at 0.0 cm) to the outer radial boundary of the conduction region. The three operating conditions are related by the parameter "$J^2/\dot{m}$", the square of the total arc current divided by the injected propellant mass flow, which is held constant at 10 kA^2-sec/g. The significance of this parameter to the anode power data will be discussed later.

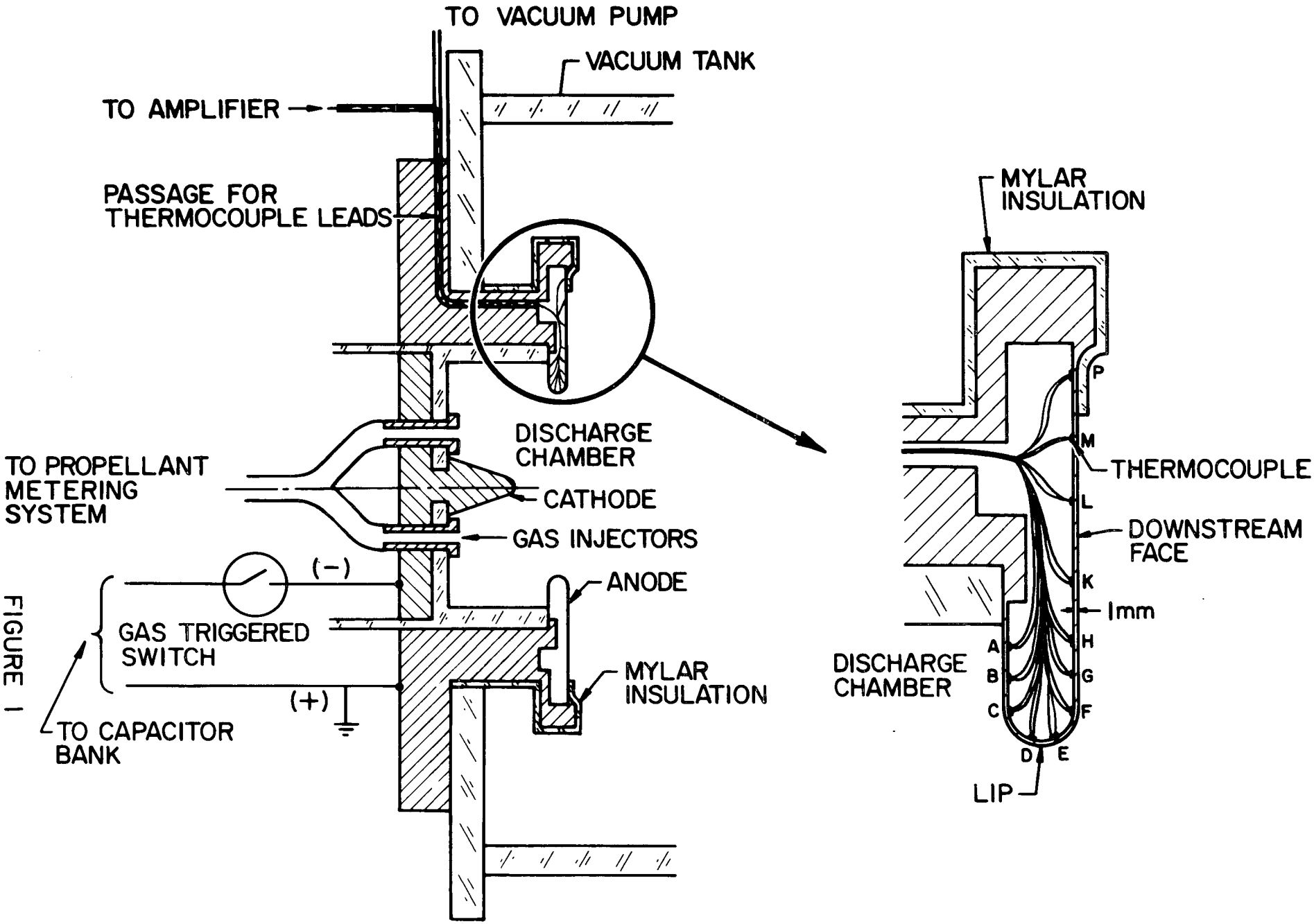

FIGURE 1
AP25-4870

MPD ARC WITH SHELL ANODE, SCHEMATIC

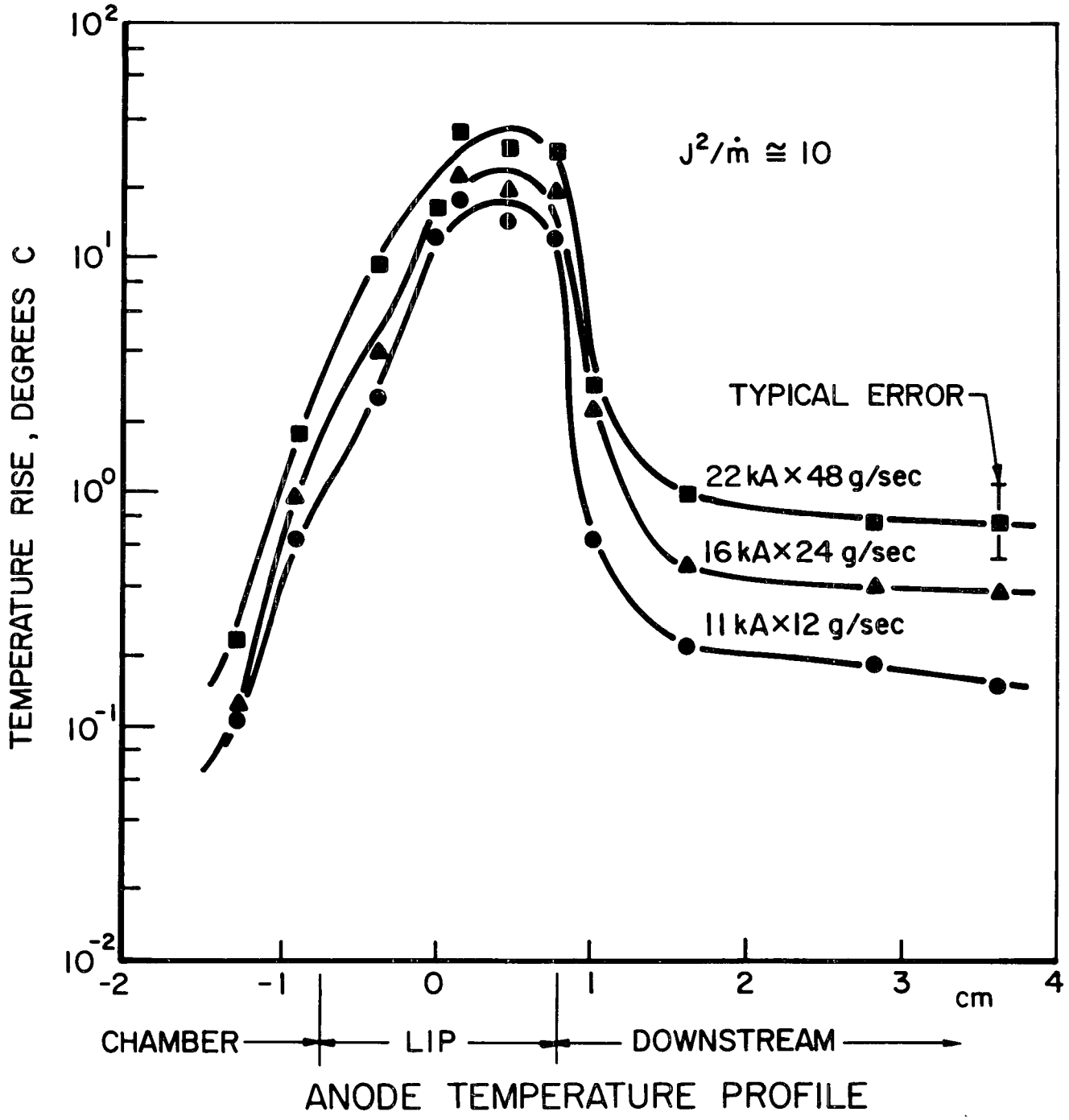

FIGURE 2
AP25-4914

For all three operating conditions, the anode temperature rise is markedly peaked about the lip and decreases by more than an order-of-magnitude along the downstream face and discharge chamber side of the anode.

Anode Heat Flux

Using anode temperature profiles such as those shown in Fig. 2 and the local one-dimensional heat flux model discussed previously,[143] the quasi-steady heat flux into the anode can be calculated. The one-dimensional model is verified by the measured negligible heat conduction along the anode shell as compared to the heat flux through the shell wall.

The anode heat flux distributions for the same three operating conditions are shown in Fig. 3. Contrary to earlier indications from the current density and potential measurements,[113] power is not uniformly deposited into the anode. Taking, for example, the 22 kA, 48 g/sec argon mass flow condition, the local anode heat flux ranges from 80 W/cm^2 on the chamber side to about 400 W/cm^2 on the downstream face peaking at 10,000 W/cm^2, over a factor-of-ten higher, at the lip.

Anode Power

By integrating the measured heat flux over the entire anode surface the power deposited in the anode during the quasi-steady pulse can be calculated. Figure 4 is a graph of anode power fraction vs. argon propellant mass flow for fixed arc currents of 11, 16 and 22 kA. It demonstrates that for any given value of current there is a maximum in the measured anode fractional power. For example, for the 16 kA condition, the anode power fraction peaks at about 0.2 when the injected argon mass flow is about 15 g/sec. For mass flows above or below this level the measured relative anode power decreases.

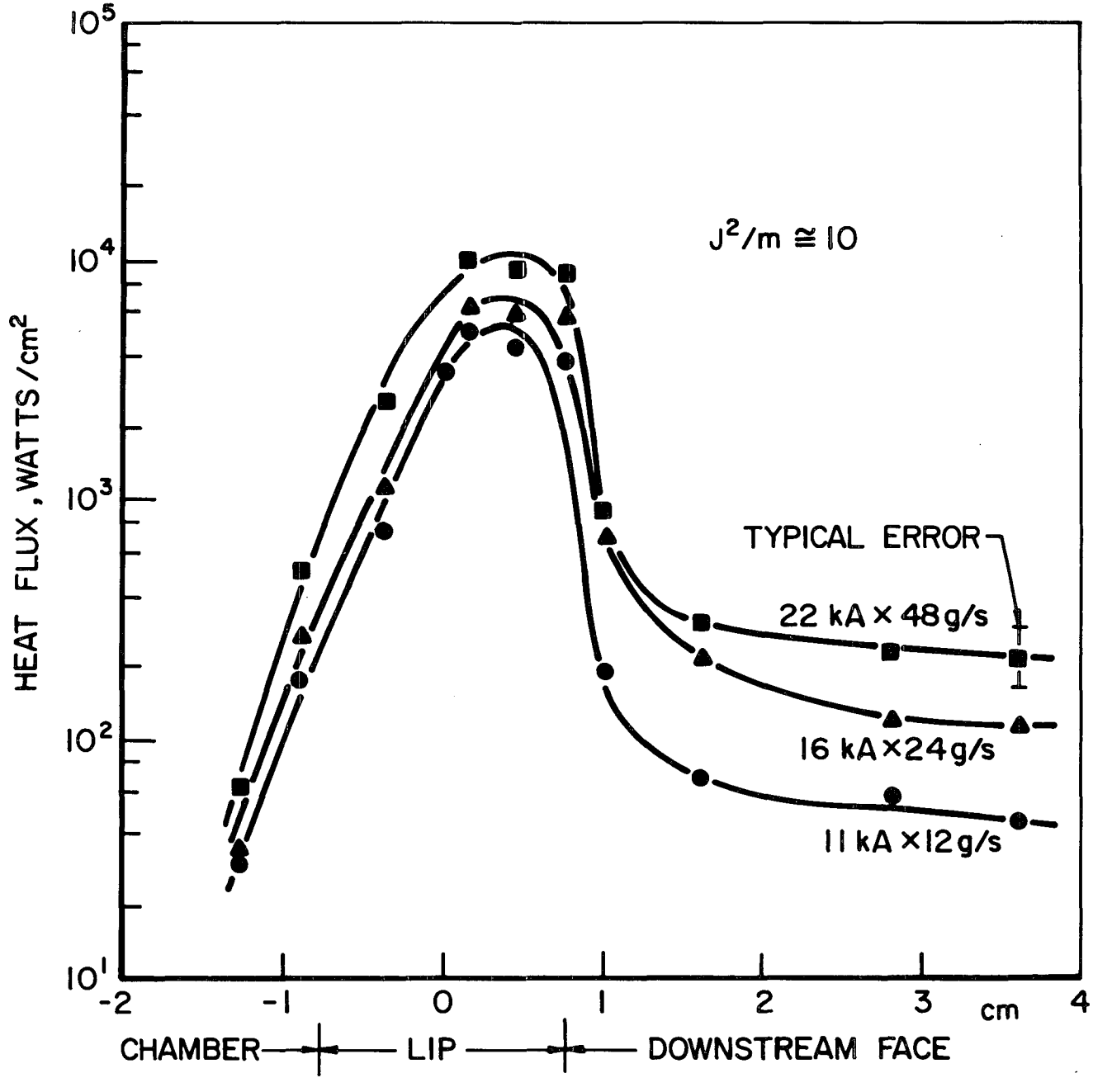

FIGURE 3
AP25 · 4916

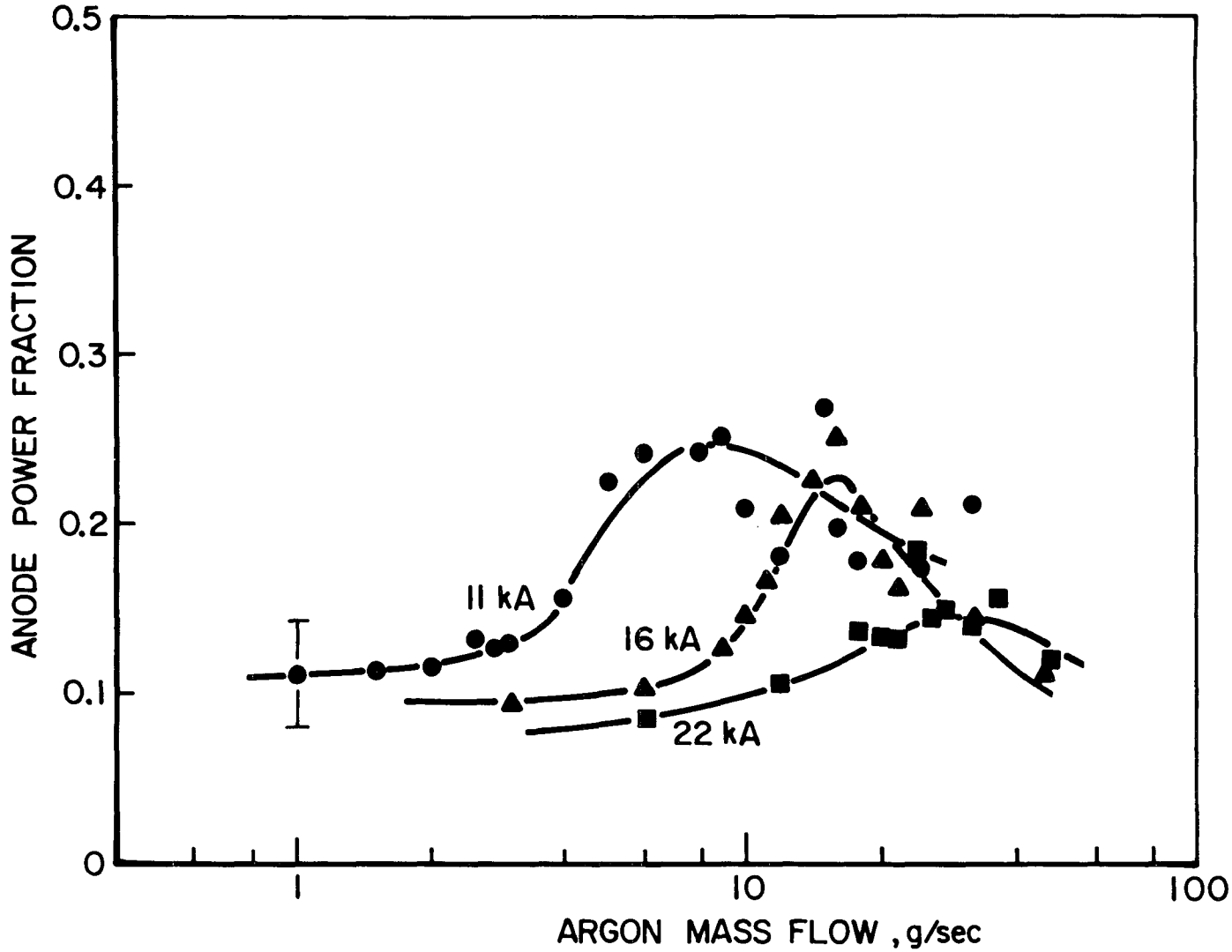

ANODE POWER FRACTION vs ARGON MASS FLOW

FIGURE 4
AP25·4915

The tendency for the peak of the fractional anode power to occur at larger mass flows for larger arc currents suggests that the data may be better characterized by plotting it against a single parameter such as $J^2/\dot{m}$. This parameter has been shown previously to correlate many features of arc radiance patterns and current and potential distributions for MPD discharges at various currents and mass flows.[141] Figure 5 shows the present fractional anode power data plotted against the parameter $J^2/\dot{m}$, where $\dot{m}$ is the injected argon mass flow. The peaks for different fixed current operation lie approximately at the same value of the abscissa ($J^2/\dot{m} \cong 16$ kA^2-sec/g) indicating that this dimensional factor may have further significance for anode power deposition studies.

The observed drop in fractional anode power when arc operating conditions are such that $J^2/\dot{m}$ is greater than 16 kA^2-sec/g may be artificial since many studies in the past have shown that above some characteristic value of $J^2/\dot{m}$ dependent upon the propellant species and arc geometry, ablation of the arc chamber insulators or electrodes begins.[A-2,118] When this occurs, the total mass flow through the discharge is greater than the injected argon flow and hence the true operating value of $J^2/\dot{m}$ is lower than what would be calculated on the basis of the argon flow alone.

The variation of anode power fraction with total arc power is shown in Fig. 6. This graph expands considerably on the amount of data and on the range of conditions examined previously. Power levels range from 200 kW to 20 MW (arc currents of 5.5 to 44 kA) with mass flows appropriate to cover values of $J^2/\dot{m}$ from 5 to 80 kA^2-sec/g. Verifying the earlier data, the anode power fraction (for any particular value of $J^2/\dot{m}$) decreases as the input power increases. The anode power fraction of 50% at about 200 kW agrees well with

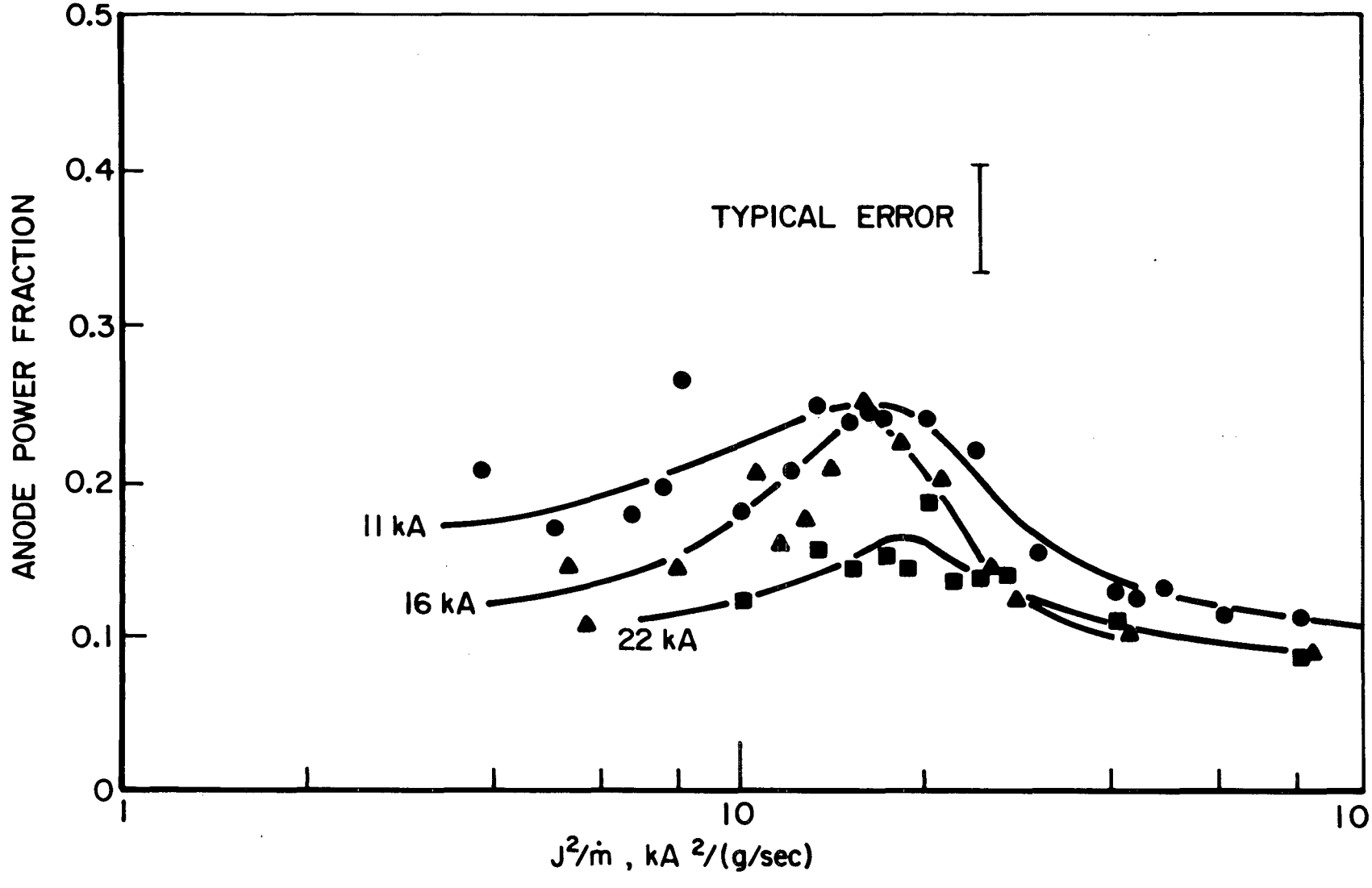

ANODE POWER FRACTION vs $J^2/\dot{m}$

FIGURE 5
AP25-4912

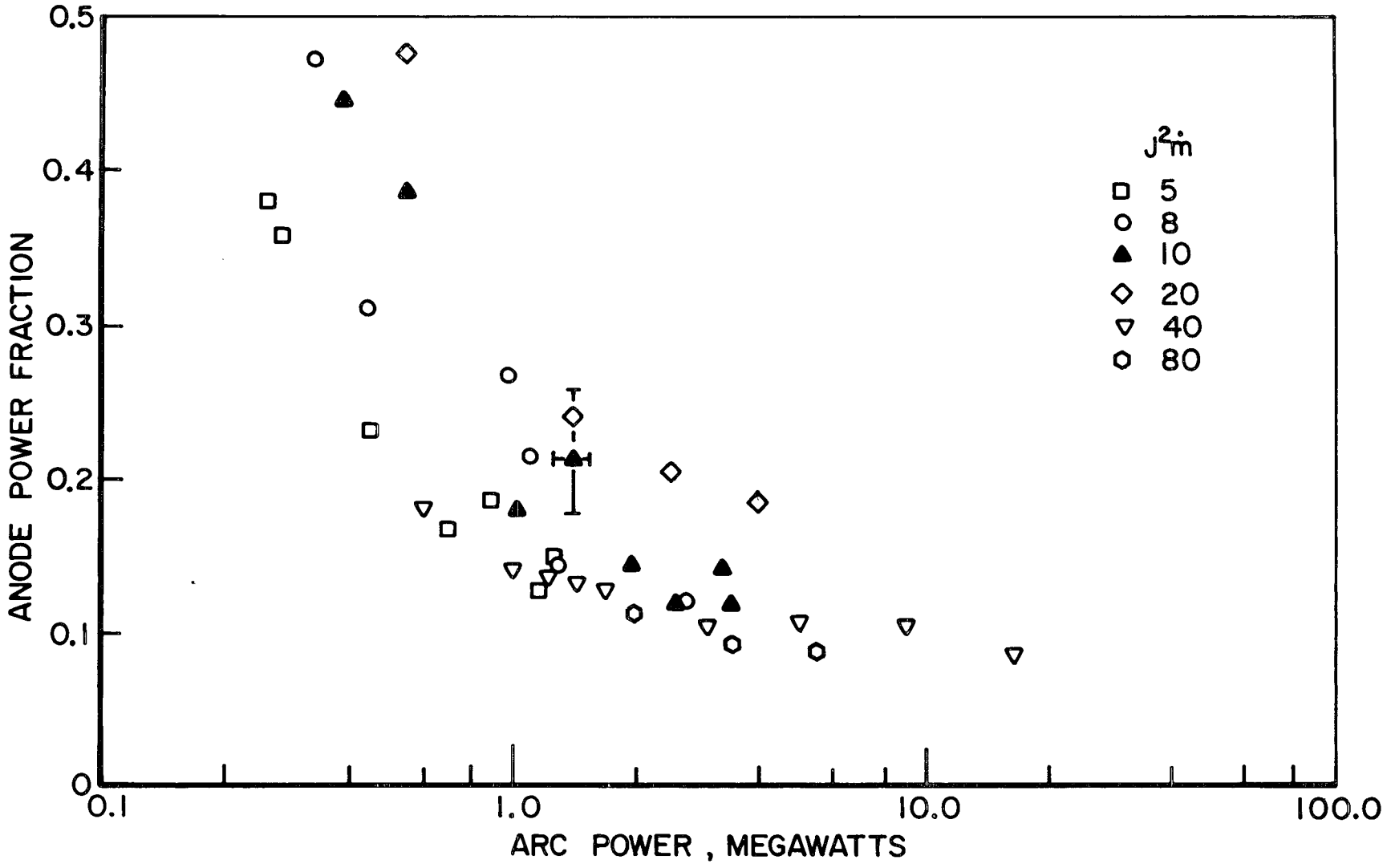

ANODE POWER FRACTION vs TOTAL ARC POWER

FIGURE 6
AP25-4910

the results for "high" power steady state arcs that have been operated at other laboratories.[A-3] As the arc power is increased to the multi-megawatt level the anode power fraction drops by nearly an order-of-magnitude to less than 10%, strongly indicating a more efficient production of thrust.

This inverse dependence of anode fractional power with arc power, even at the highest $J^2/\dot{m}$ conditions where ablated material may play a significant role in the arc operation, suggests that the trend to decreasing relative anode power applies to vacuum or ablation arcs where the propellant is completely supplied by the ablation of a solid insulating material.[A-4]

In steady state arc performance experiments, the anode loss is usually expressed as an equivalent voltage obtained by dividing the total anode power by the total current, P_A/J. This voltage is plotted in Fig. 7 against the $J^2/\dot{m}$ parameter for all of the data conditions of this study. It is of interest to note that, although the spread in the data exceeds the typical error bar, a clear peaking of the data at $J^2/\dot{m}$ = 16 kA^2-sec/g is evident. The usefulness of this curve may be limited by ablation effects which become prominent as $J^2/\dot{m}$ increases beyond the maximum in the equivalent voltage.

Applicability of the Anode Heat Flux Model

The results described in Fig. 7 suggest the definition of an equivalent local anode fall voltage V' utilizing the model commonly employed for the calculation of the anode heat flux:[143]

$$q_a = j_a\left(V_a + \frac{5}{2}\frac{kT_e}{e} + \phi_w\right) + \phi_{rad} + \phi_{conv} \qquad (1)$$

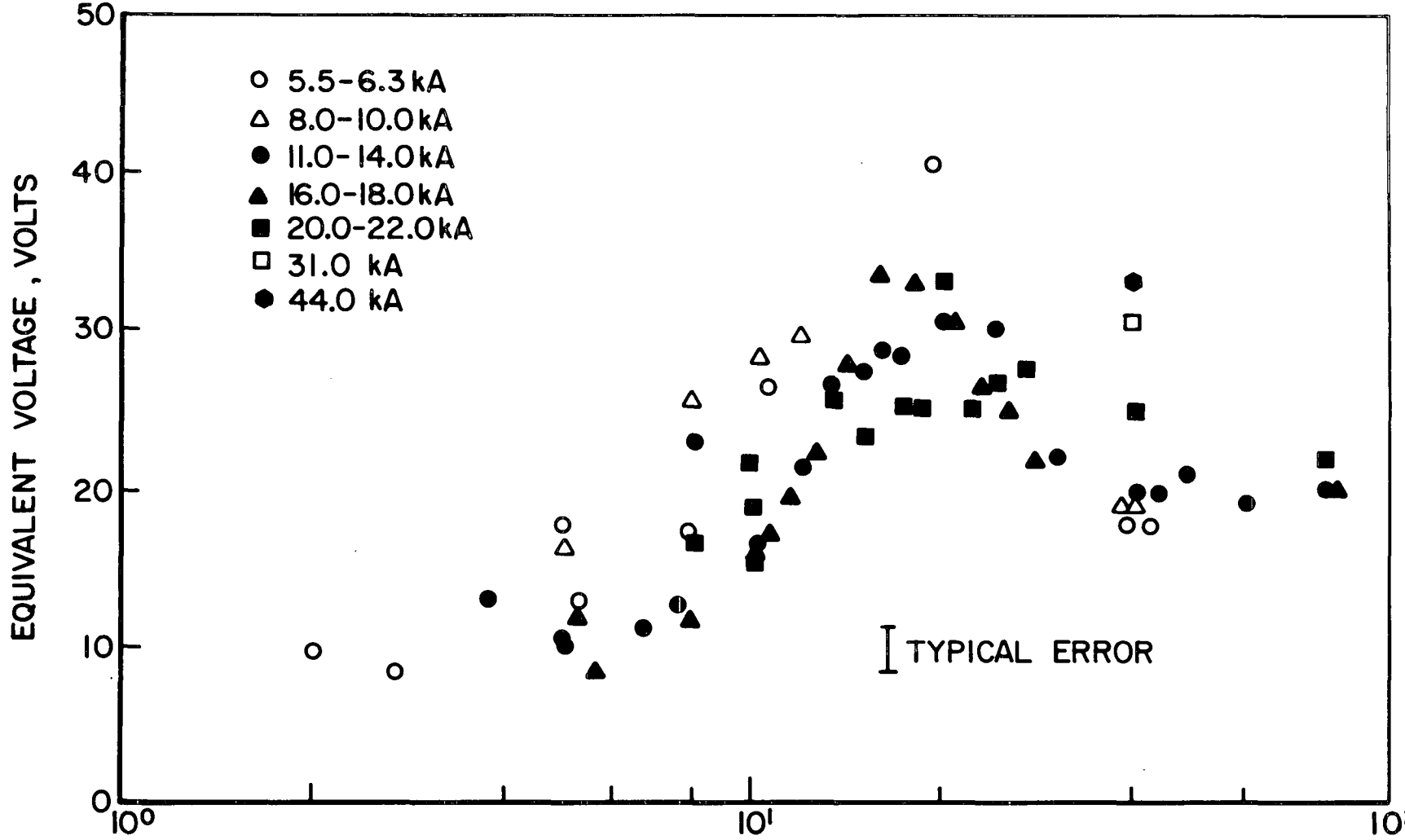

EQUIVALENT VOLTAGE vs $J^2/\dot{m}$

FIGURE 7
AP 25-4911

where q_a is the local anode heat flux, j_a the local current density at the anode, V_a the local anode fall voltage, T_e the electron temperature, ϕ_w the work function of the material, k Boltzman's constant, e the charge on an electron and ϕ_{rad} and ϕ_{conv} the contributions from radiation and convection. Radiation and convection contributions are usually neglected in steady state arcs allowing the heat flux model to become the product of two factors: the current density, j_a, and an equivalent voltage, V' where

$$V' = V_a + \frac{5}{2}\frac{kT_e}{e} + \phi_w \qquad (2)$$

The voltage V' can be determined for the quasi-steady MPD thruster by dividing the local anode heat flux by the local current density at the anode. The current density in the anode vicinity has been measured by detailed probing for the operating conditions of 11 kA x 12 g/sec, 16 kA x 24 g/sec and 22 kA x 48 g/sec. These conditions correspond to an arc operating parameter $J^2/\dot{m}$ = 10 kA^2-sec/g, where spurious propellant effects are minimal. Preliminary local anode current density profiles, shown in Fig. 8, display a peak in the vicinity of the lip just as the local anode heat flux. Further understanding of the applicability of the simple heat flux model ($q_a = j_a V'$) requires more detailed current density probing and the measurement of the local anode fall voltage, both of which are presently in progress.

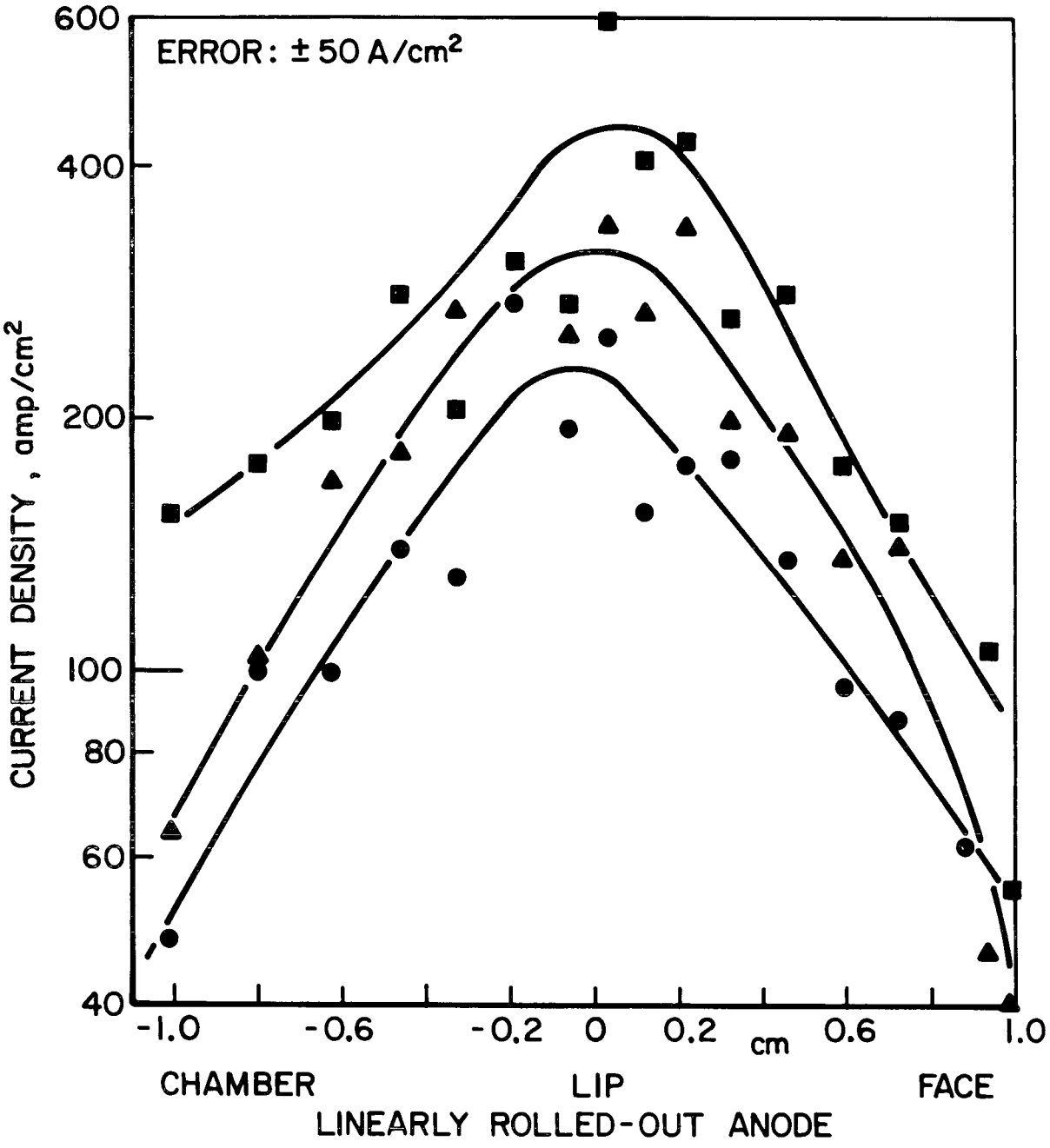

ANODE CURRENT DENSITY

FIGURE 8
AP 25·4913

II-B. Effect of Refractory Insulator Material on the Voltage-Current Characteristic (Boyle)

Recent work by Bruckner demonstrated that insulator material could have a profound effect upon the exhaust structure of a quasi-steady MPD arc accelerator.[141] As a consequence of insulator ablation an inhomogeneous species distribution arises in the discharge characterized by a complex exhaust structure of azimuthally alternating jets of argon and ionized ablation products surrounding a core of ablated materials. When this species structure is compared with a velocity profile obtained close to the anode orifice, the combination suggests that insulator ablation may also directly alter the acceleration and velocity patterns of an otherwise all argon arc. The time-of-flight velocity profile, shown in Fig. 9, consists of a central core region with an average plasma velocity of 21 km/sec and two outer wings, each with an average plasma velocity of 8.8 km/sec.[118] Superimposing Bruckner's radial species distribution upon this velocity profile, the ablation products of the Plexiglas insulator (carbon, oxygen, hydrogen) occupy the central core region while the injected argon propellant occupies the outer wings. Identifying the average mass per atom on the centerline with the mean atomic mass of Plexiglas' atomic constituents, M = 6.7 amu, one sees that the kinetic energy per argon ion and the kinetic energy per ablation particle are equal to within 6%. This suggests that the high centerline velocity may be a consequence of the low average atomic weight of carbon, hydrogen, and oxygen. The inverse dependence of average velocity on the square root of the mass has been previously observed in steady state discharges by Malliaris and Libby at AVCO.[A-5] Thus it becomes evident that a proper understanding of MPD arc processes and

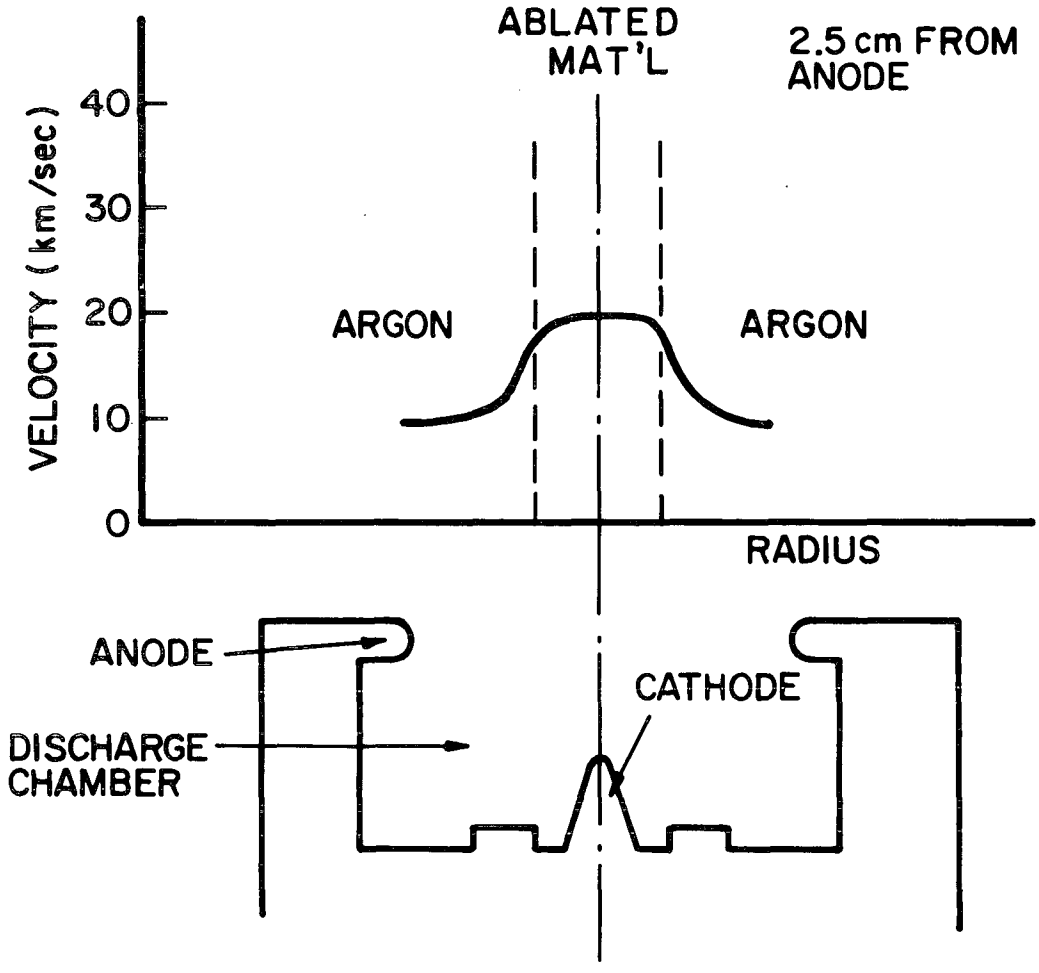

RADIAL DISTRIBUTION OF PLASMA
SPECIES AND VELOCITY
(J = 15.3 kA , $\dot{m}$ = 6 g/sec)

FIGURE 9
AP 25·4903

performance critically depends upon eliminating insulator effects from the overall problem. For this reason, two complementary programs have been undertaken; one to investigate the effects of various mass injection geometries for a given insulator material (Section II-C), and another to investigate the effects of various insulator materials for a given mass injection geometry. The results of the latter study are reported here.

Voltage-current characteristics of the accelerator are obtained for Plexiglas, boron nitride and quartz insulator backplates at injected argon mass flow rates of 6, 12 and 32 g/sec. In all cases argon propellant is axially injected into the discharge chamber through six 0.48-cm-dia flush orifices in the insulator backplate symmetrically distributed at the 2.54 cm radius. The arc current, J, measured by a Rogowski loop, and the terminal arc voltage, V, measured by a Tektronix P6013A high voltage probe are simultaneously displayed on a Tektronix 555 dual beam oscilloscope.

Plexiglas, boron nitride and quartz were selected for comparison because of the wide ranges encompassed by their different mechanical, thermal and molecular properties. Hence, equivalence among their respective V-J characteristics for a particular range of currents and injected mass flows is taken as the criterion for determining that the insulators are not partaking in arc operations for those conditions. Identifying such regions of coincidence is one of the main objectives of this study.

The voltage-current characteristics of the MPD arc running with each of the insulator materials are presented in Figs. 10a, b and c for $\dot{m}$ = 6, 12, and 32 g/sec respectively. Several general comments may be made immediately. For low values of current at a given mass flow rate, the boron nitride and quartz voltages are equal within experimental

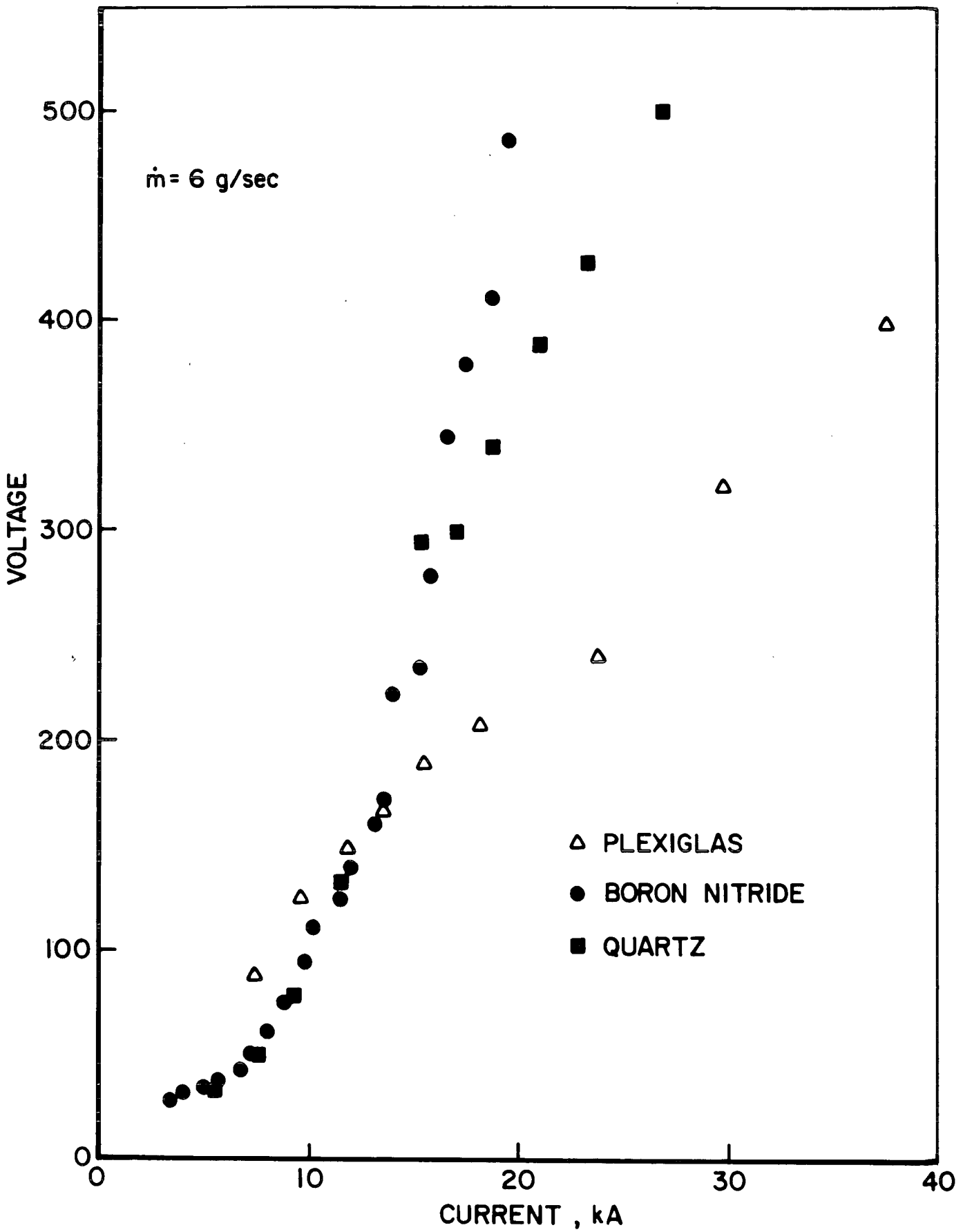

VOLTAGE - CURRENT CHARACTERISTICS

FIGURE 10 a

AP25·4902

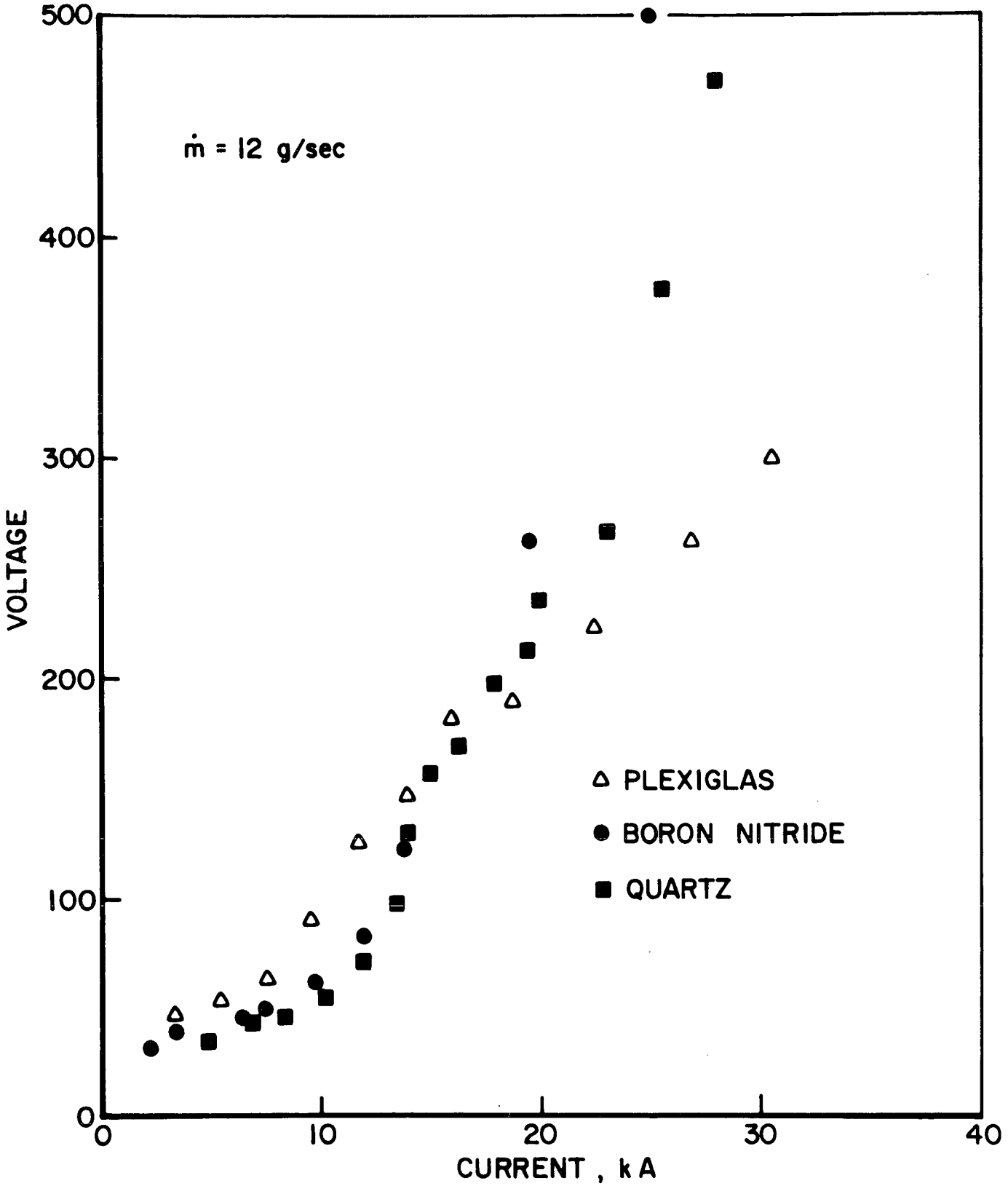

VOLTAGE-CURRENT CHARACTERISTICS

FIGURE 10 b

AP 25 · 4901

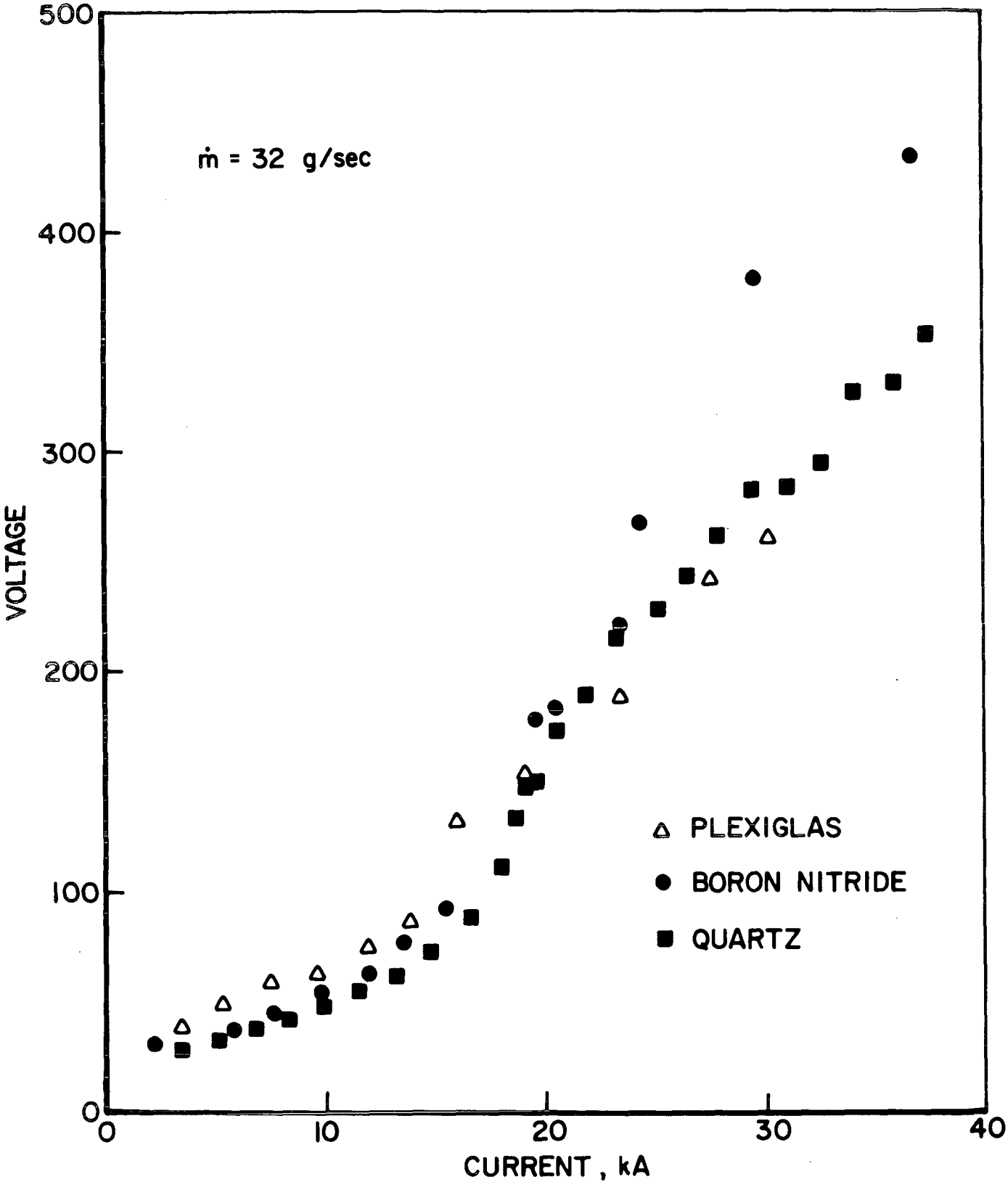

VOLTAGE - CURRENT CHARACTERISTICS

FIGURE 10 c

AP 25·4900

error, and the Plexiglas voltages are greater than the refractory insulator voltages. For currents above a crossover value J_x, the inequality reverses. In this high current regime it is further seen that the boron nitride voltages are higher than those with the quartz insulation. Referring to Table I, J_x is an increasing function of mass flow rate but shows little correlation with $J_x^2/\dot{m}$, a scaling parameter which has been used previously to correlate certain features of MPD arc operation.

However, it can be stated that to first order J_x does distinguish between regions of non-ablation and ablation for the refractory insulator materials. Consider the V-J characteristics for the $\dot{m}$ = 6 g/sec case (Fig. 10a). Below J_x = 13.3 kA, in a regime considered "overfed", the boron nitride and quartz characteristics coincide, indicative of no insulator participation in arc operation as postulated earlier, i.e. no ablation. Indeed, spectrograms of the arc discharge running with a quartz insulator at J = 7.5 kA, $\dot{m}$ = 6 g/sec show a complete absence of quartz ablation products (Fig. 11a). On the other hand spectrogram 11b observed at J = 17 kA > J_x clearly indicates presence of Si II, Si III, Si IV and 0 II, the ionized ablation products of the quartz insulator. Similarly the occurrence of boron nitride ablation is indicated by the BII, BIII and NII, NIII spectral lines identified in spectrogram 11c under similar conditions.

Table I

$\dot{m}$(g/sec)	J_x(kA)	$J_x^2/\dot{m}$ ($\frac{kA^2 sec}{g}$)
6	13.5	30.4
12	17.5	25.5
32	20.0	12.5

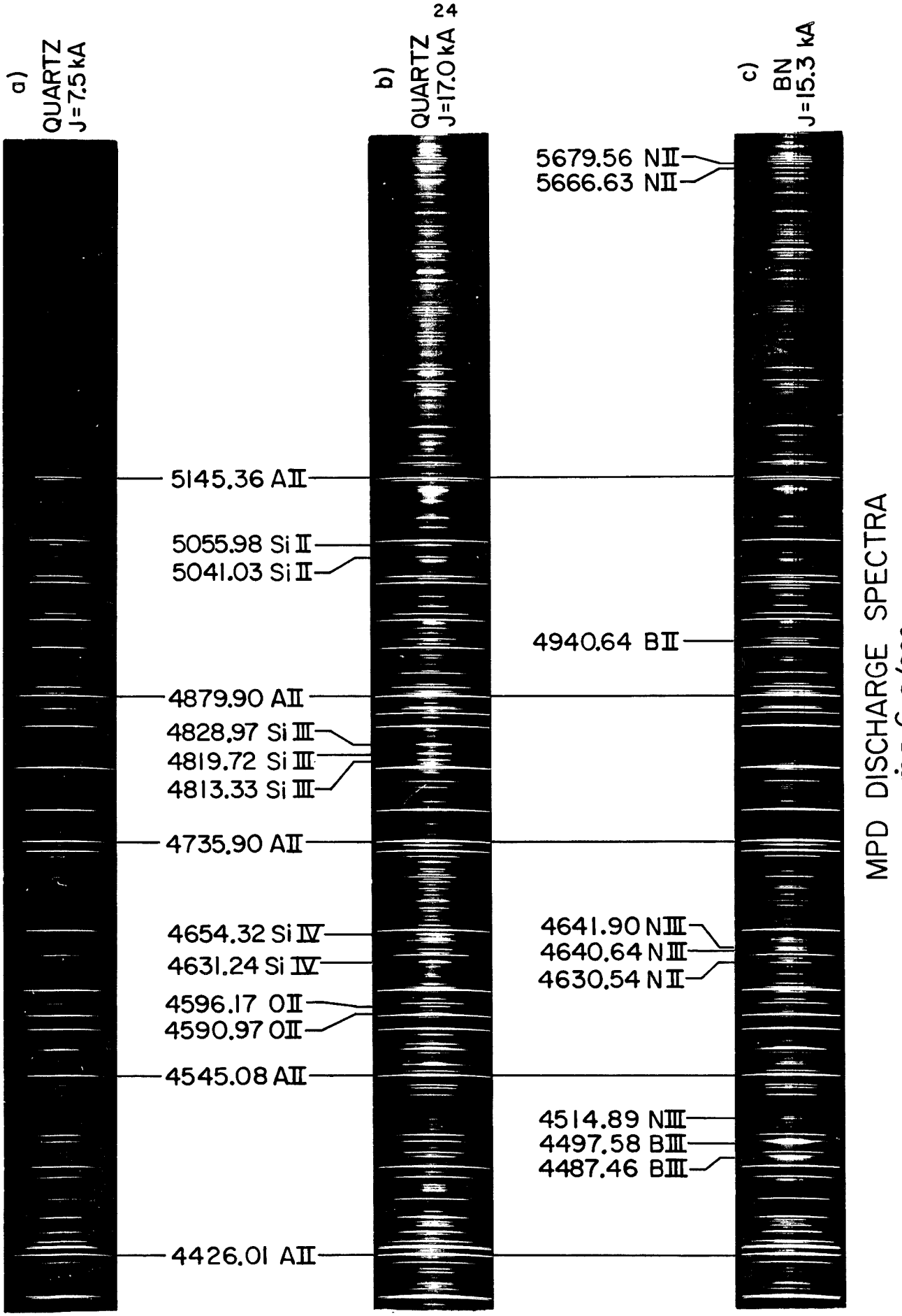

FIGURE 11
AP25-P-507

The same sharp distinction regarding the presence of ablation under certain conditions cannot be made in the case of the Plexiglas insulation. The presence of hydrogen radiance at 6563 Å observed through a narrow band interference filter when the arc is operated in the "overfed" condition implies that insulator ablation persists in spite of being overfed.[143]

As a consequence of this ablation, low atomic weight species are introduced into the discharge thereby lowering the average atomic weight of the exhaust plasma. Following the previously mentioned inverse dependence between the average exhaust velocity and the square root of the average atomic weight, ablation will thereby have the effect of increasing that velocity, which in turn increases the motional back emf contribution to the terminal arc voltage. This trend is consistent with the observed disparity between the Plexiglas and refractory material characteristics for $J < J_x$.

For $J > J_x$ spectroscopic data indicate that all the insulator materials ablate. Explanations of the differences between the three insulator voltages in this region are qualitative at best and require ad hoc assumptions regarding the ablation process which can not be justified at this time due to lack of experimental data.

Qualitatively, the V-J characteristics indicate that the MPD arc's tendency to ablate may be alleviated in two ways for a given mass injection geometry. First, as might be expected, increasing the injected argon mass flow rate substantially reduces the relative disparity among the V-J characteristics. Furthermore, the use of refractory insulator materials delays the onset of ablation as demonstrated by the large current range over which the boron nitride and quartz V-J characteristics coincide. However, even though

the region of ablation-free arc operation is extended in these ways, this extension still falls short of those conditions considered to be of propulsion interest. Thus one concludes that a complete solution to the ablation problem lies in a judicious combination of both injection geometry and insulator material.

Apart from the relative differences among the various insulator V-J characteristics, what appear to be distinct voltage modes of arc operation may be discerned upon examining the shape of an individual characteristic and the character of its associated voltage traces. For a given mass flow rate, as the current is increased, the voltage signature changes abruptly from a flat smooth response (Fig. 12b-2) to a flat, highly oscillatory signal with a frequency of order 100 kc (Fig. 12b-1). Further increase in the arc current eventually causes the voltage signature to peak early in its time history and steadily decline thereafter. The onset of high frequency voltage fluctuations is accompanied by an equally abrupt change in the curvature of the V-J characteristic in Fig. 12a, which is typical of any of the characteristics previously shown in Fig. 10a, b, and c. The current at which this "kink" occurs in the V-J characteristic, J_T, corresponds with that current for which the voltage trace becomes unstable. This voltage mode transition is found to occur for all three insulator materials examined and for all the mass flow rates employed, although evidence of the transitions in the Plexiglas case is far more subtle than in the boron nitride and quartz cases. It is interesting to note that this voltage mode transition occurs at $J_T^2/\dot{m} = 15.3 \pm 3.5$ kA^2-sec/g, a value which also appears in Saber's anode power work (Section II-A).

In an initial attempt to call forth any peculiarities associated with the modes identified above, the discharge

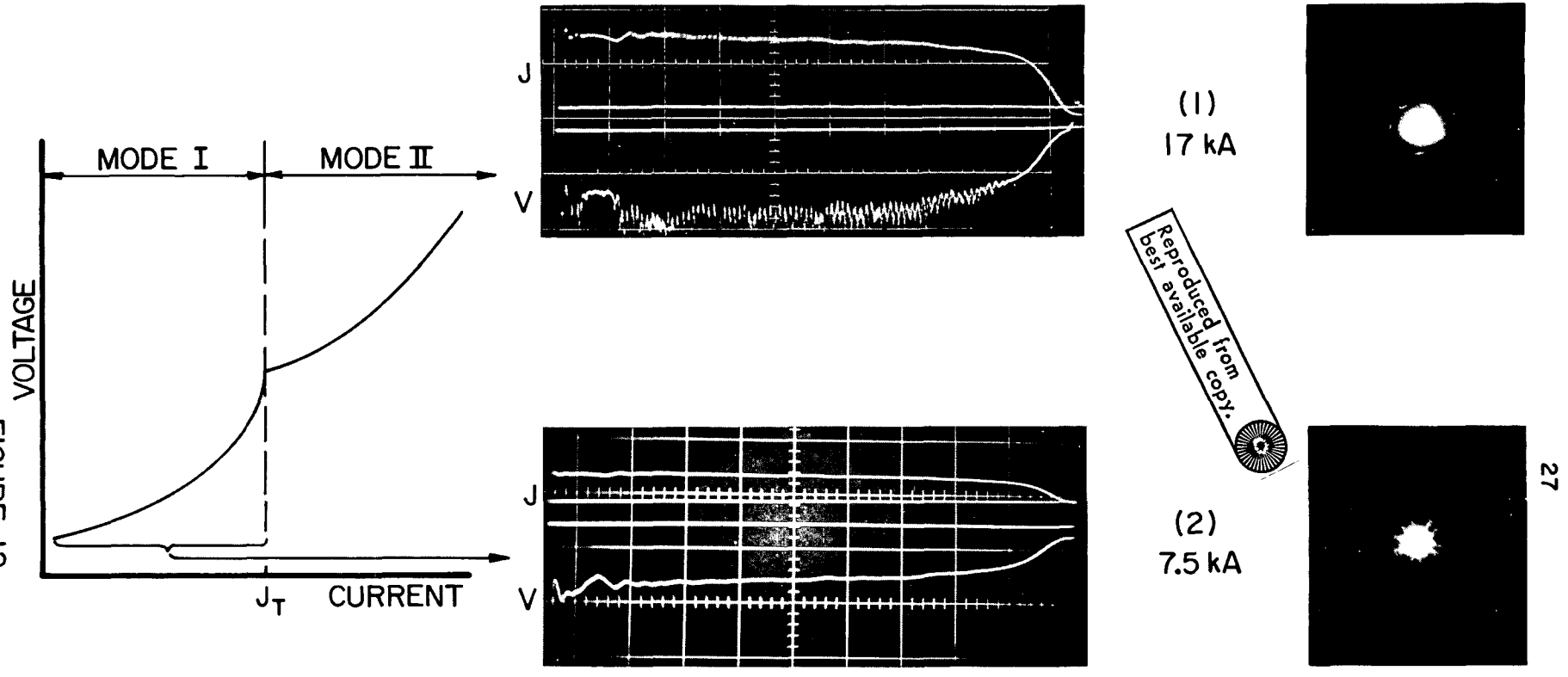

FIGURE 12
AP 25·P·503

a) TYPICAL V-J CHARACTERISTIC

b) VOLTAGE SIGNATURE

c) SPECTRAL PHOTOS OF CATHODE 5910 Å

DISCHARGE MODE CHARACTERISTICS

was photographed through various narrow band spectral filters with quartz as the insulating backplate and at a mass flow rate of 6 g/sec. The most interesting of these photos are presented in Fig. 12c. Each is an end-on view of the accelerator cathode as seen through a 5910 Å interference filter (75 Å bandwidth). Figures 12c-2 and 12c-1 correspond to current magnitudes of 7.5 kA and 17 kA, respectively. Thus according to Fig. 12a, c-2 is associated with mode I and 12c-1 is associated with mode II of arc operation. One immediately notes the striking radiation pattern associated with mode I. The spoke-like streaks originate at the base of the conical tungsten cathode, run up along the cathode surface and intersect a bright ring situated midway between cathode base and tip. For this condition the 5910 Å filter will allow only tungsten line radiation as well as continuum radiation to be transmitted. One may speculate that the radiation pattern represents the regions of current attachment and electron emission occurring on the cathode surface characteristic of mode I operation.

Mode II, represented by Fig. 12c-1, is characterized by an intense diffuse blob of continuum radiation originating from or in front of the cathode tip. Increasing the current level in mode II further constricts this cathode attachment and introduces what appears to be a luminous asymmetry emerging from the cathode tip.

In summary the following two conclusions may be drawn:

1. For this mass injection geometry, use of refractory insulator materials defines a range of currents and mass flow rates which permit ablation-free arc operation in regions where Plexiglas insulation is prone to ablate. In spite of this improvement over the Plexiglas insulator, arc operation with refractory insulators at high

currents $J \gtrsim J_x$, remains plagued by ablation phenomena indicating that the ultimate backplate will have to be a judicious combination of both insulator material and injection geometry.

2. For this mass injection geometry, the arc appears to run in different voltage modes as a function of total arc current and these modes may in part be characterized by different cathode surface phenomena.

Future work will combine the positive results of both the insulator material and injection geometry studies into an overall accelerator configuration which warrants a detailed examination of the velocity profiles and the acceleration processes devoid of any ablation phenomena. In addition such future study will attempt to further characterize and correlate the voltage modes identified herein with those same acceleration processes.

II-C. Distribution of Injected Propellant (Villani)

Using spectrally resolved photographs of the discharge radiance, Bruckner showed that the presence of a severe azimuthal species nonuniformity in the MPD exhaust flow was associated with the six propellant injection ports.[141] Subsequent accelerator operation with an annular propellant injector eliminated the azimuthal structure and also revealed a sensitivity of the terminal voltage and of the apparent ablation, as judged by photographs of the singly-ionized and molecular carbon line radiation, to the radius of this annular injector.[143] In further tests using single annulus injectors of various radii, the following restrictions on injected propellant distribution were deduced:

1. Flow is required near the anode in order to produce a flat voltage during the quasi-steady portion of the pulse.
2. Flow is required near the cathode to produce the lowest voltage for a given current.
3. Flow is required along the Plexiglas insulator in order to minimize its ablation.

Attempts to satisfy these partially conflicting requirements with a single annulus located near the cathode base and turned to divert the flow at various angles with respect to the accelerator centerline met with only partial success.[143]

To examine this problem in more detail, a special arc chamber was constructed which simplified the installation and evaluation of trial injectors.[143] In the most recent tests, double annulus injection stencils were prepared which allowed complete control of the flow rate through each annulus, independent of the shape, angle or area of the annulus. Evaluation of the double annulus injection over a limited

range of mass flows and the full range of flow division between inner and outer annuli is the subject of this report.

Apparatus

The differences in operating principles between the double annulus and the previous single annulus stencils are shown in Fig. 13. In the single annulus head (Fig. 13a), propellant flow is metered at the choked orifice of a solenoid valve (Skinner C2DB1062) and feeds into the plenum through a total of 24 holes in six injectors, passing thence through the injection stencil into the arc chamber in the desired pattern. In the differential control head (Fig. 13b), flow metering occurs at 12 small holes in the injector caps, with the plenum split by the divider ring into two separate volumes, each fed by six of the 12 orifices. Alternate sets of injector caps are available which provide percentage flow divisions of approximately 0:100, 30:70, 50:50, 70:30 or 100:0 between the inner and outer annuli. To insure that the choking occurs at the injection caps rather than the valve, a large-orifice valve (Skinner V52DB2017) with a metering area four times that of the previous type is used. Total mass flow is determined experimentally through the use of a double-action valve power supply and a fast ionization gauge as described elsewhere.[119,A-2] Flow division is calculated on the basis of orifice dimensions.

Two geometries were studied on the differential control head, one of them an interpolation and one an extrapolation of previous knowledge (Fig. 14). The interpolation (referred to as the $+45^{\circ}$ geometry, Fig. 14a) is a simple combination of two earlier geometries, each of which satisfies some of the injection design goals. As described previously,[143] it was found that if propellant is injected near the

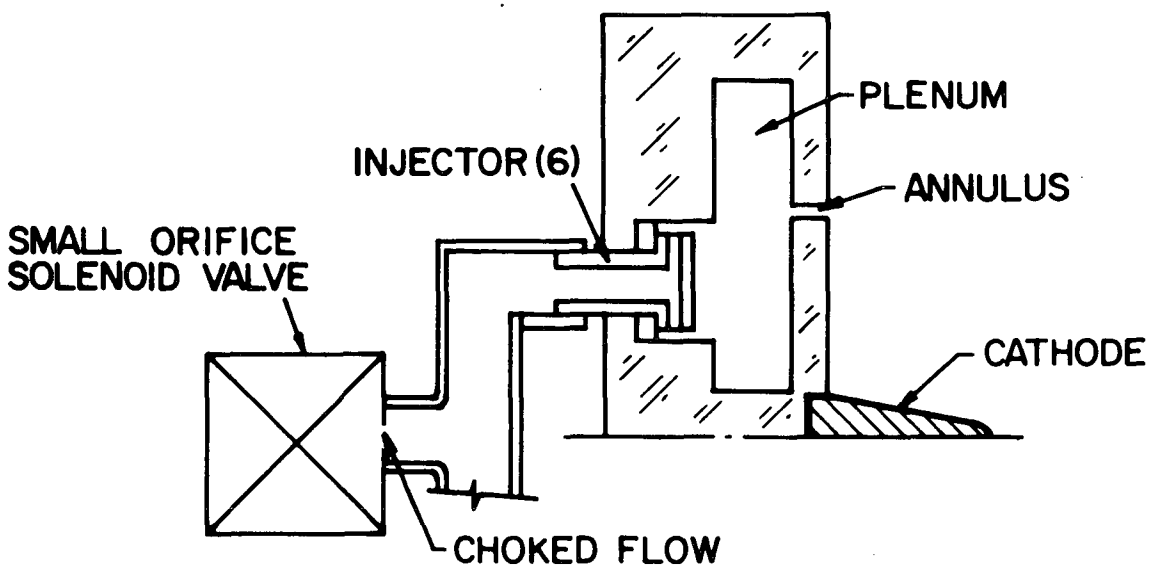

a) SINGLE ANNULUS HEAD

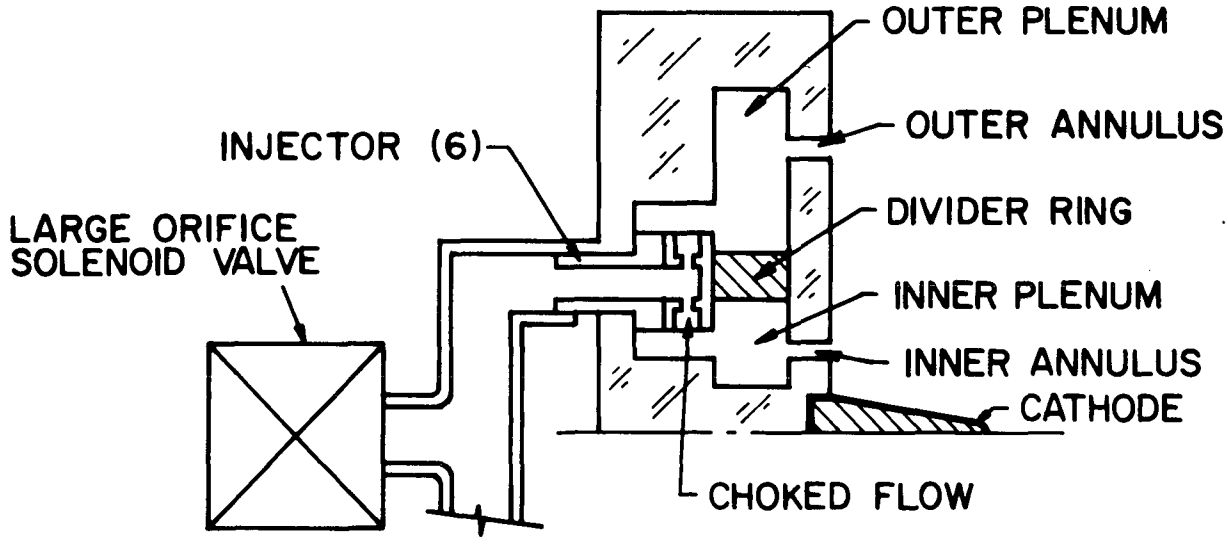

b) DIFFERENTIAL CONTROL HEAD

ANNULAR INJECTORS

FIGURE 13
AP25-4905

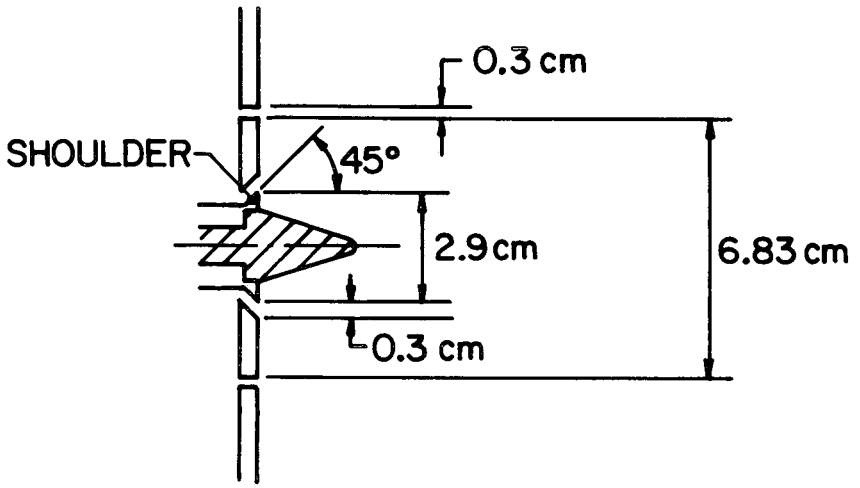

a) + 45° GEOMETRY

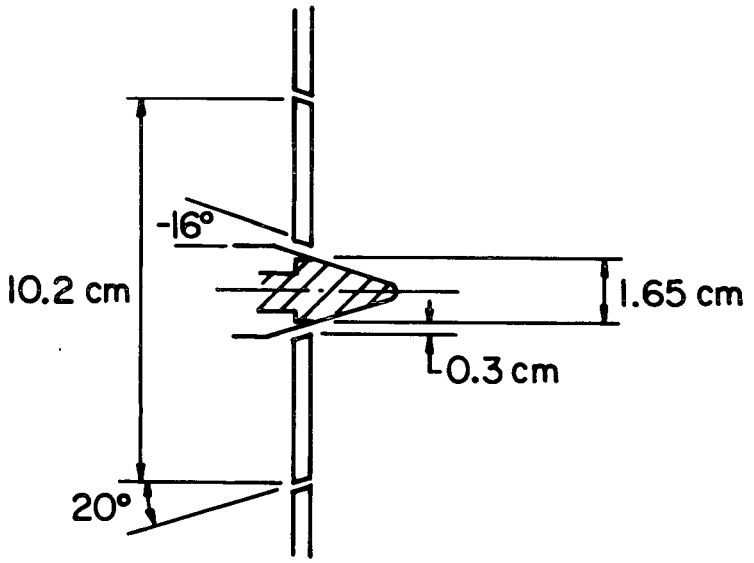

b) −16° GEOMETRY

45° AND -16° INJECTORS

FIGURE 14
AP 25·4906

base of the cathode, at a flow angle of 45^{o} radially outward, the terminal voltage is quite low, although time varying, and spectral filter photographs show very little C_2 or CII band or line radiance, indicating possibly low ablation. Injection parallel to the axis at an intermediate to large radius on the other hand produces an extremely flat voltage signature, but has the penalty of high voltage and high ablation rate. It was hoped that injection through an appropriate combination of a small-radius, $+45^{o}$ annulus and a large-radius 0^{o} annulus would provide a combination of low voltage, flat voltage, and low ablation.

The other geometry studied (referred to as the -16^{o} geometry, Fig. 14b) is an attempt to extrapolate our previous experimental range. Briefly, the flow from the outer annulus (diverted 20^{o} radially inward) should provide a flat voltage by virtue of its large injection radius and it should reduce ablation by producing inward flow along the backplate. The inner annulus should provide adequate mass flow to the intense central portion of the discharge, reducing the power losses there.

Both geometries were studied at 16.5 kiloamps, with total mass flow ranging from 6 to 12 g/sec and flow divisions of 0, 30%, 50%,70% and 100% through the inner annulus and the remainder through the outer annulus. Voltage and current were monitored on a Tektronix type 555 dual-beam oscilloscope, and spectral filter photographs were taken with a new Burleigh Brooks Super Cambo 4x5 view camera fitted with a Schneider Tele-Xenar 500 mm telephoto lens.

Results of Differential Injection Survey

It is instructive to compare the results obtained with these two geometries with the immediate goals of this injector configuration study - low voltage, flat voltage and minimum ablation for a fixed current.

Voltage Magnitude: For the +45° geometry with a current of 16.5 kA, Fig. 15 shows the dependence of peak quasi-steady voltage on total mass flow for 100% of the flow through the inner or outer annulus (Fig. 15a) and on flow division between inner and outer annuli for total mass flows of 6 and 12 g/sec (Fig. 15b). Also shown for comparison are data taken with the earlier single large radius annulus (same radius as the outer annulus of this geometry) and the single +45° annulus (same radius as the inner annulus of this geometry).[143] Similarly, Fig. 16 shows the same voltage characteristics for the -16° geometry.

Figures 15a and 16a show that regardless of the flow injection location, the voltage always decreases as the mass flow increases. This dependence has been found for any flow division between annuli. For a fixed mass flow, Fig. 15b shows that the voltage decreases monotonically in the +45° geometry as the fraction of total flow through the inner annulus increases. By contrast, the -16° geometry exhibits either a slightly increasing voltage or a decreasing voltage as the percentage flow through the inner annulus increases, depending on the magnitude of the particular total mass flow. For the 16.5 kA, 6 g/sec operating condition where considerable data has been acquired in the past, the lowest terminal voltage was measured with the +45° geometry with 100% of the flow through the inner annulus.

Voltage Flatness: Terminal voltage traces at selected conditions are shown in Fig. 17, taken with a slow sweep rate to accentuate any irregularities. It can be seen that the +45° geometry exhibits flatter voltages than the -16° geometry. For the latter case, the voltages become increasingly peaked as the flow through the inner annulus is increased (Figs. 17d, e, f). At the present time, the physical basis for the unsteady voltage is not well understood, but may be

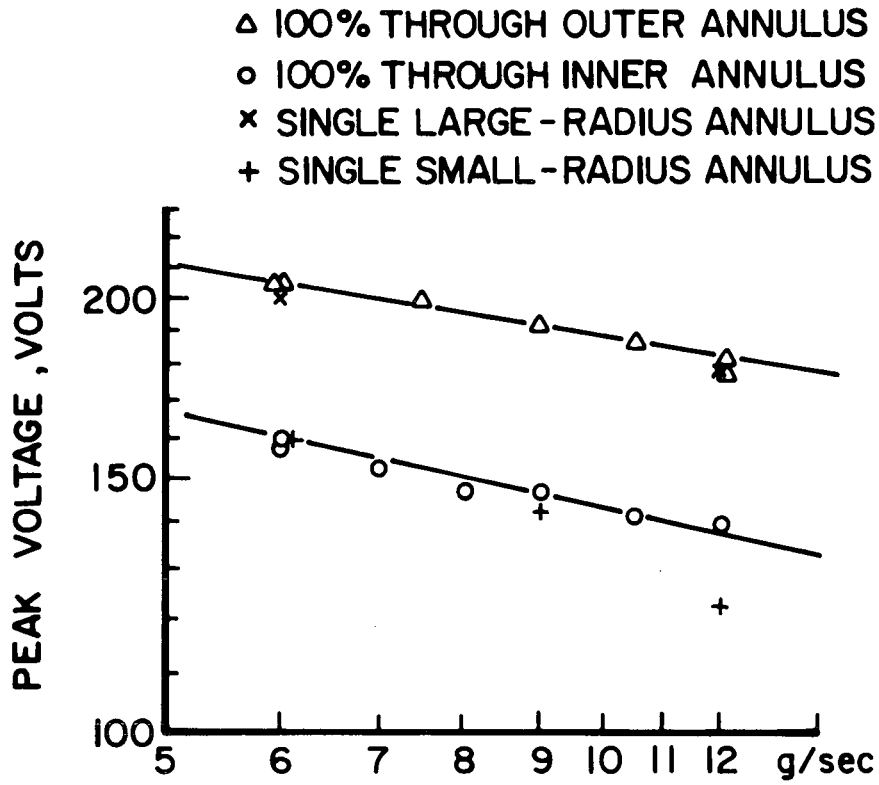

a) TOTAL MASS FLOW $\dot{m}_t$

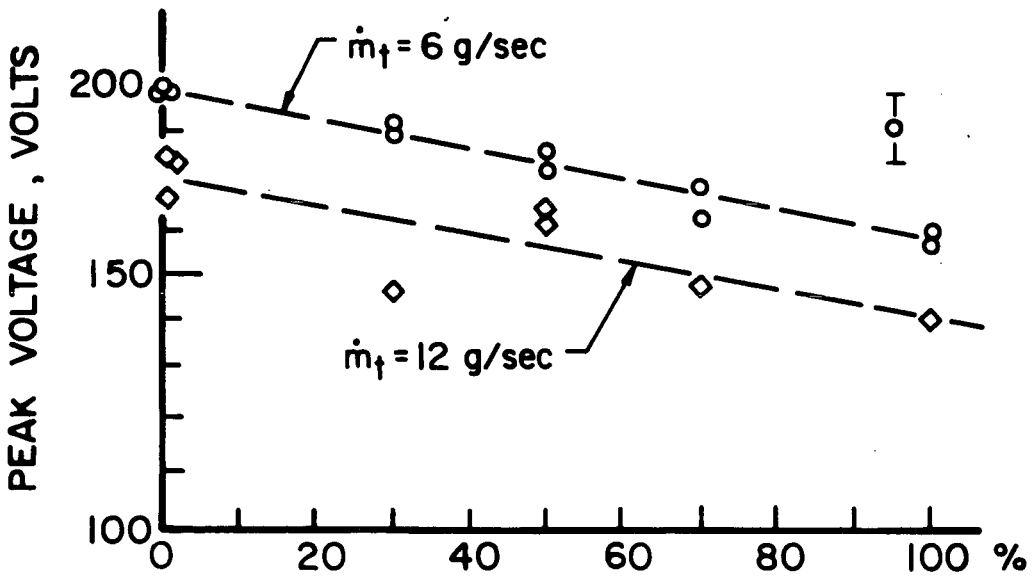

b) % OF TOTAL $\dot{m}_t$ THROUGH INNER ANNULUS

VOLTAGE CHARACTERISTICS OF +45 GEOMETRY

FIGURE 15

AP25·4907

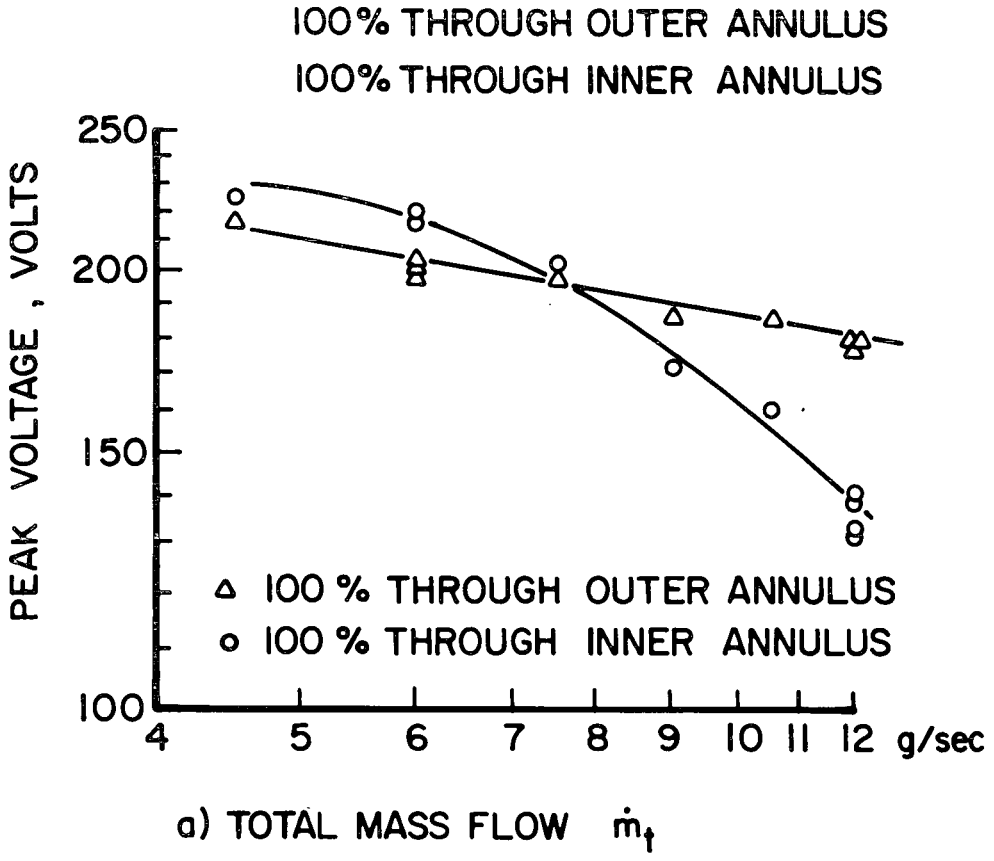

a) TOTAL MASS FLOW $\dot{m}_t$

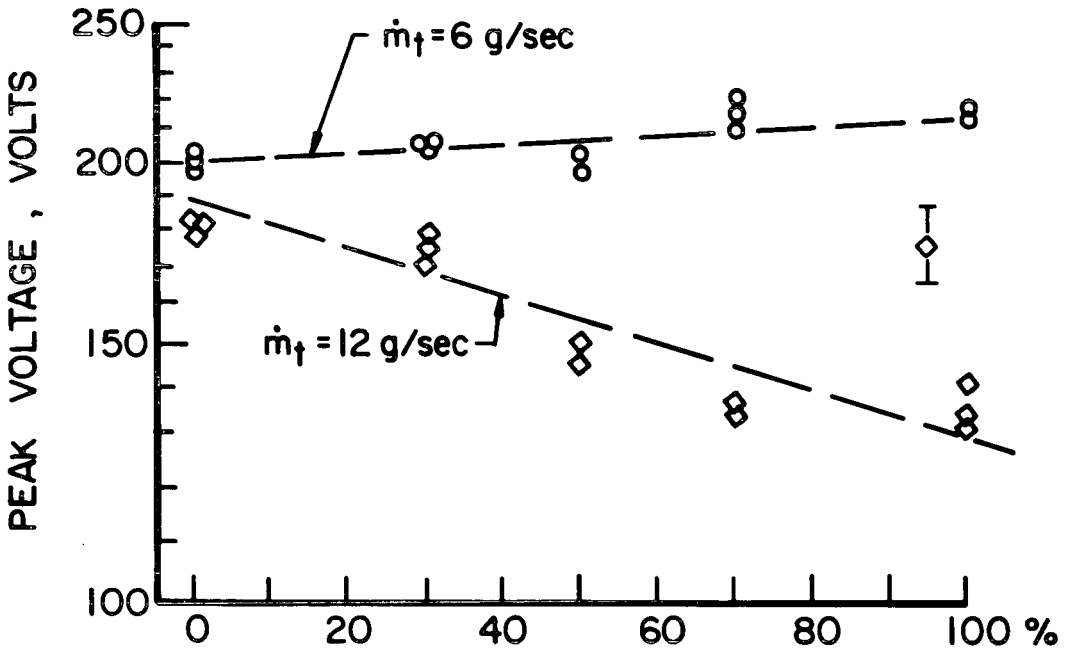

b) % OF TOTAL $\dot{m}_t$ THROUGH INNER ANNULUS

VOLTAGE CHARACTERISTICS OF -16° GEOMETRY

FIGURE 16
AP25·4908

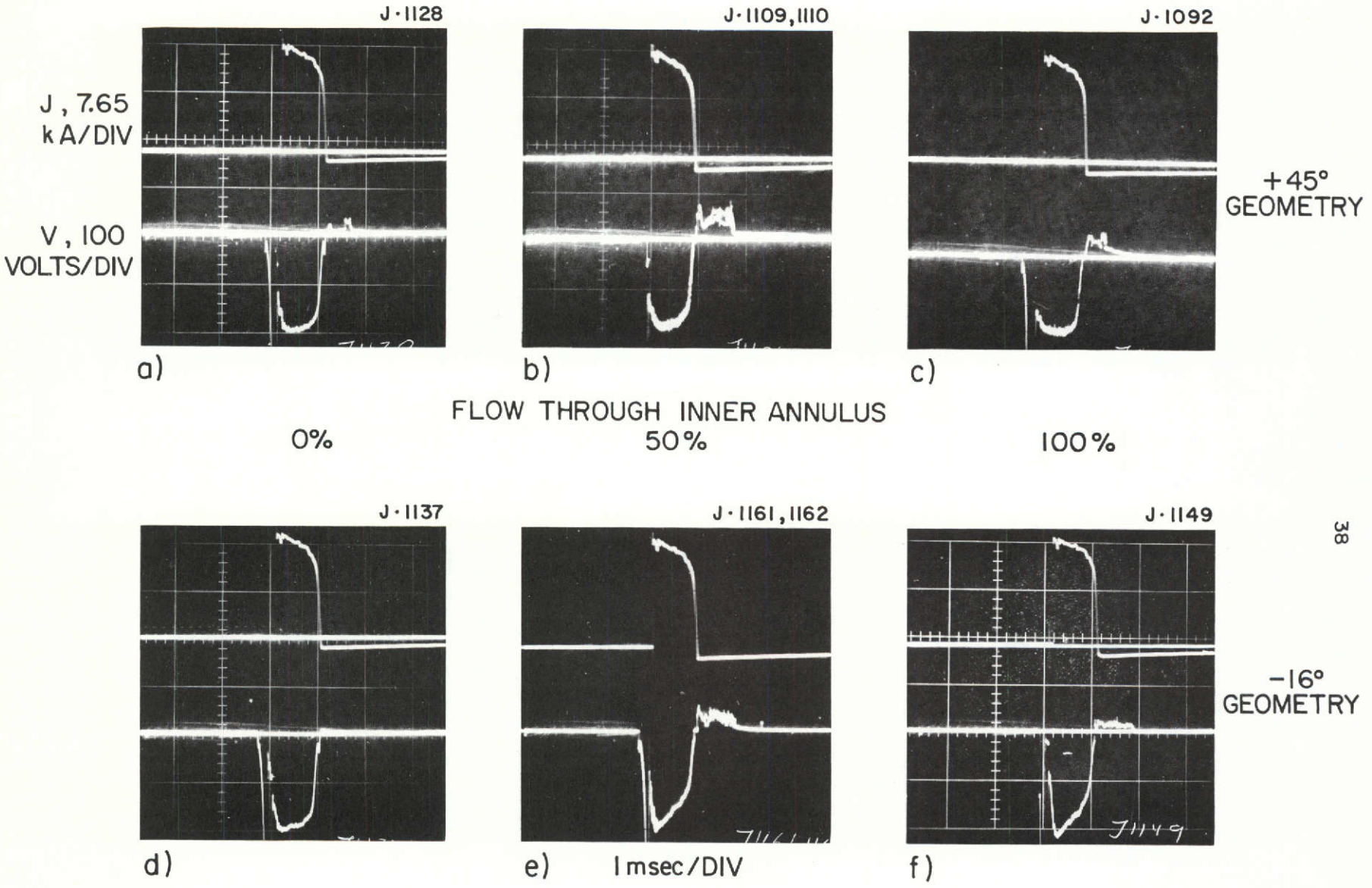

FIGURE 17
AP 25·P·504

VOLTAGE AND CURRENT SIGNATURES OF ANNULAR INJECTORS

related to lack of charge carriers near the anode. For the $+45^{o}$ geometry, the curious trend of the 0% and 100% inner annulus flow cases exhibiting the flattest voltages (Figs. 17a and 17c) may still be related to the charge carrier density at the anode since the inner annulus diverts the flow toward the anode.

Luminosity Patterns: Argon and carbon line-radiation photographed through spectral filters at the 16.5 kA, 6 g/sec condition are shown in Figs. 18 and 19 at selected flow divisions for both geometries. The argon photos (left side) show, as expected, an increase in argon ion line radiation in the vicinity of the cathode as the flow division is shifted toward the inner annulus. In addition, comparison of Figs. 18 and 19 for the same flow division shows a greater argon ion line radiation on the centerline for the -16^{o} geometry, consistent with the more direct injection into this area. The carbon photos of both geometries (right side) contain an interesting feature: a ring of light with well defined inner and outer boundaries which moves inward as the flow division shifts toward the outer annulus. Photos taken at intermediate flow divisions confirm the continuous movement of the luminous ring, which may be identified as the region of the insulator not protected by the injected argon. Close examination of the carbon photos shows that, except for the small bright ring at the base of the cathode, the total luminosity of ablated carbon appears to be a minimum for the $+45^{o}$ geometry with 100% of the flow through the inner annulus. Referring back to Fig. 14a, it is seen that the bright ring is associated with the unprotected surface of the inner insulator between the cathode and inner annulus.

Based on the results of these experiments, the $+45^{o}$ geometry with 100% of the flow through the inner annulus appears to be the most interesting of the two injection configurations from the standpoint of minimum voltage, minimum

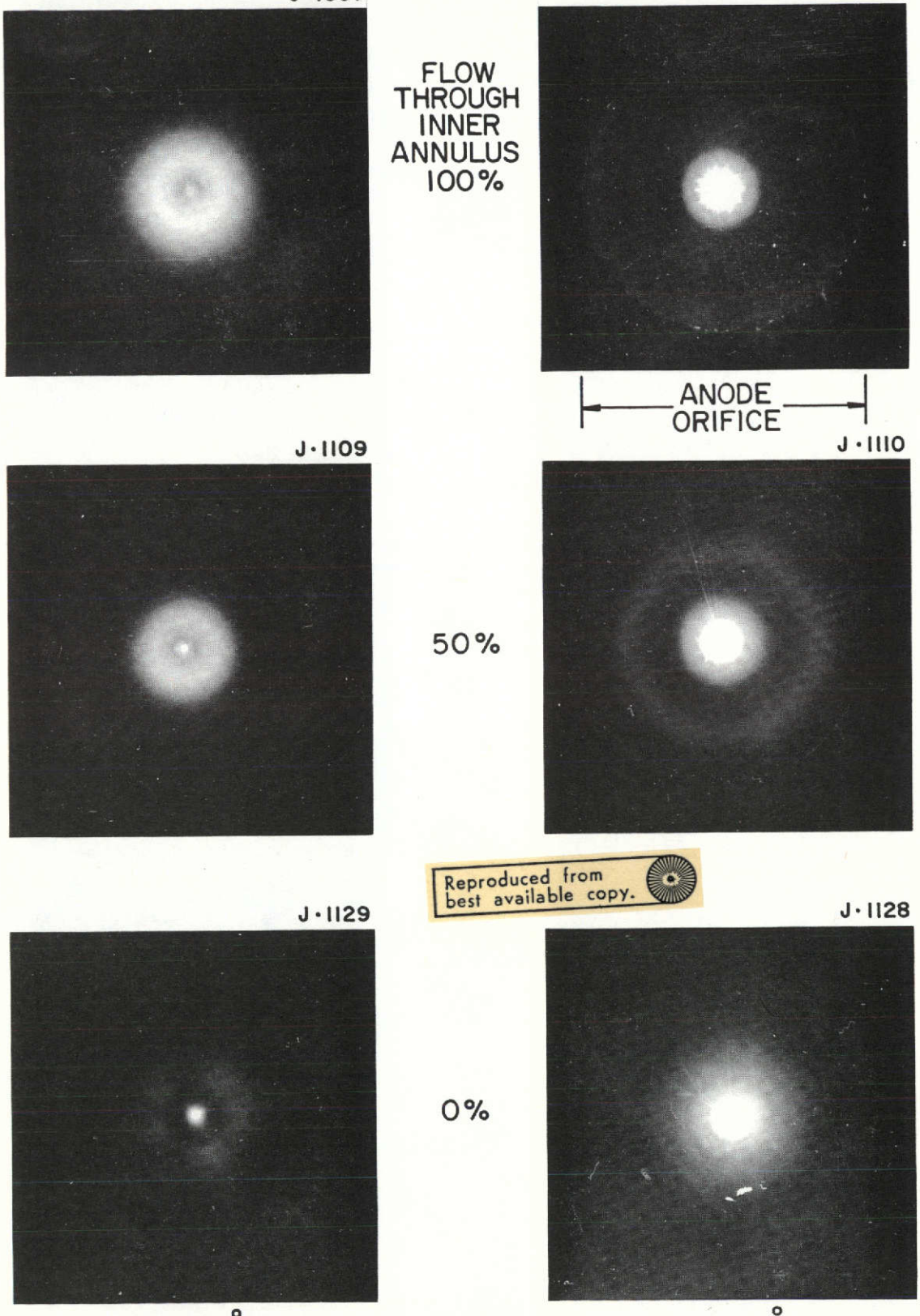

SPECTRAL FILTER PHOTOGRAPHS; +45° GEOMETRY

FIGURE 18
AP 25·P·506

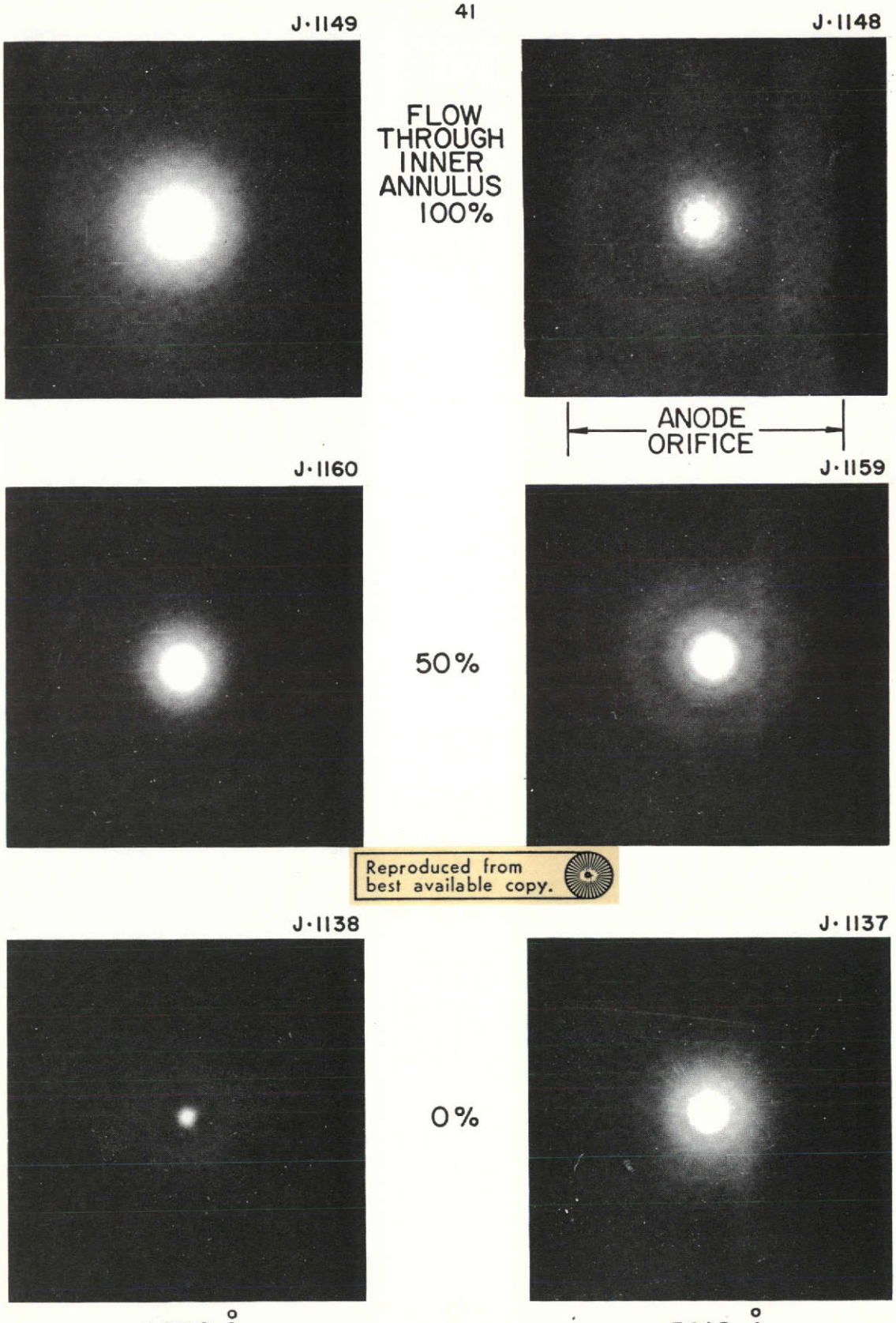

SPECTRAL FILTER PHOTOGRAPHS; -16° GEOMETRY

FIGURE 19
AP 25·P·505

ablation, and reasonably flat voltage record. In order to determine whether the 45^{o} injection is in fact a local optimum, data have been obtained for single annulus injectors of $+90^{o}$, $+22^{o}$, 0^{o} and -16^{o}, all with an exposed inner insulator shoulder comparable to the 45^{o} injector (approximately 4 mm). In addition, a 67^{o} annulus with an 8-mm-shoulder was also tested. Since the inner annulus of the original -16^{o} geometry injected flow along the cathode surface (zero shoulder), the -16^{o} annulus with the 4-mm-shoulder was included to evaluate the effect of this shoulder.

The results for these various annuli are plotted in Fig. 20 for the 16.5 kA, 6 g/sec condition. For the present electrode geometry and a fixed insulator shoulder between the inner lip of the annulus and the cathode base, the optimum propellant injection angle appears to be greater or equal to 45^{o} which again suggests the importance of delivering propellant to the anode region. The effect of the shoulder is seen in the circular data points. The open circle, which is for the $+67^{o}$, 8-mm-shoulder case, produces an arc voltage which is 30 volts greater than the voltage trend implied by the 4-mm-shoulder data. The solid circle is the earlier data point acquired with the zero-shoulder configuration. Injection at -16^{o} with a 4-mm-shoulder produced a voltage of 240 volts, the largest yet observed with a Plexiglas injector stencil.

The latter results strongly suggest one other test to answer the following interesting question. Since increasing the shoulder dimensions produces an apparent 30 volt increase in the terminal voltage ($+67^{o}$ case) and alternatively, eliminating the shoulder in the -16^{o} case produces a 30 volt decrease, the question arises whether the minimum observed voltage (160 volts for the $+45^{o}$ case) can be further reduced by yet an additional 30 volts simply by removing the 4-mm-shoulder.

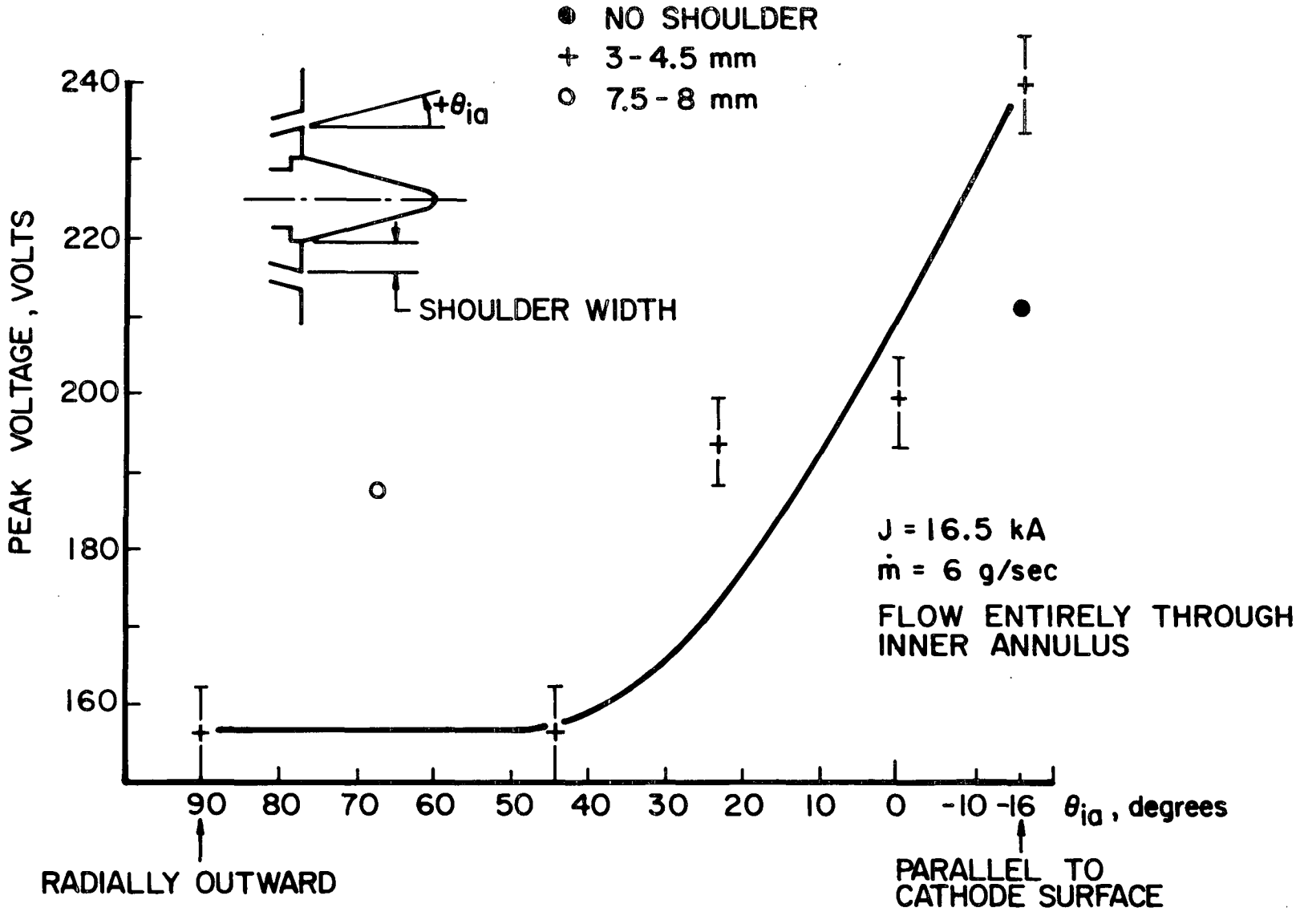

VOLTAGE DEPENDANCE ON INJECTION ANGLE

FIGURE 20
AP25-4909

An injection configuration to answer this question is presently under construction.

Future Work

Subject to the result of the above test with the $+45^{o}$ geometry, it will be possible to identify for the present electrode geometry a local optimum injection configuration, i.e. one which is relatively free of extraneous loss mechanisms. The next experimental step consists of mapping the enclosed current contours and floating potential distributions in the arc chamber at the optimum and selected non-optimum conditions. This will serve a number of purposes: First, it will determine whether the current pattern is altered radically in the presence of changes in the propellant injection pattern. Since acceleration through the MPD discharge depends strongly on the local profile of the current and self-magnetic field interaction, the current distribution could greatly affect the profile and divergence losses in the exhaust flow. Second, knowing the current and floating potential distributions, the power deposition per unit volume can be calculated. This can be correlated with the propellant injection configuration to provide information relating local energy sinks with local propellant density. In addition, local measurements of E-field and current density vectors will assist in the determination of local conductivity and vector flow-field.

II-D. Impact Pressure Measurements with a Piezoelectric Probe (Dutt)

A piezoelectric pressure probe has recently been developed which is capable of measuring the local momentum flux in the quasi-steady MPD exhaust.[125] In conjunction with local measurements of flow velocity and flow angle obtained with biased double electrostatic probes, a detailed mapping of the mass, momentum and energy fluxes over the entire exhaust plume is possible.[138,143]

The accuracy with which previous pressure probe signals could be reduced to local values of the momentum flux was limited by incomplete information in two areas:

1. The static pressure, p, could not be separated from the measured total pressure, P_t, without certain ad hoc assumptions based on a limited amount of spectroscopic data.

2. The response of the pressure probe to flows that are not parallel to the probe axis, i.e. flows not normally incident on the probe tip, was not fully understood.

The experiments described here are directed toward improving our understanding in this second area.

Yaw Correction

When supersonic flow is normal to the flat probe tip, there is a detached bow shock wave in front of the probe. The probe tip in our case is sufficiently blunt so that the shock wave may be approximated by a normal shock in the region in front of the probe, after which the flow is assumed to stagnate isentropically on the probe tip. When the incident flow is not normal to the probe tip, many complex phenomena are introduced:

(a) The detached shock wave may no longer be approximated by a normal shock,

(b) the flow is turned after passing through the oblique shock,

(c) for sufficiently large angles of incidence the shock may not be detached at all, and

(d) the components of velocity parallel to the probe surface cause transverse forces to act on the probe tip. These forces excite transverse and shear modes in the thin Plexiglas rod in which the piezoelectric crystal is embedded, which in turn cause spurious signals to be generated in the crystal.

Since the strength and structure of the bow shock depend on the free stream Mach number, M, and the ratio of specific heats, γ, it is possible that the response of the probe will depend on the particular arc operating condition as well as on the angle of incidence of the flow on the probe tip. In the present experiment, the probe was rotated through various angles of flow incidence while maintaining the operating conditions at a current of 16 kA and a mass flow of 6 g/sec.

Probe Characteristics

The piezoelectric probe has been described in detail previously.[125,143] Briefly, it consists of a piezoelectric crystal (PZT-5) embedded in a Plexiglas acoustic delay rod 1 m long and 0.95 cm in diameter. The rod is suspended inside a tube of 7 cm diameter, the front end of which is closed except for a 2.5 cm diameter extension with a 1.3 cm diameter hole to accommodate the probe tip. The probe tip is recessed about 1 mm behind the front end of the tube extension.

The tube and probe assembly is mounted in the vacuum tank on a new movable platform whose position is altered using four electric motors. With this new platform, it is possible to remotely move the probe in the accelerator axial direction as well as the horizontal and vertical directions perpendicular to the axis. In addition it is possible to rotate the probe to an arbitrary angle of incidence in the horizontal plane. Figure 21 shows a top view of a typical probe arrangement in the vacuum tank.

Piezoelectric pressure probes are susceptible to spurious pickup of electromagnetic noise associated with the discharge. The noise alone can be measured in the present case by shielding the probe from the plasma with a small cap on the end of the tube housing. With this shield in place, a survey throughout the exhaust plume showed the noise, or null signal, to be approximately constant with respect to both probe location and time during the discharge at a value of 17 $\pm$ 4 mV. The 4 mV average deviation is small compared to the centerline probe response to plasma flow ($\approx$ 200 mV). The response of the probe to all stresses, R_2, is thus obtained by subtracting the null signal, N , from the total probe output, R_1.

Flows not normally incident on the probe exert a force which may be resolved into components normal and tangential to the probe tip, each of which generates a different probe response. The normal force excites longitudinal stress waves which propagate down the Plexiglas rod, reflect off the end surface and return to the crystal after 0.86 msec. Thus, the time for undistorted measurements of the longitudinal stresses is the 0.86 msec following the first probe response.

The tangential component has an effect on the probe which is dependent on the direction of the force because the stress-measuring crystal is not isotropic. Since the probe

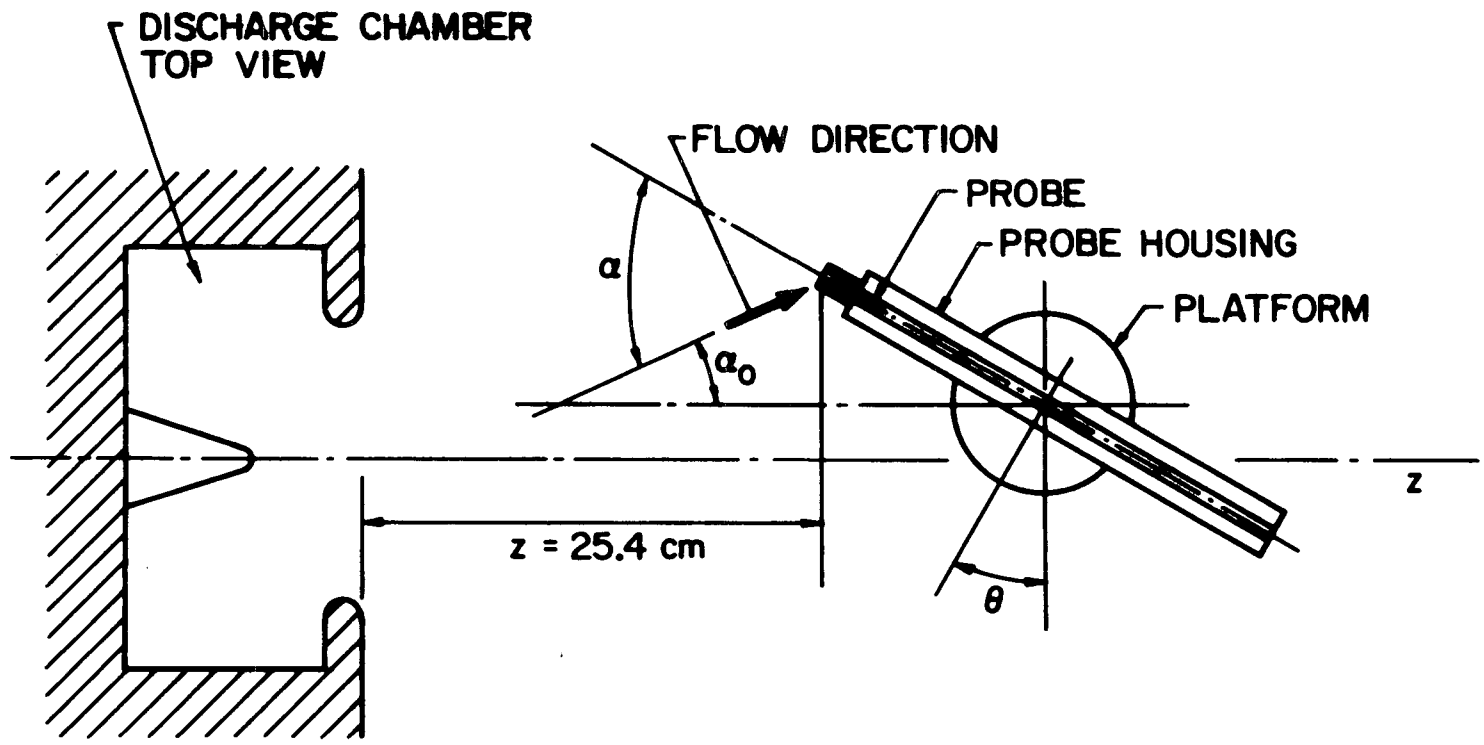

PRESSURE PROBE ARRANGEMENT, SCHEMATIC

FIGURE 21
AP25·4927

was maintained on the horizontal plane through the accelerator centerline for the present experiments, the tangential component was horizontal, i.e. it had only 2 possible directions depending on whether the angle of flow incidence on the probe (α) was positive or negative. Separate calibration studies using the Hertzian impact of a small steel ball on the probe tip show that the probe response due to equal and opposite tangential forces is also equal and opposite. Furthermore, the tangential force excites transient vibrations in the probe which are of much lower frequency than the longitudinal oscillation so that over the 1 msec discharge period, the effect of the tangential force is to shift the baseline of the oscillogram trace such that the probe response with respect to the shifted baseline is entirely due to the normal component of the force. In other words, approximately 0.05 msec after discharge termination the probe response due to the normal force falls to zero while the response R_3 due to only the transverse force persists and reaches a maximum in about 1.5 msec. The magnitude of this response R_3 at 0.05 msec after discharge termination is approximately the same level as just before it and can therefore be accounted for as the mentioned baseline shift.

Consequently, in order to determine the normal component of the force, the following procedure was used (refer to the oscillograms and their schematic representations in Fig. 22): Using a 0.75 msec current pulse (Fig. 22a) the baseline shift (R_3) was measured at 0.81 msec after current pulse initiation. Then, using a 1 msec pulse (Fig. 22b) the total signal (R_1) was measured at 0.81 msec at the same location and probe orientation. From these two values, the net signal (R_4) due to the normal component of force at 0.81 ms was obtained.

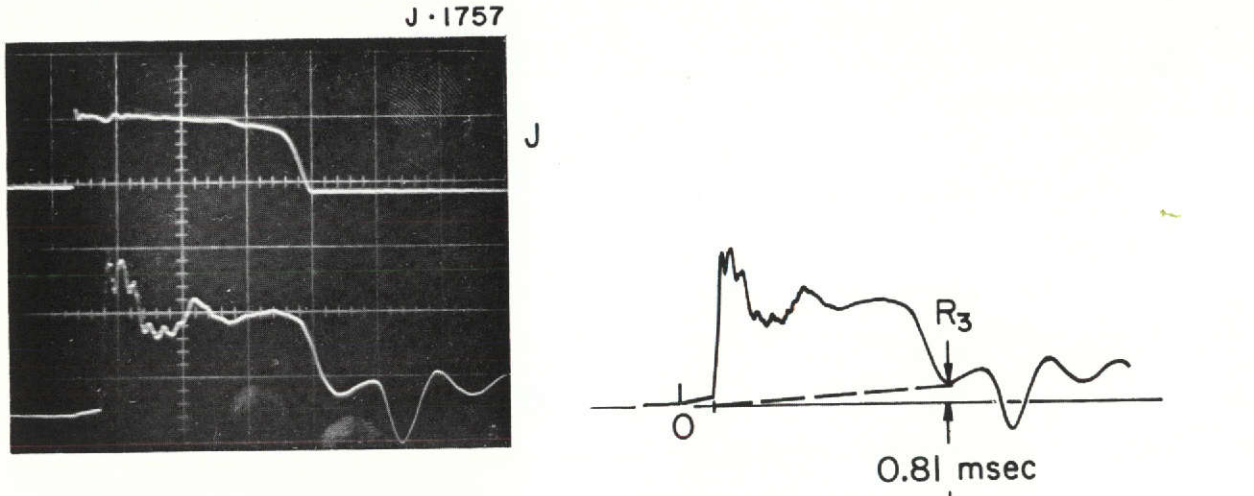

a) 0.75 msec CURRENT PULSE

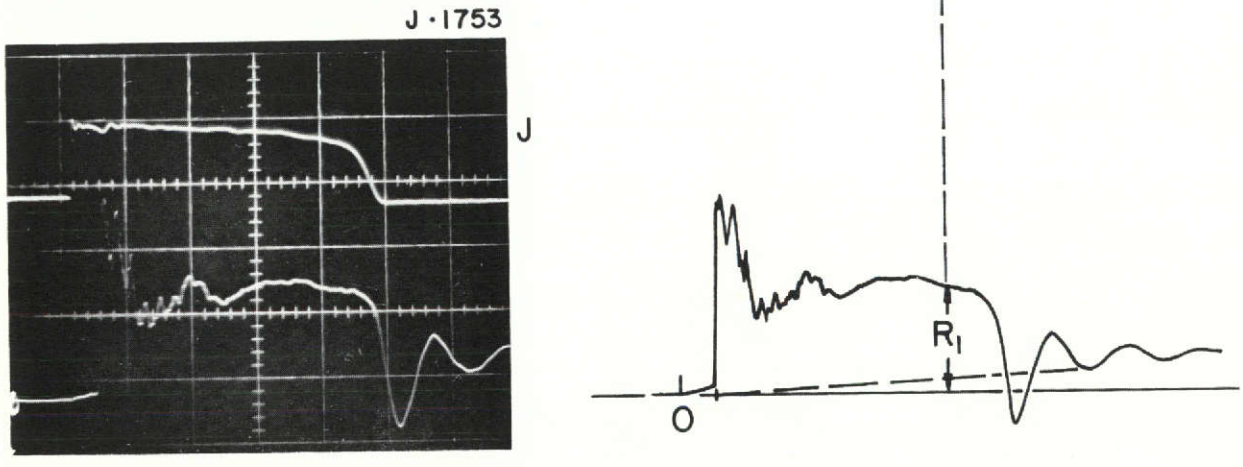

b) 1.0 msec CURRENT PULSE

PROBE RESPONSE WITH TRANSVERSE FORCE

FIGURE 22
AP25·P·508

The purpose of the present experiment was to determine the dependence of the probe normal force on the angle of flow incidence. Profiles of probe signals (R_1 and R_3) were taken at Z = 25.4 cm with three different fixed orientations of the probe of $\theta = 0^\circ$, + 10°, +20°. (Larger probe angle settings were not possible in the 90-cm-dia vacuum tank.) The signal (R_4) due to the normal force was calculated in each case as described above. The true angle of flow incidence to the probe, α, was given at each position by

$$\alpha = \alpha_o(r) + \theta \tag{3}$$

where $\alpha_o(r)$ is the flow angle with respect to the accelerator centerline, as determined from a biased double probe,[131,138] and θ is the fixed probe angle with respect to the accelerator centerline (see Fig. 21). Thus, for each location of the probe tip, the variation of the probe normal force over a 20° range of incident flow angle is recorded.

Results

A typical profile of the normal component of force has been plotted in Fig. 23a for a probe inclination of $\theta = 0^\circ$ and radial locations out to 20 cm. For comparison, Fig. 23b shows the previously measured flow angles for the same axial station. Although the size of the probe and vacuum tank precludes determining the yaw sensitivity for a continuously changing incidence angle at a given position, data from Fig. 23a and similar profiles at probe inclinations of 10° and 20° may be patched together to obtain a nondimensional variation of R_4 with α in the range of 0° to 40°. The resulting probe angular response is shown in Fig. 24. This plot shows that the response of the probe is relatively insensitive to flow incidence angle up to angles of 30°. For

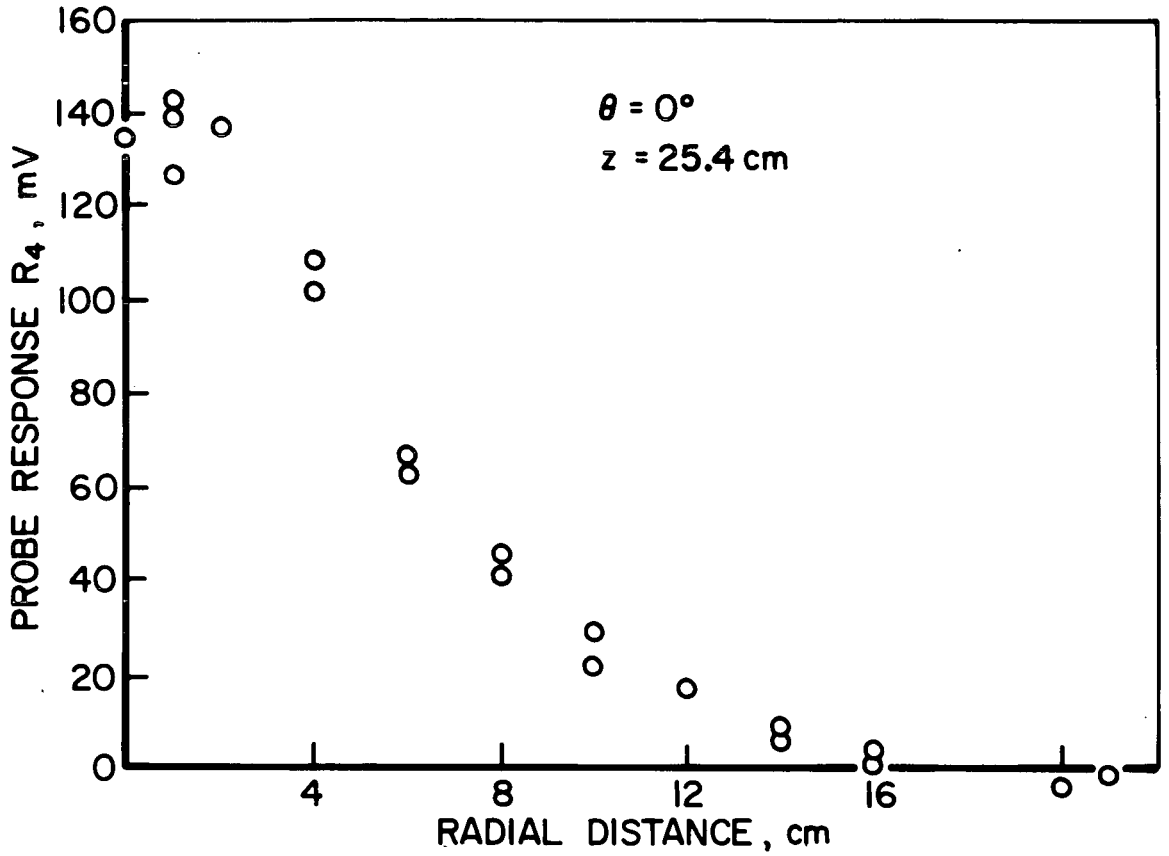

a) PROBE RESPONSE TO NORMAL STRESS

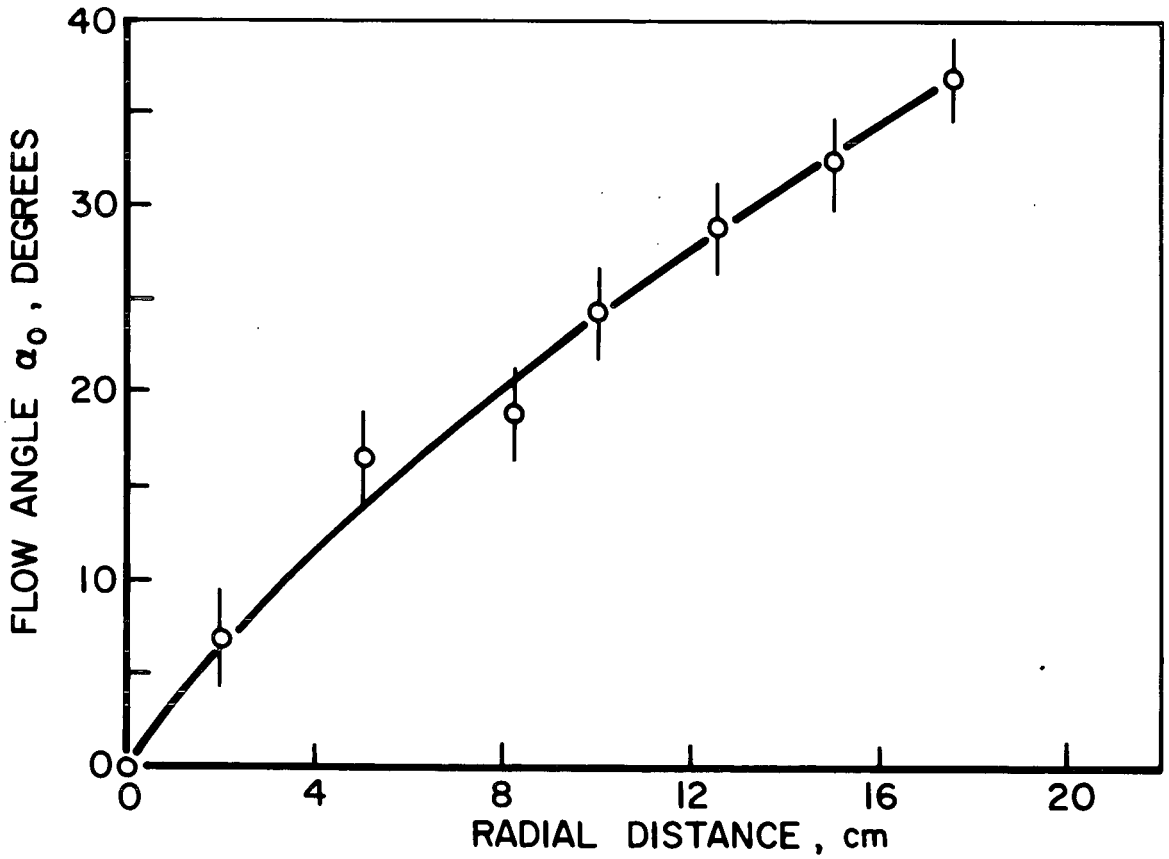

b) MEASURED FLOW ANGLE

FIGURE 23
AP25·4926

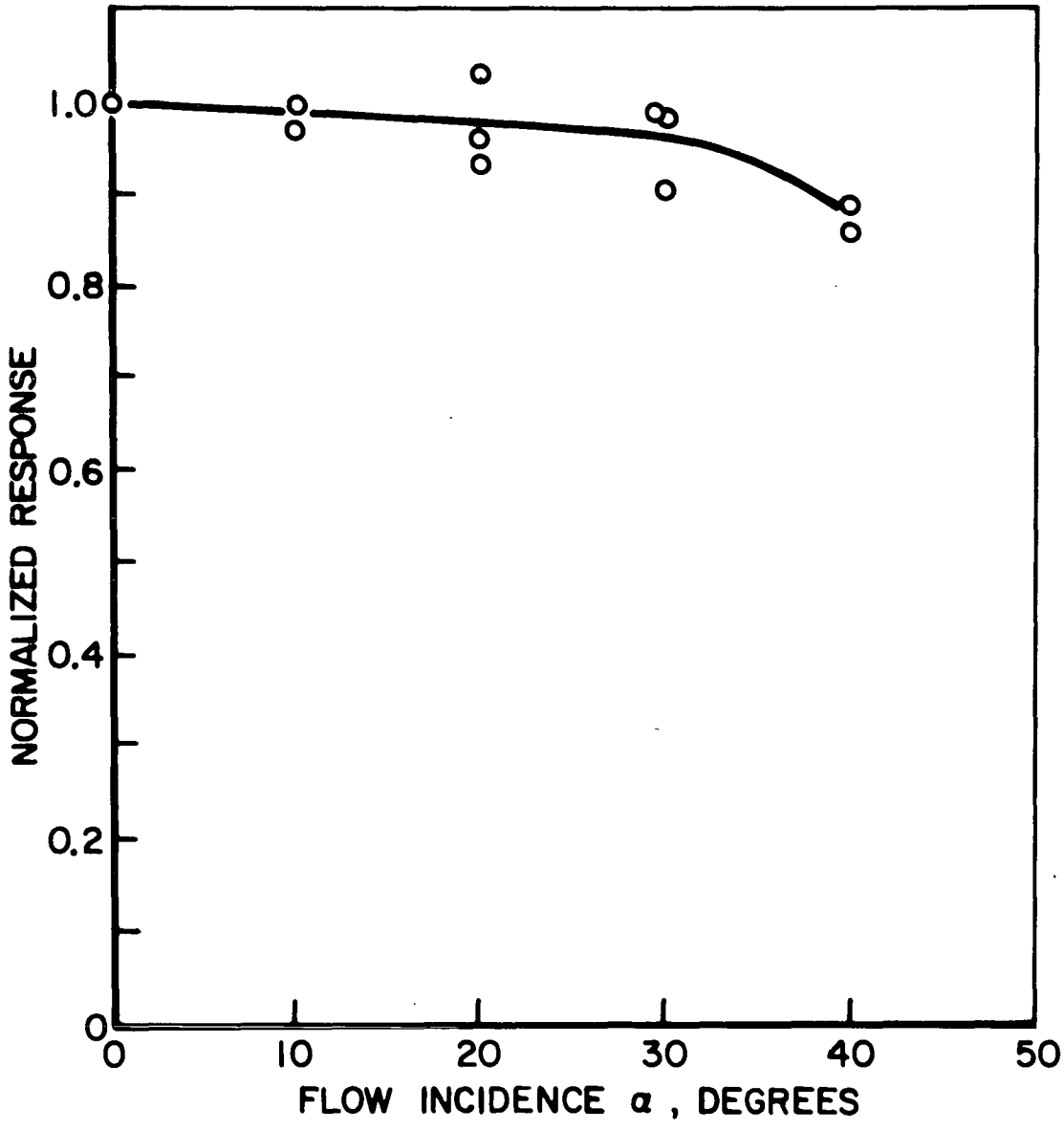

YAW CORRECTION

FIGURE 24
AP25·4928

larger angles, the response appears to decrease rapidly. This result is in reasonable agreement with plots of the effect of yaw on various impact pressure probes in a wide range of ambient flow conditions.[A-6]

Conclusions

By accounting for the effect of the transverse component of force, it is possible to determine the piezoelectric pressure probe response to an arbitrarily directed flow. Additional data at large radii, where the probe signal is small but the contribution to integrated quantities is large, are necessary to complete the yaw sensitivity correction. Future experiments will provide this information as well as measure the ratio of static pressure to total pressure.

III. THE HOLLOW CATHODE DISCHARGE (Krishnan)

Hollow cathodes were first used to advantage in spectroscopic studies where they were shown to be capable of simultaneously providing high electron number density and relatively low temperature ions and neutrals in the essentially field-free cathode cavity.[A-7] More recently, hollow cathodes have been used in ion engines where they exhibit a lower specific heating power and longer lifetime than previously used oxide coated or liquid mercury cathodes.[A-8] However, only few detailed analyses of the physical processes inside the hollow cathode have been attempted,[A-9] and the scaling parameters and laws for hollow cathodes have not yet been developed.

The objectives of the experimental hollow cathode research in this laboratory are: 1) to determine whether hollow cathode operation can be achieved in the multi-megawatt MPD discharge, 2) to compare the characteristics of this operation to those of the ion engine hollow cathode, 3) to examine whether the same advantages for hollow cathode operation in ion engines (most notably increased efficiency, decreased erosion, and stable operation) prevail for the MPD accelerator with a hollow cathode, 4) to determine the scaling laws for characteristic hollow cathode operation in order to bridge the gap between the high current MPD arcs and the important low current regime of the ion engine, and 5) to provide, wherever possible, direct support for the ion engine hollow cathode program.

Throughout this program, diagnostic probing directly within the cavity will provide a detailed account of the current and potential distributions as well as the thermodynamic state of the propellant. This probing is possible because of the larger diameter cathode required for the high power MPD discharge. The hollow cathode used in the present investigations

(diameter of 1.27 cm) is large enough to permit access into the cavity for optical observations and diagnostic probes while maintaining good resolution and minimal perturbation of the cavity plasma.

Description and Calibration of Apparatus

A schematic of the apparatus is shown in Fig. 25. Argon propellant is injected into the discharge chamber through a solenoid valve to six injection ports and also through the hollow cathode orifice. These orifices are arranged symmetrically at a radius of 25.4 mm from the centerline of the discharge chamber. The mass flow rate is determined by the reservoir pressure and the total area of the seven injector orifices. (The precise control of the mass flow by varying this area is discussed in detail later.) Power is supplied as an essentially rectangular current pulse from a 936-μfd, high voltage capacitor bank. A typical trace of the current pulse is shown in Fig. 26a. The current is monitored by a Rogowski loop around the cathode lead and the terminal voltage of the discharge is measured with a Tektronix P-6013A voltage probe. Both are recorded by a Tektronix dual beam oscilloscope.

In addition to discharge voltage, discharge current and total mass flow, another parameter must be added for MPD arc operation with the hollow cathode - namely, the fraction of the total mass flow that passes through the cathode cavity. If the propellant flow chokes (Mach No. = 1) at the inlet orifices, then the total mass flow rate can be changed simply by varying the area of these orifices. Furthermore, the fractional division of the total flow through the hollow cathode cavity and the outer injectors can be controlled precisely by changing the relative areas of the orifices. (Previously the flow choked at the solenoid valve orifice and hence the supersonic flow entering the discharge chamber orifices could not be accurately divided into "outside" and

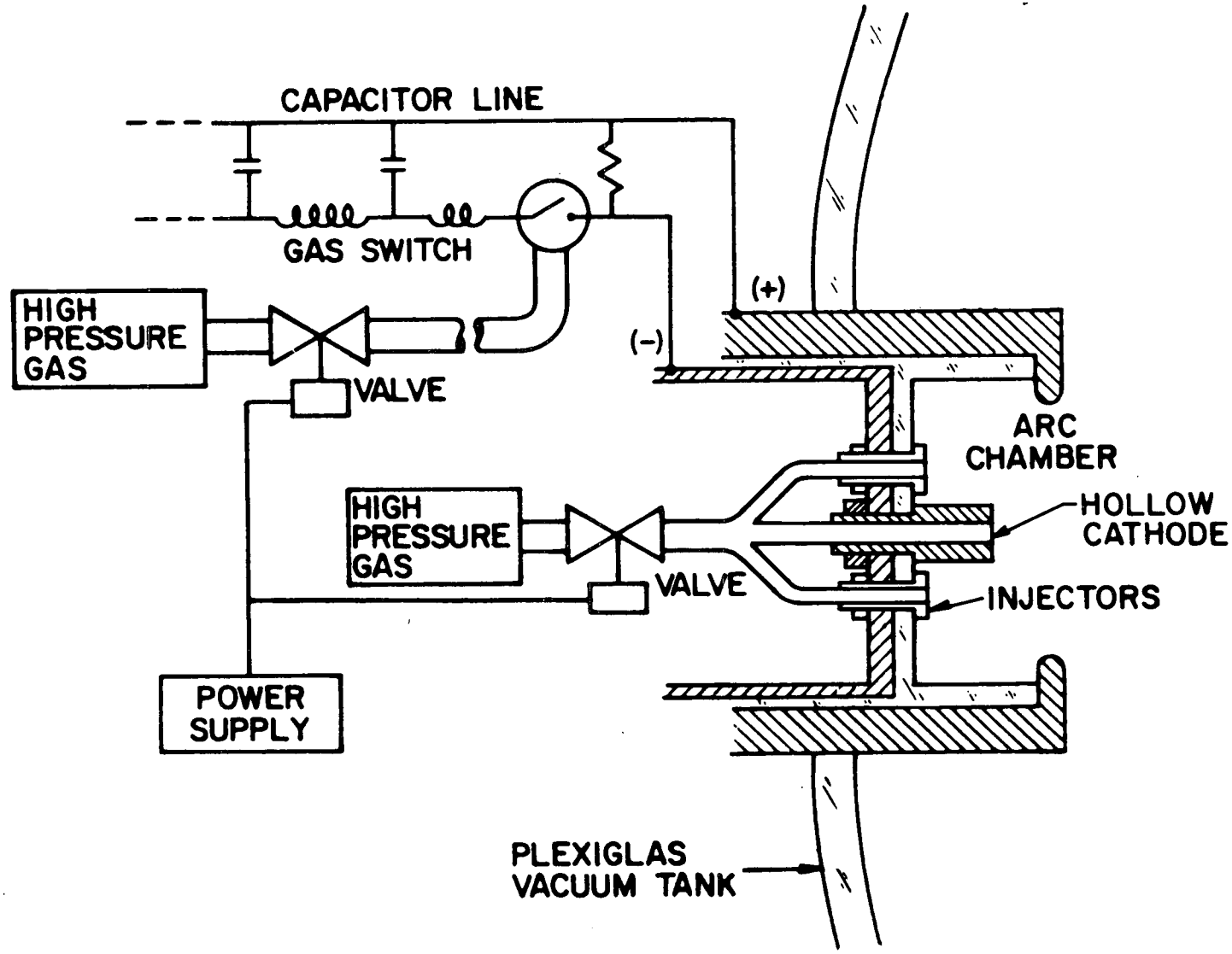

HOLLOW CATHODE EXPERIMENTAL CONFIGURATION

FIGURE 25
AP25-4681

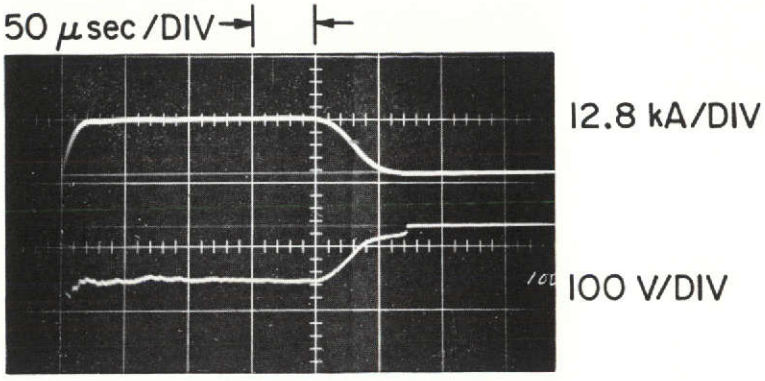

a) DISCHARGE CURRENT AND VOLTAGE

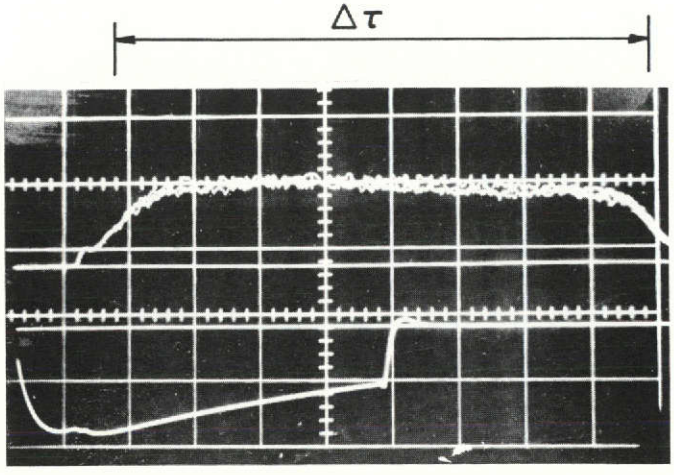

b) MILLITORR GAUGE SIGNAL

MILLITORR GAUGE RESPONSE

FIGURE 26
AP 25·P·509

"inside" flow.) Several injector plugs were then fabricated such that 5, 10, 25, 50, 75 or 100% of the total flow can be injected through the hollow cathode. The largest total area of the orifices is restricted to 16 mm^2 or about 30% of the 50 mm^2 valve orifice area to ensure that the choking of the propellant flow occurs at the injector orifices.

The calibration of this mass flow system proceeded in the following three steps:

Step A: The hollow cathode cavity was plugged and the 6 outer injectors, of total area 16 mm^2, were installed. The vacuum tank was separated from the vacuum pump by closing a valve, and the solenoid valve was activated by a rectangular current pulse from a Hewlett Packard pulse generator. For a given reservoir pressure the density-time history inside the discharge chamber was monitored by a Varian Millitorr (T.M.) fast ionization gauge. The ion gauge signal and valve current for a typical flow test without discharge are shown in Fig. 26b. The pressure in the vacuum tank before and after the current pulse was measured with a McLeod gauge. For successively increasing pulse lengths from the pulse generator the pressure rise per pulse Δp in the tank and the half width $\Delta\tau$ of the millitorr gauge response were measured each time. A plot of Δp against $\Delta\tau$ reveals a linear relationship, as expected, the slope of which is the mass flow for the given reservoir pressure. This procedure was then repeated at several other reservoir pressures. A graph of the mass flow $\dot{m}$ versus the reservoir pressure is shown as line A in Fig. 27.

Step B: Two of the six injector plugs were then blanked off and the procedure outlined in step A was repeated. Another straight line, line B, of reservoir pressure versus argon mass flow rate was obtained (Fig. 27). The slope of this graph is 67% of the slope of the graph produced in step A. The total

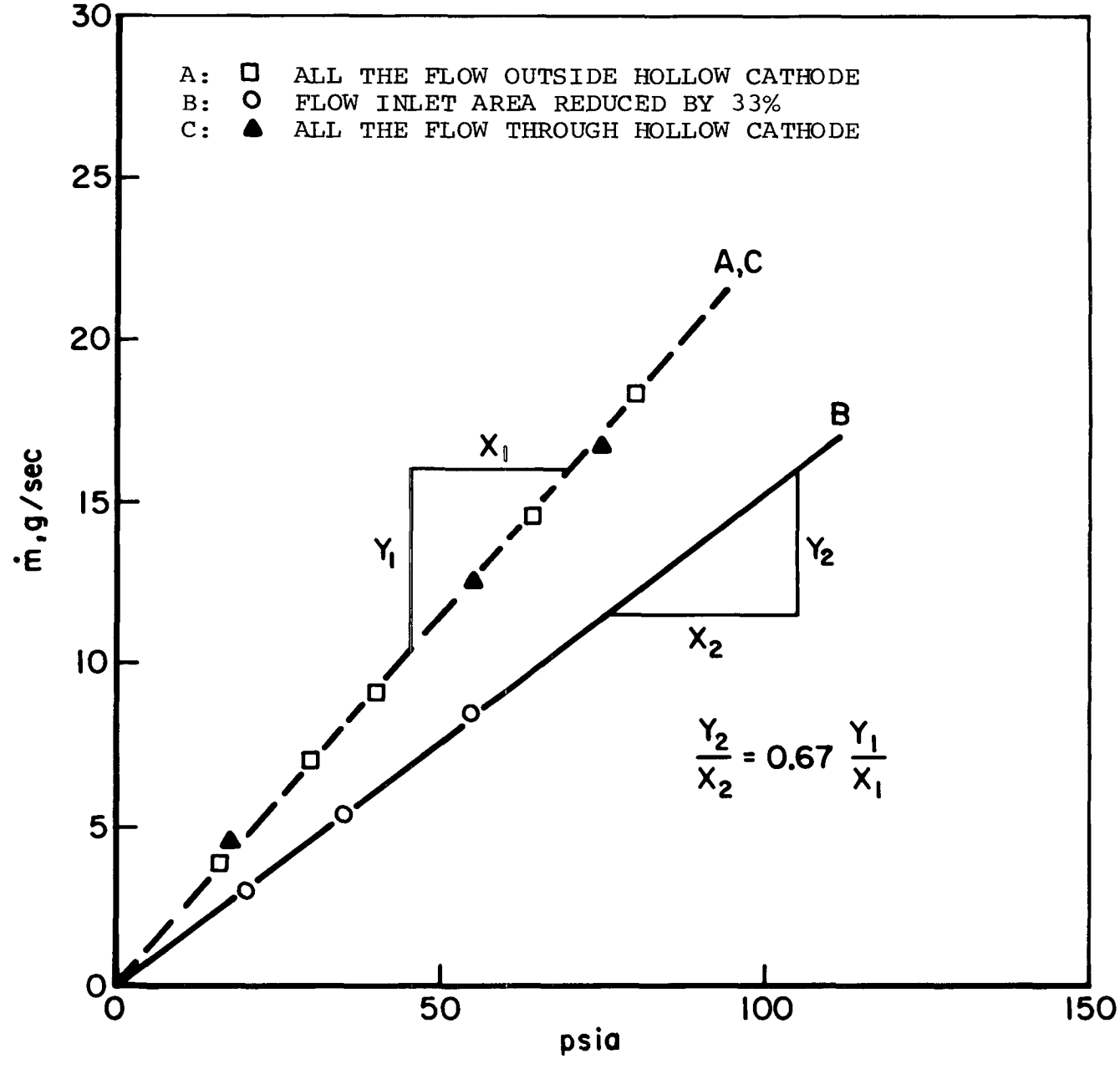

MASS FLOW CALIBRATION

FIGURE 27
AP25·4929

cross sectional area of four injectors used in step B is also 67% of the total area of the six injectors of step A, verifying that the cold gas flow indeed chokes at the inlet orifices to the discharge chamber. As further corroboration, the Skinner valve catalog flow chart was used to compute a choked argon mass flow of 17 g/sec through the 0.795-cm-dia valve orifice for a reservoir pressure of 1.8×10^5 N/m^2. The experimental calibration, however, shows an argon mass flow of 6 g/sec at this pressure proving that the flow through the valve orifice indeed occurs at a Mach number much smaller than unity.

Step C: The outer six injectors were sealed off and a single 16 mm^2 orifice was inserted coaxially into the hollow cathode about 10 mm behind the plane of the discharge chamber backwall insulator. In this configuration all the gas enters the hollow cathode cavity through an area equal to the total area of the six outer injectors used in step A. The calibration technique of step A was repeated and a straight line dependence of the reservoir pressure on argon mass flow rate was found (Fig. 27, line C). Line C for all the flow through the cathode is seen to be identical (within the margin of the error bars) to line A for the entire flow through the outer six injectors. Thus, the choked mass flow rate is proportional to reservoir pressure and the total area of the injector orifices and is insensitive to fractional divisions of that area. The only constraint is that the total area must be less than or equal to 16 mm^2 to produce a choked flow over the given range of reservoir pressures.

Experimental

1) Flow both inside and outside the hollow cathode

With the entire 6 g/sec argon mass flow through the outer six injectors the current to the discharge was varied from 5 kA to 20 kA while monitoring the discharge voltage to obtain

the voltage-current characteristic (a) shown in Fig.28. Then the mass flow rate was reduced to 3 g/sec (still all outside flow) to obtain the voltage-current characteristic (b) in Fig. 28. The voltage at a given current is observed to be higher for the lower mass flow rate consistent with previous results obtained with a conical solid tungsten cathode. However, the voltages are lower than those with a solid conical cathode discharge at the same mass flow which are shown for comparison at $\dot{m}$ = 6 g/sec as a dashed line (c) in Fig. 28. Thus, by changing only the configuration of the cathode in an MPD discharge, significant changes in the voltage-current characteristic are produced.

Next, the injectors were arranged to permit a total $\dot{m}$ of 12 g/sec of argon flow with 6 g/sec through the hollow cathode and 6 g/sec outside flow. For this total mass flow of 12 g/sec, voltage-current characteristic (d) was recorded (Fig. 28). Another characteristic, total mass flow of 6 g/sec with 3 g/sec through the cathode and 3 g/sec on the outside, is shown as line (e) in Fig. 28. It is remarkable that the $\dot{m}$ = 12 g/sec V-J characteristic (d) with 6 g/sec flow through the cathode and 6 g/sec outside flow is identical to the $\dot{m}$ = 6 g/sec characteristic (a) with all the flow outside and similarly that the $\dot{m}$ = 6 g/sec characteristic (e) with 3 g/sec flow through the cathode is also identical to the $\dot{m}$ = 3 g/sec characteristic (b) with all outside flow. The conclusion is that for the relatively high flow rates of 6 g/sec and 3 g/sec through the cathode, the participation of the cavity in the discharge is not manifest on the V-J characteristics. This is further supported by a photograph of the discharge at $\dot{m}$ = 12 g/sec through a 4880 Å narrow bandpass filter shown in Fig. 29 (b). The luminous regions of the discharge are all seen to be outside the hollow cathode cavity, while the cavity itself appears quite dark.

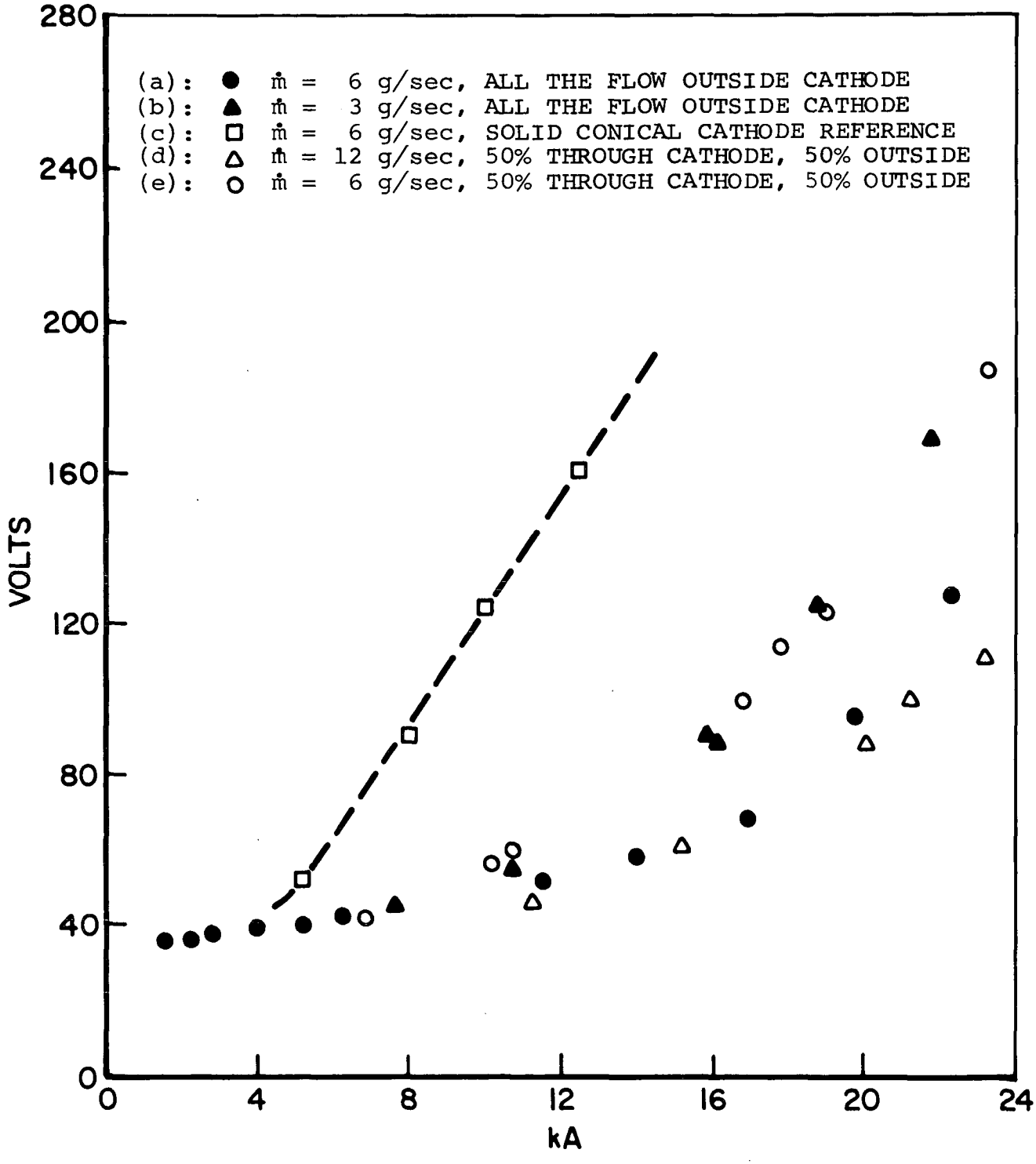

TUNGSTEN HOLLOW CATHODE CHARACTERISTICS

FIGURE 28
AP25-4930

FRONT VIEW

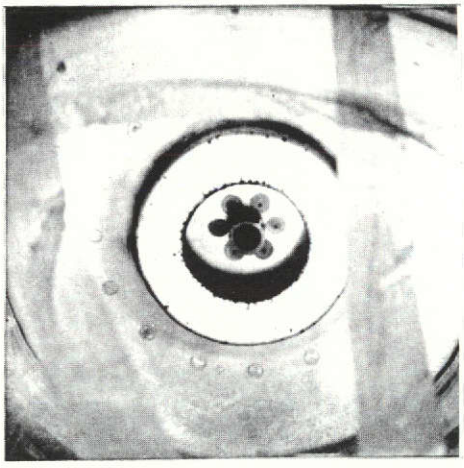

a) CHAMBER

$\dot{m}$ = 12 g/sec
50 % HC FLOW
50 % OUTER FLOW

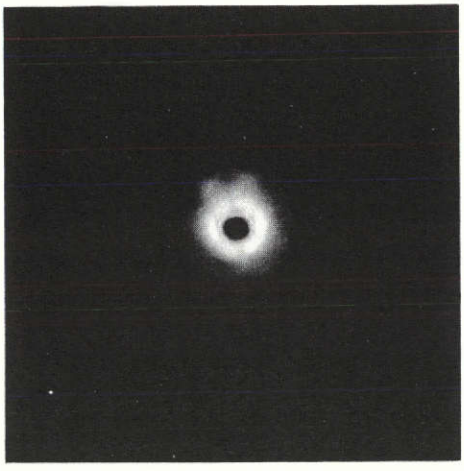

b) DISCHARGE @ 16 kA

DISCHARGE THROUGH 4880 Å AII FILTER

FIGURE 29
AP 25·P·510

This suggests the possibility that the 6 g/sec flowing through the hollow cathode may not ionize and possibly passes right through the cathode cavity as neutral argon. The outer flow of 6 g/sec of argon is ionized, as evidenced by its luminosity in the photograph, and determines the electrical properties of the discharge.

2) Flow solely through the hollow cathode

Since the above experiments suggested that current was not attaching inside the hollow cathode when flow was equally divided between the inside and outside of the cathode, the outside flow was cut off altogether. Spectral photographs (4880 Å) of the discharge at 11, 18 and 26 kA and a 6 g/sec flow entirely through the cathode are shown in Fig. 30. Figure 30a shows the view of the discharge chamber used for the photographs in Fig. 30b) and c), while Fig. 30d) shows the arrangement for the photograph in Fig. 30e).

The hollow cathode cavity appears as a dark region at 11 kA in Fig. 30b and at 18 kA in Fig. 30c and all the luminosity of the discharge is observed principally beyond the cavity orifice. The photograph of the discharge at 26 kA in Fig. 30e) still shows the dark cavity but the luminosity now emanates from a "pinched" region of the discharge in front of the cathode. Thus, although increasing the discharge current to 26 kA has the effect of "pinching" the discharge to smaller radii, the gasdynamic pressure of the flow in the cavity may still be too high to allow current penetration into the cavity. Similar results were obtained when the injected hollow cathode flow was reduced to 2 g/sec.

The next phase of the experiment may be introduced by the following qualitative examination of the dynamics of the hollow cathode cavity flow for the case where the current attaches to both the inside and outside of the cavity.

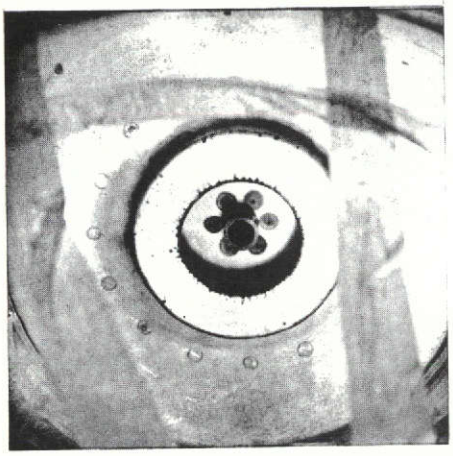

a) FRONT VIEW

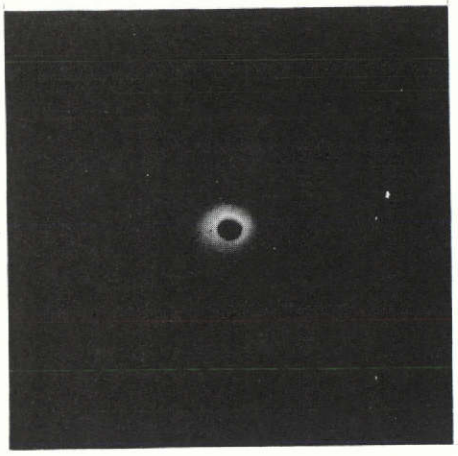

4880 Å FILTER

b) 11 kA

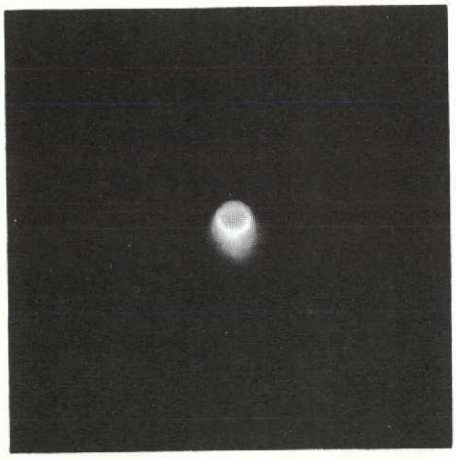

4880 Å FILTER

c) 18 kA

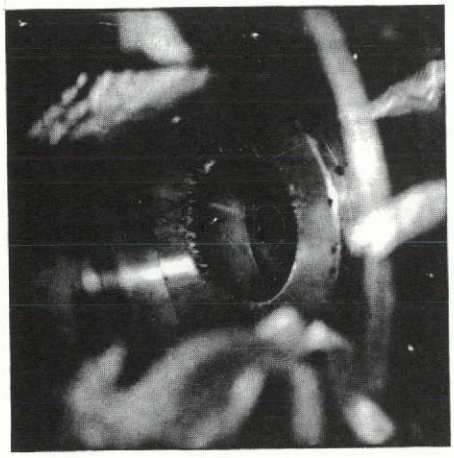

d) SIDE VIEW

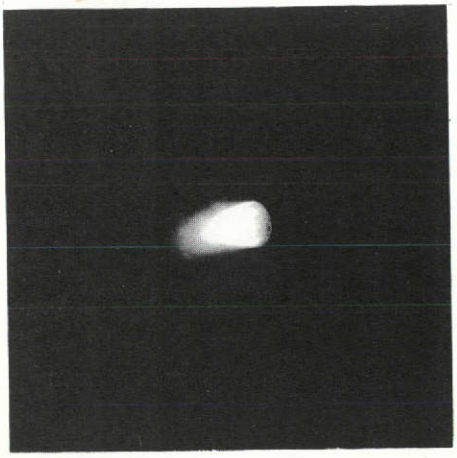

4880 Å FILTER

e) 26 kA

DISCHARGE AT 6 g/sec ARGON FLOW
(100 % HC FLOW)

FIGURE 30
AP 25·P·511

Figure 31 shows an assumed current pattern for the hollow cathode. The electromagnetic $\vec{j} \times \vec{B}$ interaction produces a radial "pumping' force, $f_z = - j_z B_\theta$, and an axial "blowing" force, $f_z = - j_r B_\theta$, inside the hollow cathode. The fact that inside the cavity the magnetic pressure $(B_\theta^2/2\mu_o)$ acts in an upstream direction opposing the downstream gas flow suggests the requirement of a dynamical balance between these two opposing pressures. Thus, it might be speculated that at the relatively high argon mass flow rates of 6 g/sec and 2 g/sec the gasdynamic pressure is high enough to blow the discharge out of the cavity (see Appendix). To test this simple model the mass flow rate in the hollow cathode was reduced by a large factor to 0.30 g/sec and the discharge current was increased to 29 kA. Figures 32b and 32d show, in frontal and side views respectively, that there is now a bright luminosity emanating from inside the cavity orifice implying current attachment inside the hollow cathode.

Another set of spectral photographs heightens the comparison between a discharge at 12 kA and 6 g/sec inside flow with no luminosity inside the hollow cathode (Fig. 33a, b, and c) and a discharge at 29 kA and 0.3 g/sec inside flow with bright argon AII radiance emanating from the cavity (Fig. 33f). The photograph through the 5910 Å spectral filter in Fig. 33e) further illustrates that the radiance from the orifice in Fig. 33d) is not due to impurity radiation.

3) Hollow cathode discharge characteristics

Three voltage-current characteristics for 6 g/sec, 2 g/sec and 0.30 g/sec argon mass flow through the hollow cathode for currents between 10 kA and 30 kA are shown in Fig. 34. All three characteristics show abrupt changes in their slopes between 15 kA and 18 kA. If each characteristic is approximated by two straight lines shown in Fig. 34, then the slope ($\Delta V/\Delta J$) of each characteristic changes from about 25 mΩ (for $J < 15$ kA) to 3 mΩ (for $J > 18$ kA).

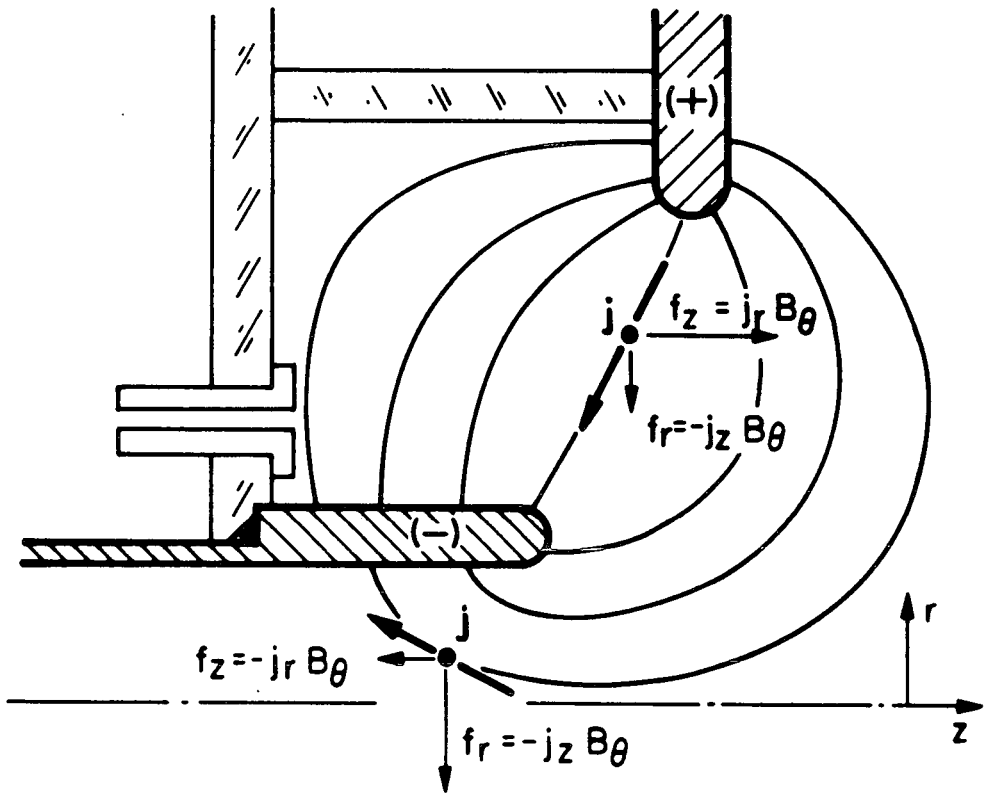

HOLLOW CATHODE CURRENT PATTERN

FIGURE 31
AP25·4798

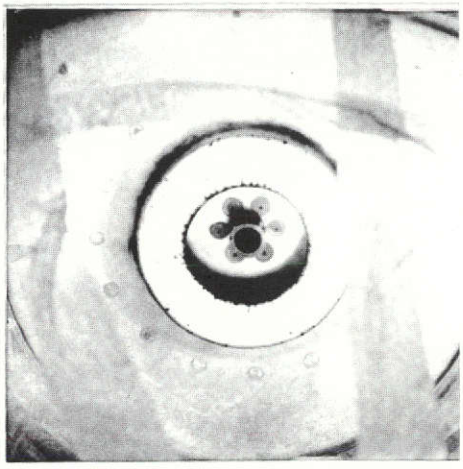

a) FRONT VIEW

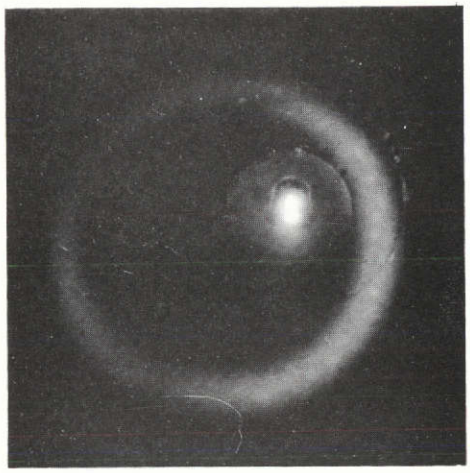

4880 Å FILTER

b) 29 kA

c) SIDE VIEW

4880 Å FILTER

d) 29 kA

DISCHARGE AT 0.3 g/sec ARGON FLOW
(100% HC FLOW)

FIGURE 32
AP 25·P·512

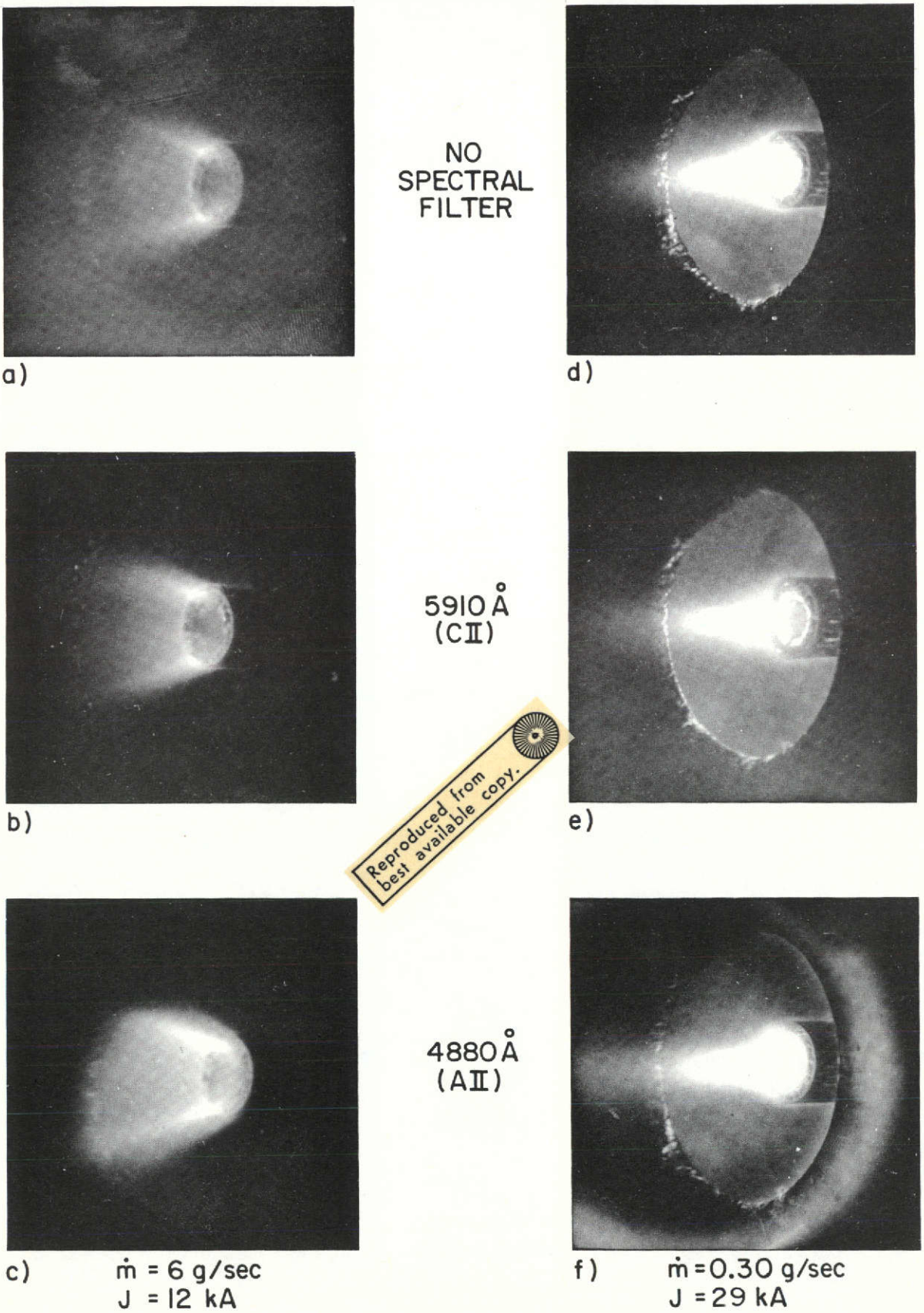

DISCHARGE WITH 100% HC FLOW

FIGURE 33
AP 25·P·513

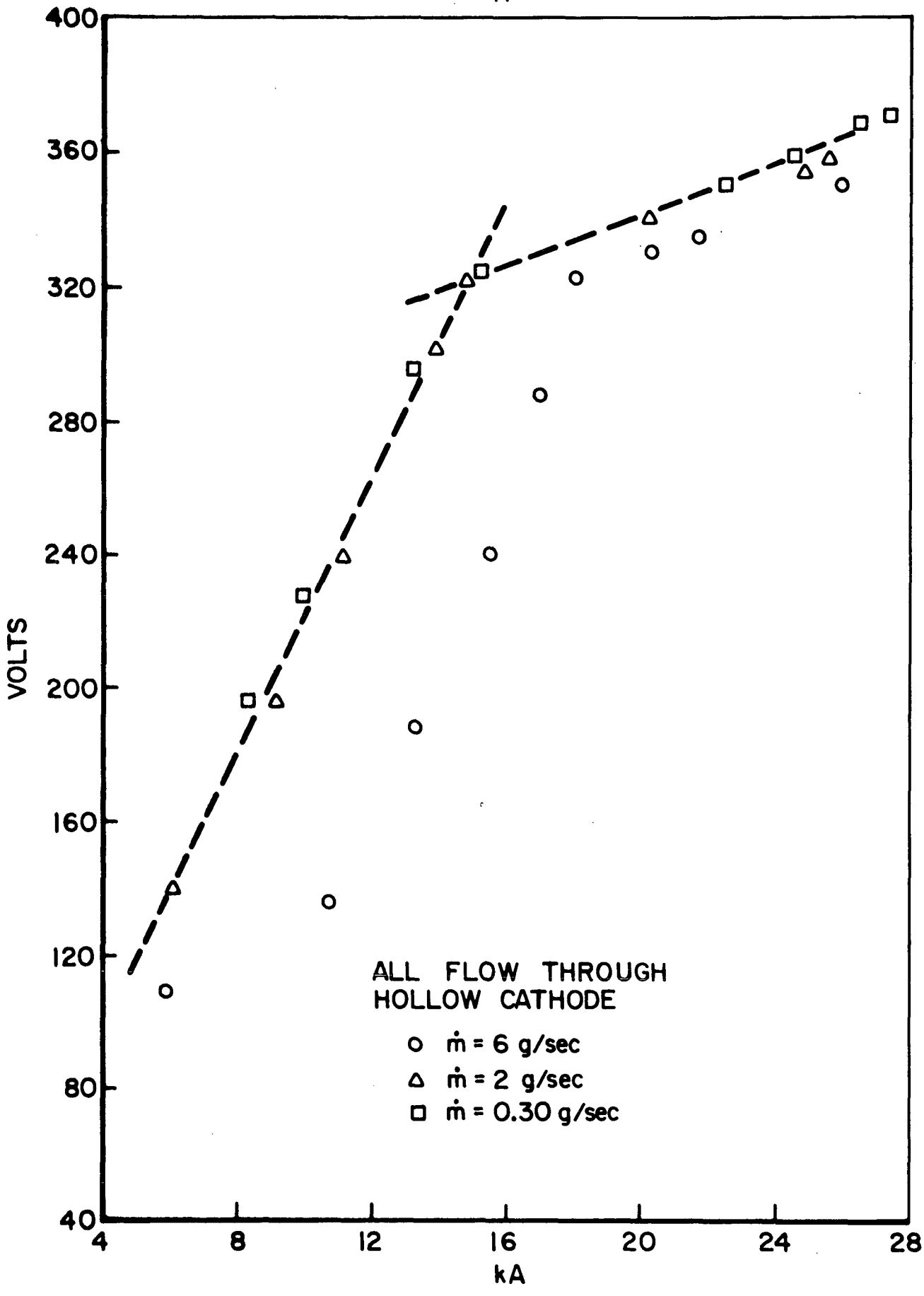

TUNGSTEN HOLLOW CATHODE CHARACTERISTICS

FIGURE 34
AP25·4931

Abrupt changes in the operating characteristics of low current hollow cathodes have been traced to the transition from a "plume" mode to a "spot" mode attachment as the current is increased. The relation between this transition, which is usually accompanied by an appreciable drop in discharge voltage, and the observed slope change in the voltage-current characteristic for the large hollow cathode is presently under investigation.

One of the significant experimental results is the demonstration of ionized argon AII radiance from the hollow cathode cavity at a low argon mass flow rate of 0.3 g/sec through the cathode at a relatively high current of 29 kA. The absence of such luminosity at a higher mass flow rate of 6 g/sec of argon and a lower current of 12 kA has also been demonstrated. These two modes of operation of the hollow cathode discharge may also be distinguished on the voltage-current characteristic which changes from a steep slope at low currents to a much smaller slope at high currents. The mapping of profiles of potential and current distributions with electrostatic and magnetic probes inside and about the hollow cathode, currently in progress, can be expected to yield detailed information regarding when "hollow cathode mode operation" is achieved.

Appendix

Earlier a qualitative argument was presented for a dynamical balance between gasdynamic and magnetic pressures inside the hollow cathode cavity. A simple quantitative determination is now presented.

An estimate of the gasdynamic pressure inside the cavity for any given mass flow rate can be obtained using the supersonic isentropic flow tables for argon ($\gamma = 1.67$) assuming an isentropic expansion of the cold gas flow from a Mach

number of one at the hollow cathode inlet to one corresponding to the cross sectional area of the cavity, which is thirteen times the choking area.

The one-dimensional momentum equation for the flow inside the hollow cathode cavity in the cirection z is:

$$\rho u \frac{du}{dz} + \frac{dp}{dz} = \frac{-B}{\mu_o} \frac{dB}{dz} \tag{4}$$

where ρ = density
u = velocity, and
p = pressure

A first integral of (4) is

$$(\rho u)u_o + p_o = (\rho u)u + p + \frac{B^2}{2\mu_o} \tag{5}$$

where subscript "o" refers to a point upstream in the hollow cathode cavity where no current and hence no magnetic pressure is assumed to exist and no subscript refers to conditions well downstream in the cavity near the front face of the cathode where the current density can be assumed to be uniform.

An average magnetic pressure over the area must be assumed to make the problem one-dimensional. For an assumed uniform current density over the hollow cathode cavity cross section, the magnetic field is axisymmetric and given by

$$B = \frac{\mu_o j r}{2} \tag{6}$$

The average magnetic pressure over the cross section is

defined by

$$\overline{\left(\frac{B^2}{2\mu_o}\right)} = \frac{1}{\pi r_c^2} \int_0^{r_c} \frac{B^2}{2\mu_o} \; 2\pi r \, dr \qquad (7)$$

where r_c is the radius of the hollow cathode cavity. Integration yields:

$$\overline{\left(\frac{B^2}{2\mu_o}\right)} = \frac{u_o \; j^2 r_c^2}{16} \qquad (8)$$

or in terms of total current

$$\overline{\left(\frac{B^2}{2\mu_o}\right)} = \frac{u_o \; J^2}{16 \pi^2 r_c^2} \qquad (9)$$

At a current level of 12 kA, with all of the current assumed to attach inside the hollow cathode cavity, the average magnetic pressure is

$$\overline{\left(\frac{B^2}{2\mu_o}\right)} = 3 \times 10^4 \text{ N/m}^2$$

The left hand side of equation (5) is equal to the total pressure of the cold flow entering the hollow cathode cavity and for a mass flow rate of 0.3 g/sec it is known to be 8800 N/m^2. Thus, equation (5) reads:

$$8800 \text{ N/m}^2 = (\rho u) \; u + p + 30{,}000 \text{ N/m}^2 \qquad (10)$$

This equation is balanced only if there is flow of gas in the upstream direction during the discharge. Since no effects of such an upstream flow have been observed (heating

of the injector orifice and burning of the tygon feed tube to the hollow cathode) we must conclude that not all the current attaches inside the hollow cavity. How much current is carried by the hollow cathode can be determined by magnetic probes in the cavity.

The preceding analysis exhibits the role that the mass flow and gasdynamic pressure play in initiating and subsequently sustaining a hollow cathode discharge in this configuration. Preliminary calculations show that probably not all the current is carried by the hollow cathode cavity. Further diagnostic probing of the potential and current distribution in the discharge will shed more light on this problem.

IV. PLASMADYNAMIC LASER STUDIES

IV-A. Photoelectric Measurements of Radiance Profiles and Optical Depth (Hixon)

Time-resolved photoelectric spectroscopic studies of the MPD arc jet with the boron nitride (BN) backplate insulator (containing six injector ports) were undertaken to 1) record radial and axial intensity profiles for various species in the discharge, and 2) measure the optical depth of the discharge plasma for certain transitions.

The equipment employed consisted of a Bausch & Lomb grating monochromator and an RCA 1P28 photomultiplier tube shown in Fig. 35. The monochromator has a linear dispersion of 16 Å/mm. It was calibrated with a mercury lamp, and its wavelength settings were found to be reproducible to ± 2 Å with 60% confidence. An entrance slit width of 200μ and an exit slit width of 500μ were chosen so that 1) the exit slit would be much larger than the entrance slit, and 2) the photomultiplier would see an 8 Å spectral interval, large enough to contain a given line and its wings even if the line center were mislocated by 2 Å.

The discharge was imaged on the monochromator entrance slit through a 42 cm focal length f/6 quartz lens and a first surface plane mirror as shown in Fig. 35. The entrance slit was masked in such a way that radiance from a region 1 cm high and 0.8 mm wide in the discharge was permitted to enter the monochromator. Different positions in the discharge were viewed by realignment of the lens and mirror and by movement of the entire apparatus. For initial work, the optics were aligned at $Z = 2.5$ cm, $R = 0.0$ cm.

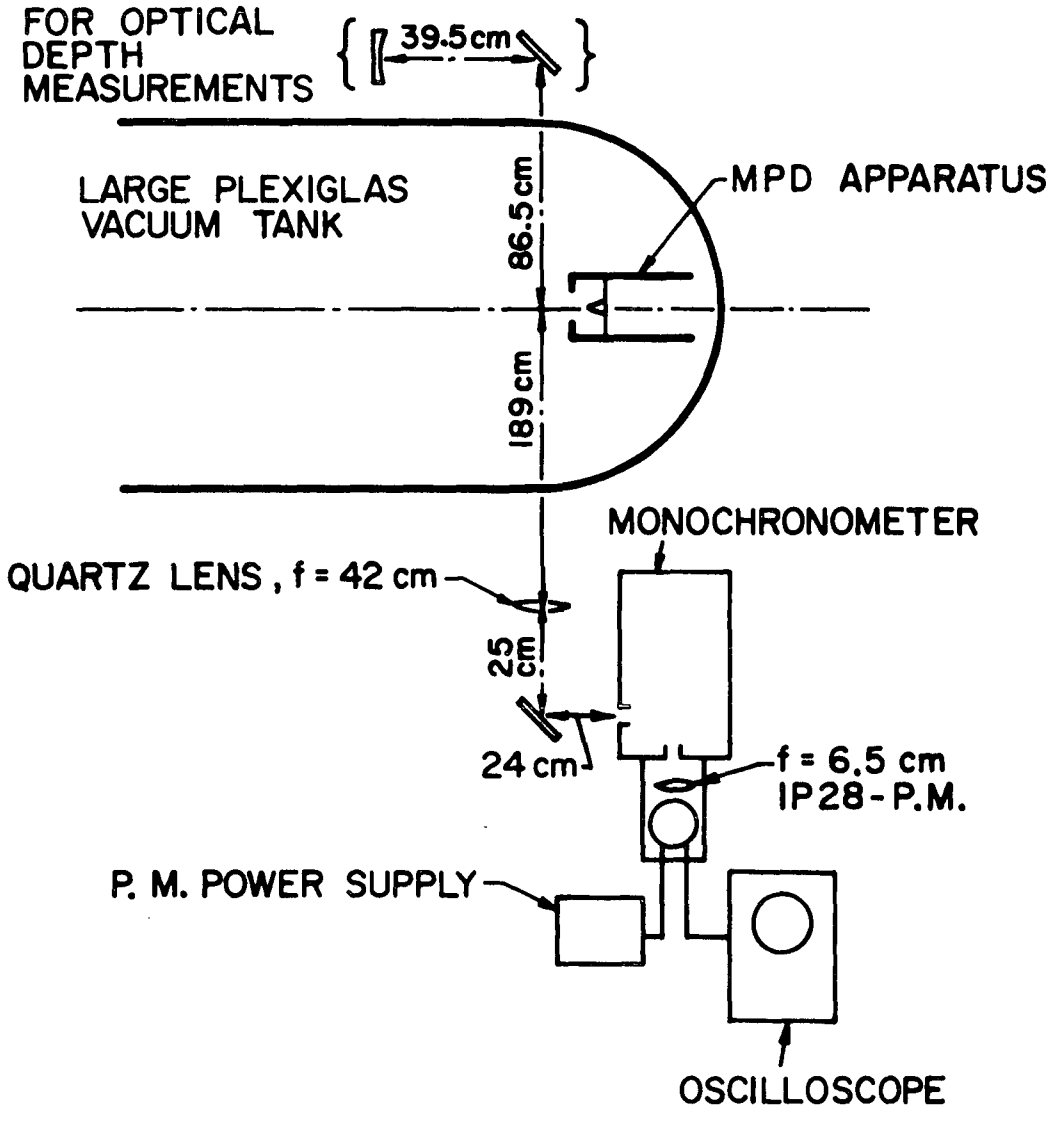

PHOTOELECTRIC STUDIES

FIGURE 35
AP25·4922

The 1P28 photomultiplier circuitry involves a load resistor R_L which was chosen as 1.8 MΩ which, together with the parallel 1.0 MΩ scope impedance and an estimated stray capacitance of 10^{-11} F yielded a time constant RC = 7 μsec. This limits the decay time of the signal and not the rise time. The value $R_L C = 7$ μsec employed in this study is still small compared to the 1000 μsec scale of the discharge duration. The present study was conducted at photomultiplier operating conditions such that a signal to noise ratio > 100 always prevailed.

It was determined that the J = 16 kA, $\dot{m}$ = 32 g/sec condition gave the maximum value of $J^2/\dot{m}$ (8 $kA^2 \cdot sec/g$) which allowed 1) a flat voltage trace, 2) a voltage trace free of noise, and 3) a quasi-steady AII PM trace. For this nominal condition, the axial and radial species surveys were undertaken. The interesting species are AI, AII, AIII, BII, NII, and continuum radiation. The discharge radiation is largely AII radiation, and a strong, isolated AII line at 4806 Å was selected as the standard line for AII measurements. AII traces showed excellent shot-to-shot reproducibility. Spectrograms of the BN arcjet discharge[143] were used for guidance in selecting a vacant region of the spectrum for continuum measurements. Since they show no line radiation between 4823 and 4843 Å, an 8 Å spectral region centered at 4833 Å was chosen to sample the continuum.

In order to verify that continuum radiation was being recorded, two tests were devised. One, called the "linearity test", consisted of plotting signal voltage against spectral region size. If the radiance being recorded was distributed in a continuous fashion, the plot should be linear. If it is line radiation, it should be quite nonlinear. A second, the "side-stepping test," tested for continuous radiation by measuring the radiance at increasing wavelength intervals from the line center and looking for a

drastic reduction. Both of these tests depend on the condition that the exit slit be much larger than the entrance slit. The entrance slit was set at 200μ. The exit slit setting was 500μ or more. The 8 Å spectral region centered at 4833 Å was verified by both of the tests to be continuum.

Searches for the particular spectral lines were conducted in a similar manner. The AIII lines at 3336 Å, 3344 Å, and 3285 Å, each of which is prominent on spectrograms taken of the MPD arc with a Plexiglas backwall in the discharge chamber,[143] were determined by linearity or side-stepping tests to be not visible relative to the continuum background. The NII line at 4631 Å which was previously recorded in the discharge chamber could not be identified since the measurement showed no significant decrease in radiance when subjected to the side-stepping test. One may conclude that the line radiation at 4631 Å is not significant relative to the continuum background. It should be remembered that the photomultiplier optics look across the exhaust plume centerline 2.5 cm downstream of the anode face and a small NII density, visible in the chamber, might be quite invisible further downstream. A BII line previously recorded at 3451 Å was also not present. As a control, the strong AII lines at 3491 Å and 4806 Å were also subjected to the linearity and side-stepping tests; they were quite easy to identify as line and not continuum sources.

Using only the 4806 Å AII line and the continuum at 4833 Å, the radial and axial surveys of radiance were undertaken and the results are presented in Figs. 36 and 37. The expected functional form for the argon line radiance is given by:

$$I_{AII} \sim n_i \; e^{-E/kT_e} \qquad (11)$$

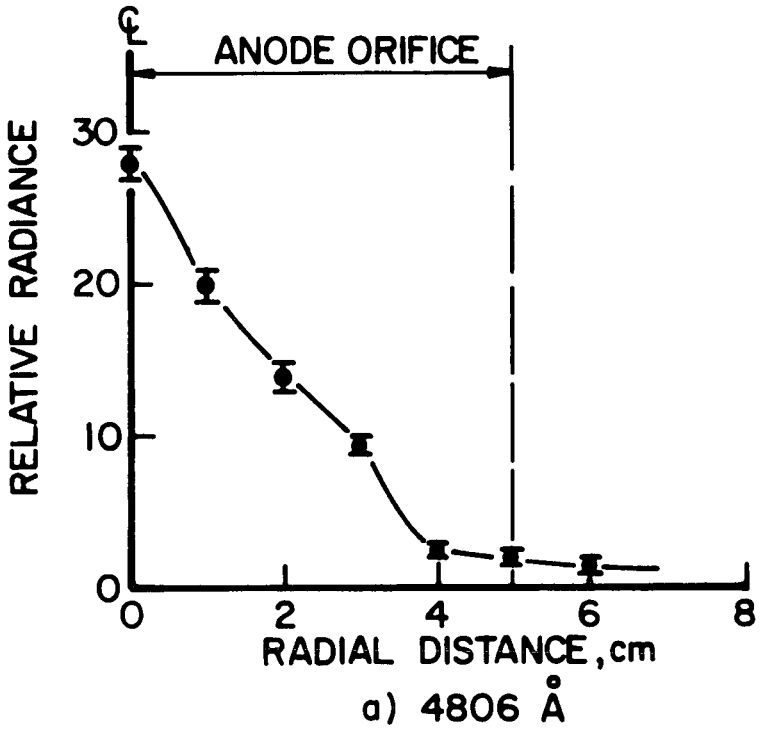

a) 4806 Å

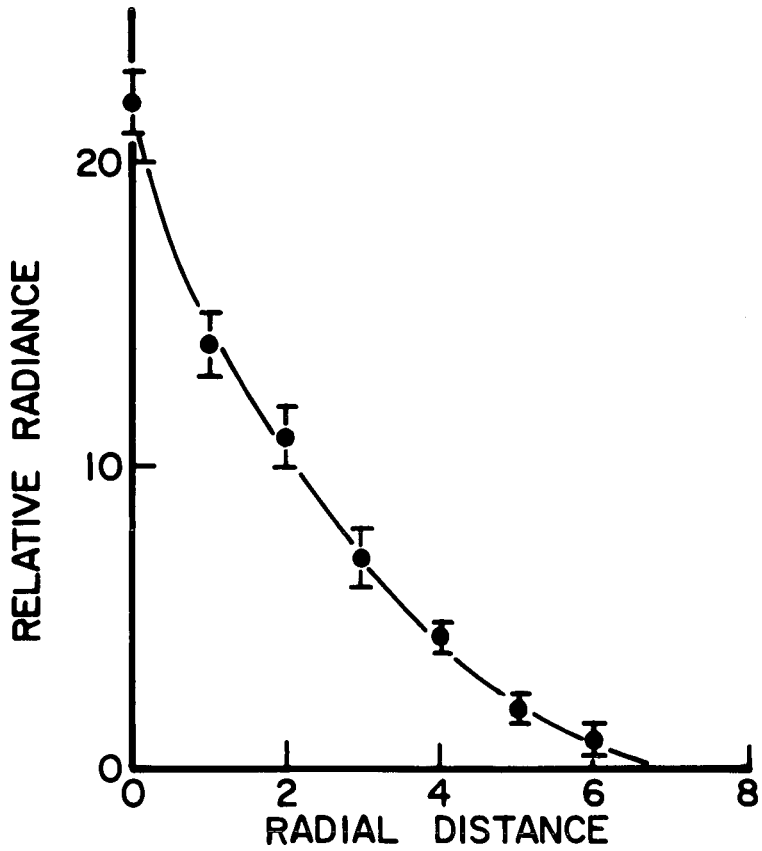

b) CONTINUUM AT 4833 Å

RADIAL PROFILES OF RADIANCE AT z = 2.4 cm

FIGURE 36
AP25·4920

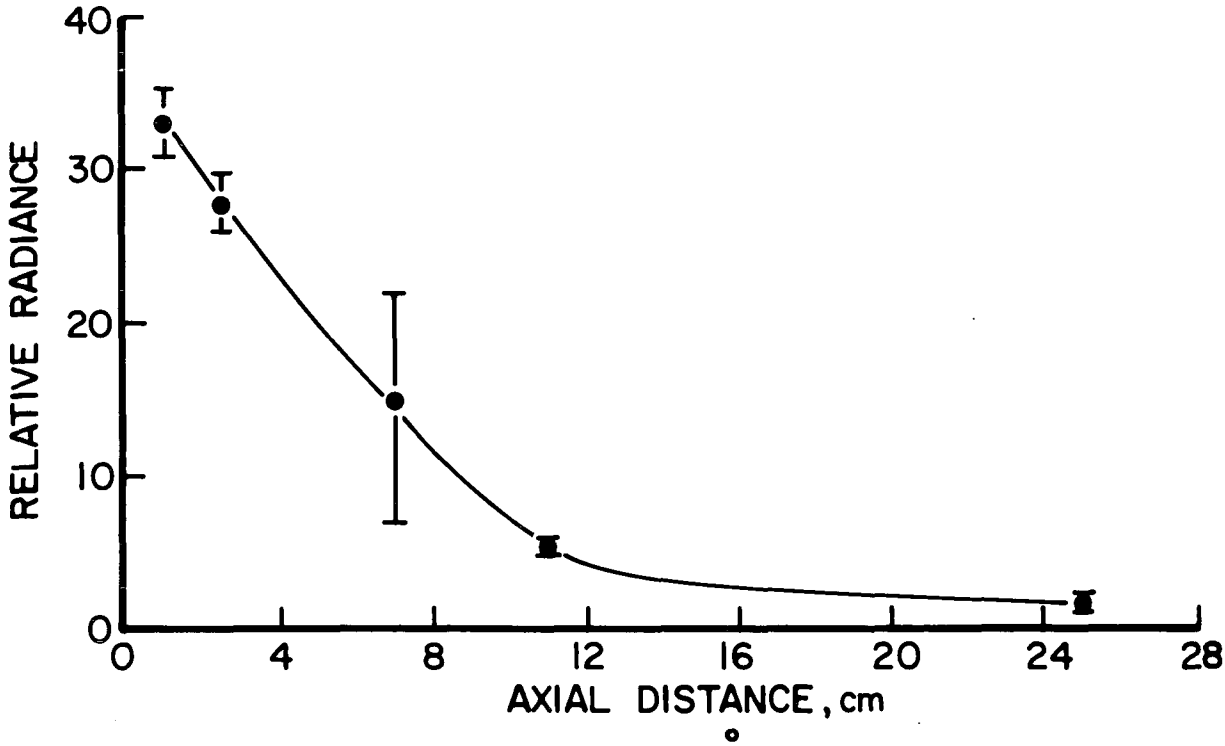

a) 4806 Å

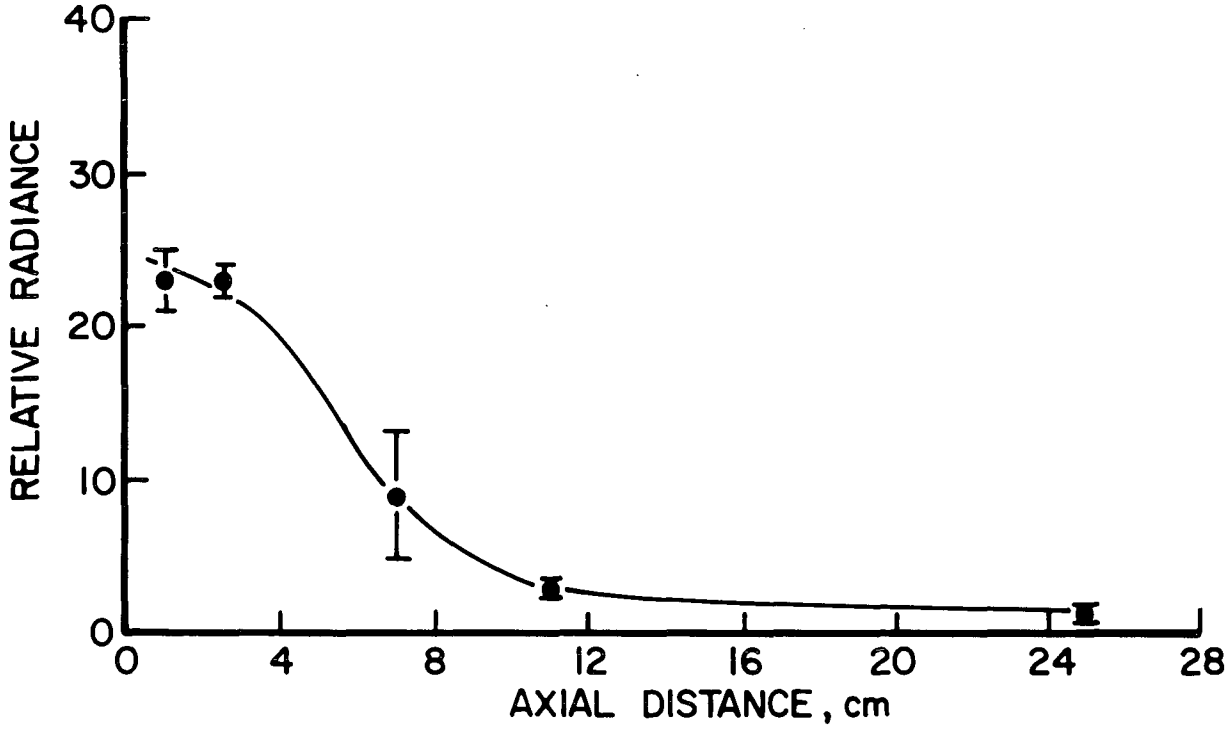

b) CONTINUUM AT 4833 Å

AXIAL PROFILES OF RADIANCE

FIGURE 37
AP25·4921

and for the continuum by:

$$I_{CONT} \sim n_i \, n_e \, T_e^{-\frac{1}{2}} \, e^{-h\nu/kT_e} \qquad (12)$$

where n_i and n_e represent the densities of ions and electrons, T_e is the electron temperature, E the energy of the initial level of the transition and ν the frequency of the radiation. In order to examine the measurements for their functional dependence the data were replotted versus axial distance on a log-log graph (Fig. 38). From approximately 4 cm to 25 cm from the anode the graph is linear indicating a power dependence on distance. The slope of the AII radiance is approximately -1.6 and that for the continuum -1.4. It is of interest to note that a previous survey of AII radiance at 4880 Å for the MPD arc with a Plexiglas backplate at the 16 kA, $\dot{m} = 6$ g/sec condition plotted a straight line of slope -2 on a similar log-log presentation.[141] A comparison of the radiances in (11) and (12) would indicate a slope for the continuum on the log-log presentation twice that of the ionized argon if the electron temperature were approximately constant, and if $n_e = n_i$ over the region of the measurements. However, Fig. 38 shows the radiances for the ionized argon and the continuum at approximately the same slope indicating a decay of the electron temperature along the direction of the flow. No further conclusions shall be attempted because, as yet, little is known about the temperatures, densities and the exhaust plume structure of the discharge with the boron nitride insulator.

The modifications to the apparatus for optical depth experiments are also shown in Fig. 35. An f = 63 cm spherical concave mirror was placed at 2 focal lengths from a point 1.6 cm downstream of the anode face on the discharge centerline. The mirror images the discharge onto itself from the

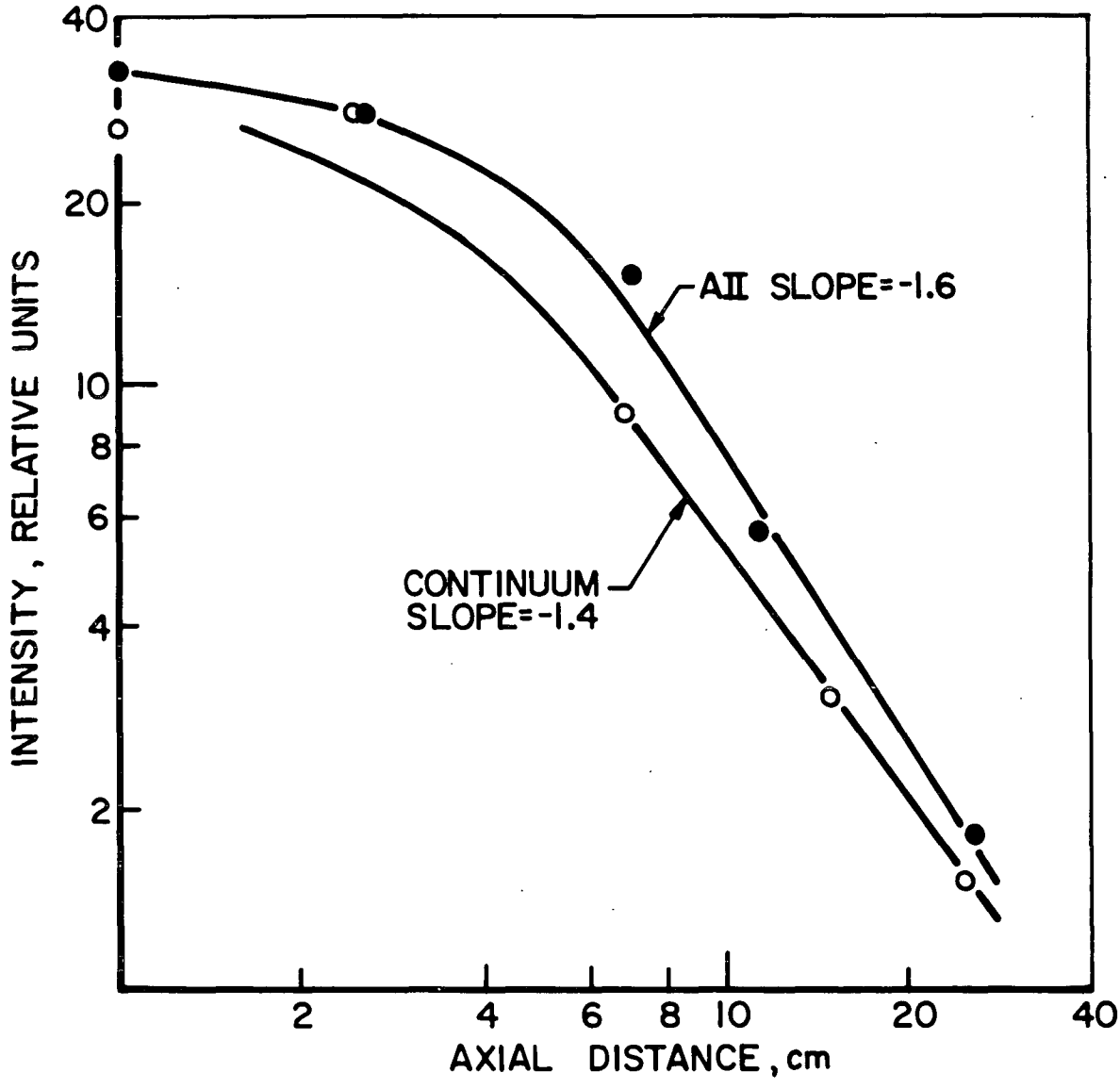

AXIAL PROFILES OF AII AND
CONTINUUM INTENSITY

FIGURE 38
AP25·4932

backside. The photomultiplier was then aligned to look at both the discharge and its reflected image along the common optical axis. If the discharge is transparent to its own radiation, then the reflected radiation should add on to the direct radiation from the discharge. The reflective optics of f/8 return the entire cone of radiation that the photomultiplier optics of f/16 can accept. For this preliminary test a direct calibration of the transmission and reflection losses of the optical components was not performed. It can only be stated that perfect transparency of the discharge corresponds to a slightly less than 100% increase in radiance.

In order to test for self-consistency of the measurements, a $T = 0.8$ transmission neutral density filter was inserted in the reflective optics. Since the radiation passed through it twice, a total transmission of 0.64 resulted.

Optical depth measurements were undertaken for the 4806 Å AII line at operating conditions of 16 kA at mass flows $\dot{m} = 32$ and 6 g/sec, and for the 4765 Å AII line and the continuum at 4833 Å with $\dot{m} = 32$ g/sec mass flow only. The results are presented in Fig. 39.

For the $\dot{m} = 32$ g/sec condition, the 4806 Å AII line shows an approximately 80% radiance increase with the reflective optics added. Accounting for the losses mentioned above, one may conclude that the discharge is nearly transparent for this transition. For the same arc operating conditions, the 4765 Å AII line shows only a 36% increase in radiance with the reflective optics, indicating considerably larger optical depth. The continuum also shows optical depth of magnitude comparable to the 4765 Å AII line as does the 4806 Å AII line for the $\dot{m} = 6$ g/sec operating condition. One may conclude that, under certain conditions, significant absorption occurs.

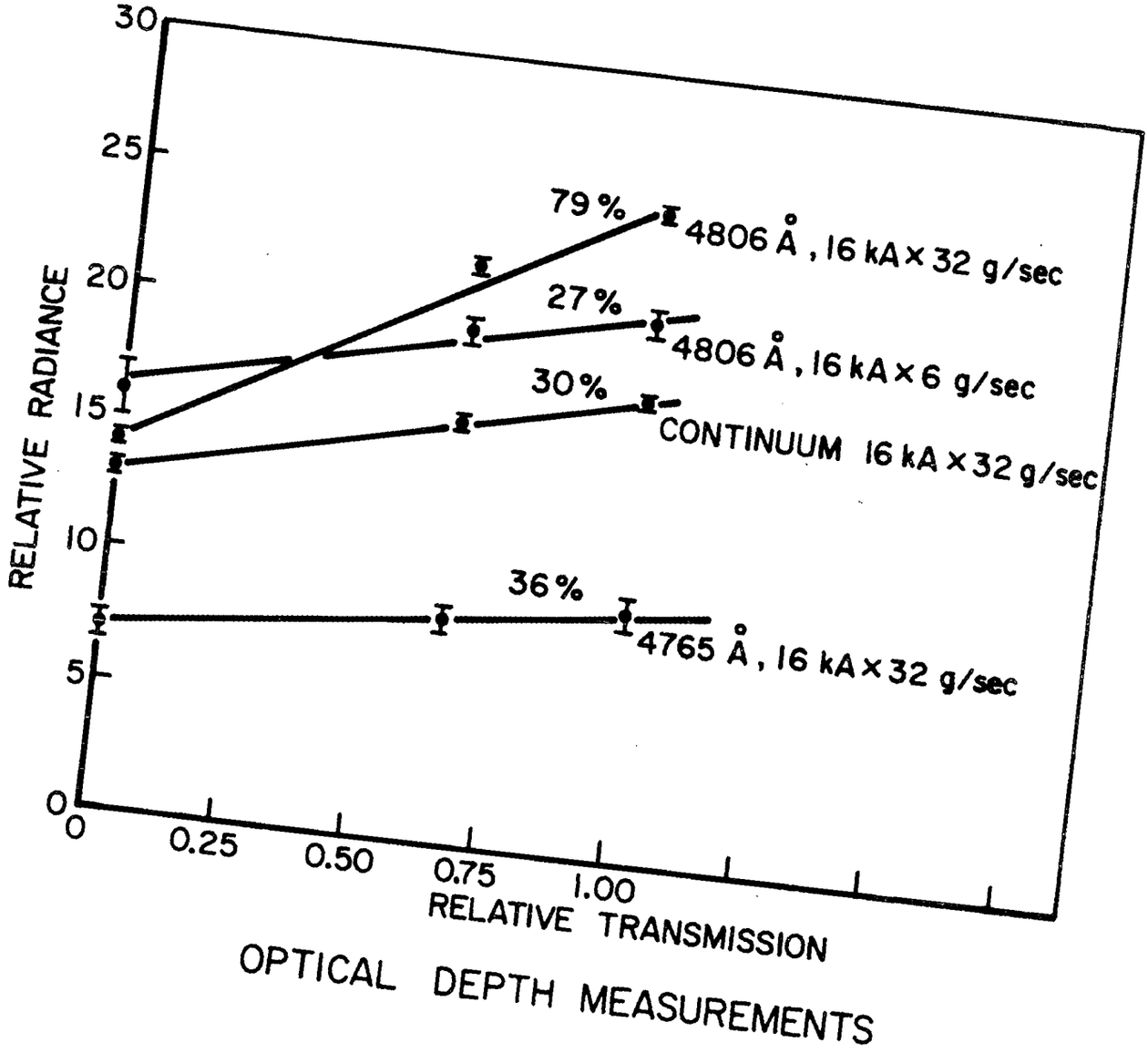

FIGURE 39
AP 25 · 4917

The accuracy of the measurements of the axial and radial radiance profiles has been limited in these exploratory experiments in the interest of obtaining initial results promptly. These studies can and will be resumed in the near future with the appropriate choice of injection geometry and materials used in the construction of the discharge chamber.

The measurements of the optical depth can be considered as further initial steps of the on-going plasmadynamic laser studies. The results differ considerably in optical depth for the 4806 Å AII line, and other AII lines and the continuum; therefore further experimental examinations are presently in progress with optical components whose transmission and reflection coefficients are calibrated. These measurements include larger regions of the exhaust flow in which the electron densities and electron temperatures can be lowered and raised when the operating currents and mass flows are changed. The studies will then be extended to a more appropriate injection geometry and propellants possibly more suitable for the investigation of plasmadynamic laser phenomena.

IV-B. Spectrographic Study of Neutral Argon in the MPD Discharge (von Jaskowsky)

In earlier spectroscopic work with MPD discharges in this laboratory[105] as well as elsewhere, neutral argon has failed to manifest its presence on spectrographic records in the visible and near-ultraviolet range. The presence of AI is, however, of considerable interest especially in plasmadynamic laser studies in the relaxing and recombining flow of argon plasma from the MPD arc. Any preferential population of the upper levels of either neutral or singly ionized atomic constituents of a relaxing plasma may be understood as a non-equilibrium recombination process with subsequent cascading of the higher state population by electron collisions at relatively low electron temperatures.[143] The increasing density of the neutral or lowest state of ionization therefore constitutes a measure of recombination in the relaxing flow with decaying electron temperature.

Earlier during this reporting period a series of spectrographic experiments were undertaken to determine the locations where neutral argon existed inside the discharge chamber and in the exhaust flow of the MPD arc with the conventional Plexiglas backplate insulator. The discharge was operated with a 1 msec pulse of 16 kA with 6 g/sec argon mass flow. The exhaust flow up to 54 cm from the exhaust orifice was examined for AI radiance.

For the studies the discharge chamber was viewed side-on through a glass window of full chamber diameter inserted into the anode cylinder. A Steinheil GH glass prism spectrograph was adjusted to record the radiation over the spectral region from 4400 Å to over 9000 Å on Kodak High Speed Infra-Red Sheet Film at a demagnification of the object of approximately 8.5:1 on the film. Parts of two typical spectrograms

of the discharge across the discharge chamber, Fig. 40a, taken at 1.2 cm from the chamber backwall, and Fig. 40b, taken just in front of the tip of the cathode, show lines of neutral and ionized argon, of hydrogen and of carbon impurities and continuum radiation on the centerline. The spectrograms exhibit distinctly different distributions of the radiance of AI and of the other constituents over the 12.8 cm inside diameter of the discharge chamber. While the AI radiance of the neutral argon flow is seen to be concentrated in narrow radial regions just in front of the injector ports in Fig. 40a, it has spread appreciably just 1 cm further downstream in Fig. 40b. The map in Fig. 41 showing the observed distribution of the plasma constituents has been obtained by superimposing the regions of highest radiance of neutral and singly ionized argon from this and other spectrograms on a diagram of the discharge apparatus. For clarity of the illustration only the neutral and singly ionized argon components are shown, while AIII, the continuum and the impurities have been omitted. For comparison, the boundaries and the line of maximum AII radiance in the previously observed exhaust jets[141] have been superimposed and are seen to correspond quite well. In near ultra-violet spectrographic work reported earlier,[134,143] the presence of doubly ionized argon AIII in the discharge has been established for the same operating conditions. It was shown to prevail inside the discharge chamber at somewhat closer proximity to the axis when compared with AII and was observable in the exhaust flow in a region of approximately 2 cm diameter about the axis, 4 cm downstream of the anode face.

Neutral argon is manifest immediately upon entering the discharge chamber and is seen to skirt the ionized argon flow which prevails at smaller radii. The presence of neutral argon surrounding the ionized flow extends into the regions

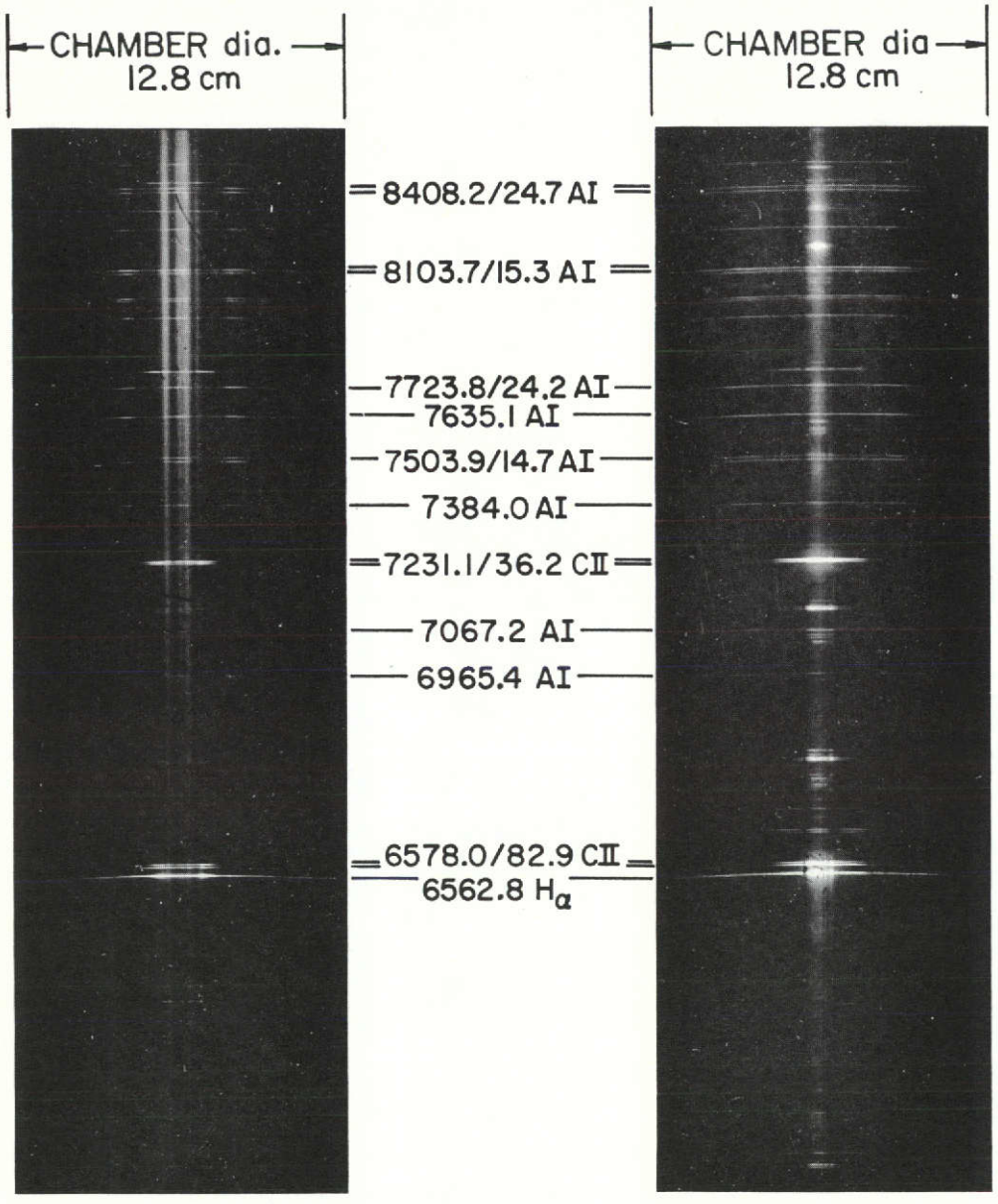

a) 1.2 cm FROM BACK WALL

b) IN FRONT OF CATHODE

SPECTROGRAMS OF MPD DISCHARGE

FIGURE 40
AP25-P-502

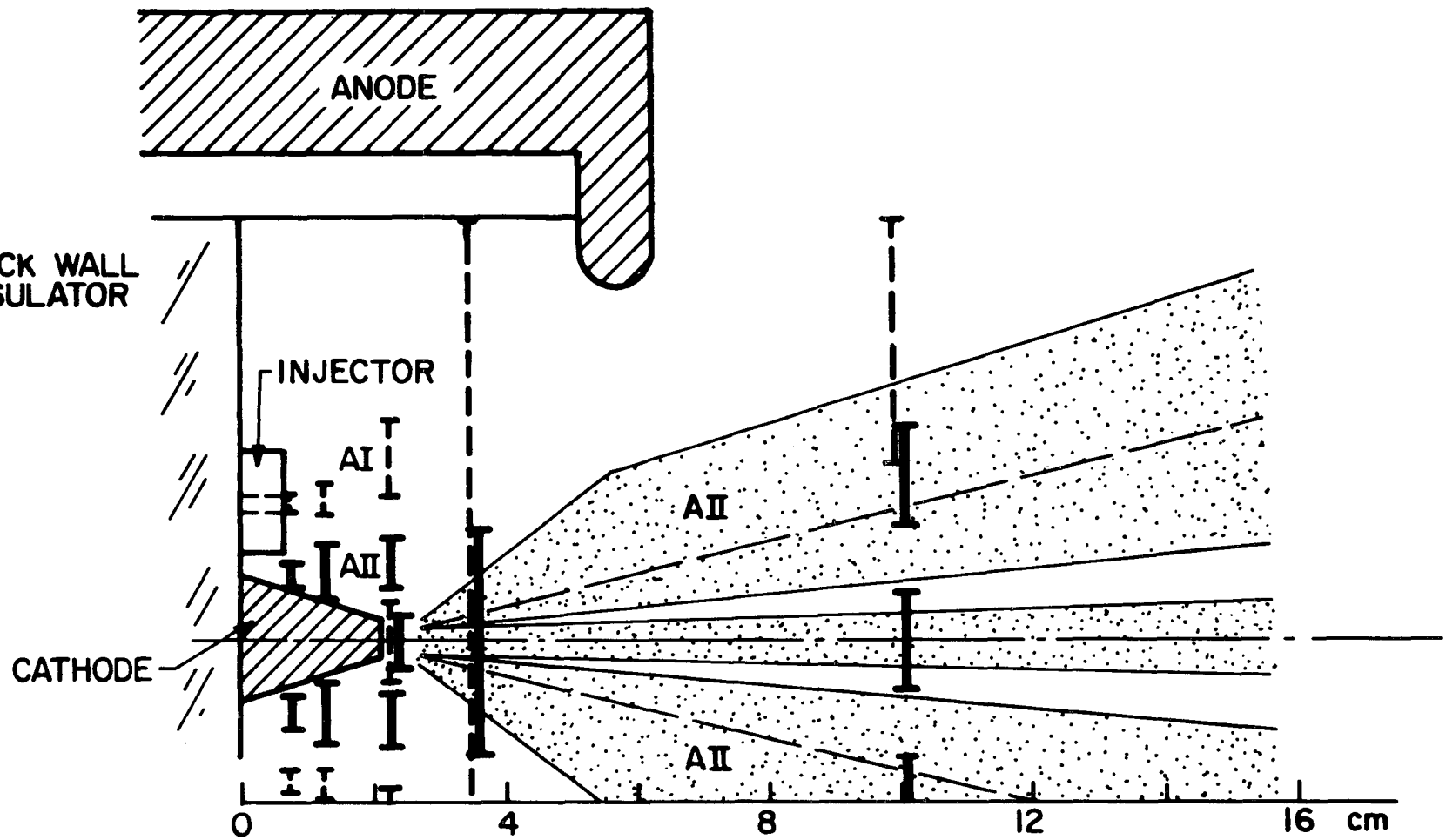

FIGURE 41
AP25-4904

DISTRIBUTION OF AI AND AII

C2

downstream of the anode. This observation allows the possibility that some fraction of the propellant passes through the discharge chamber without direct participation in the electromagnetic acceleration and is exhausted at a relatively low velocity.

Further downstream at 36 cm and 54 cm from the anode, spectrograms show only the lines of neutral argon AI and the H_α and H_β lines; the AII lines are not seen at these downstream locations indicating the progress of relaxation and recombination in the flow.

The observation of essentially completed recombination at the 36 cm downstream location permits the identification of the relaxation time for recombination. Using an average velocity of 1.5×10^4 m/sec, as determined from time-of-flight measurements, a relaxation time of 0.25 msec is obtained. Assuming an electron temperature of 1 eV the expression for the recombination rate[A-10,A-11] can then be used to compute a residual electron density of 1.3×10^{14} cm^{-3} at that location. This density is quite close to the value of an electron density of $10^{14} cm^{-3}$ which is obtained from the measured line width due to Stark broadening of the H_β line of 0.46 Å on the spectrographic record. The decreasing electron temperature in the flow has not been taken into account; a smaller temperature would reduce the computed electron density providing an even closer agreement.

The region directly in front of the cathode has already been characterized in earlier work[105] to contain a high electron density in a small volume of about one cm diameter. Therefore the continuum radiation in Fig. 40b can be identified as "brems" continuum. In contrast, the radiance of the striated continuum originating on the cathode surface in Fig. 40a exhibits the texture of the cathode surface and decreases with wavelength much more rapidly than the brems continuum. Therefore, it may be assumed to originate at thermal

radiation at the cathode surface consistent with a relatively low surface temperature. A high electron density layer is known to exist adjacent to the cathode surface[105] and can also be recognized in Fig. 40a where the H_α and H_β profiles are broadened. However, at the corresponding radial positions there is no recorded continuum; hence, the optical depth is small and the assumption of the thermal origin of the continuum appears to be justified.

When the argon mass flow was increased from 6 g/sec to 24 g/sec at the same current of 16 kA the levels of the radiance of AI and AII 1.5 cm upstream of the anode were significantly raised and its structure became less pronounced, while the continuum radiance remained about the same. On the other hand, raising the current from 16 kA to 32 kA at $\dot{m}$ = 6 g/sec significantly decreased the AI radiance relative to that of AII and increased as might be expected the brems continuum radiance. In order to ascertain that the spectrograms were representative of the quasi-steady part of the duration, a typical spectrogram of the middle of the discharge chamber recorded under nominal operating conditions of 16 kA for 1 msec at $\dot{m}$ = 6 g/sec was compared with one recorded at the same current and mass flow, but at only one quarter of the nominal 1 msec pulse duration. Any initial or terminal transient radiative phenomena with the short pulse should record at the same densities as those for the long pulse while the steady state part would appear at a correspondingly lower exposure. It was found that most spectral features were preserved but at considerably reduced exposure, thus permitting the conclusion that the spectrograms are representative of the quasi-steady part of the discharge.

PROJECT REFERENCES

[1]Jahn, R. G., Bernstein, I. B. and Kunen, A. E., "Proposed Studies of the Formation and Stability of an Electromagnetic Boundary in a Pinch," Proposal for NASA Research Grant NsG-306-63, Mar. 5, 1962, Princeton Univ., Princeton, N. J.

[2]Jahn, R. G. and von Jaskowsky, W. F., "Pulsed Electromagnetic Gas Acceleration," NASA NsG-306-63 progress report for the period 1 July 1962 to 31 December 1962, Aeron. Eng. Rept. No. 634, Jan. 1963, Princeton Univ., Princeton, N. J.

[3]Jahn, R. G. and von Jaskowsky, W. F., "The Plasma Pinch as a Gas Accelerator," A.I.A.A. Preprint 63013, A.I.A.A. Electric Propulsion Conference, Colorado Springs, Colo., 11-13 Mar. 1963.

[4]Jahn, R. G. and von Jaskowsky, W. F., "Pulsed Electromagnetic Gas Acceleration," NASA NsG-306-63 progress report for the period 1 January 1963 to 30 June 1963, Aeron. Eng. Report No. 634a, June 1963, Princeton Univ., Princeton, N. J.

[5]Jahn, R. G. and von Jaskowsky, W. F., "Structure of a Large-radius Pinch Discharge," A.I.A.A. Journal, Vol. 1, No. 8, Aug. 1963, pp. 1809-1814.

[6]Jahn, R. G., von Jaskowsky, W. F. and Casini, A. W., "A Gas-triggered Inverse Pinch Switch," NASA NsG-306-63, Aeron. Eng. Tech. Note No. 660, Aug. 1963, Princeton Univ., Princeton, N. J.

[7]Jahn, R. G., von Jaskowsky, W. F. and Casini, A. L., "Gas triggered Inverse Pinch Switch," The Review of Scientific Instruments, Vol. 34, No. 12, Dec. 1963, pp. 1439-1440.

[8]Jahn, R. G. and von Jaskowsky, W. F., "Pulsed Electromagnetic Gas Acceleration," (Paper delivered at the 4th NASA Intercenter Conference on Plasma Physics, Washington, D. C., 2-4 Dec. 1963), p. 8.

[9]Jahn, R. G. and von Jaskowsky, W. F., "Pulsed Electromagnetic Gas Acceleration," NASA NsG-306-63 progress report for period 1 July 1963 to 31 December 1963, Aeron. Eng. Rept. No. 634b, Dec. 1963, Princeton Univ., Princeton, N. J.

PROJECT REFERENCES

[10]Jahn, R. G. and von Jaskowsky, W. F., "Current Distributions in Large-radius Pinch Discharges," A.I.A.A. Preprint 64-25, A.I.A.A. Aerospace Sciences Meeting, New York, N. Y., 20-22 Jan. 1964.

[11]Jahn, R. G. and von Jaskowsky, W. F., "Current Distributions in Large-radius Pinch Discharges," A.I.A.A. Bulletin, Vol. 1, No. 1, Jan. 1964, p. 12.

[12]Jahn, R. G. and von Jaskowsky, W. F., "Pulsed Electromagnetic Gas Acceleration," NASA NsG-306-63 renewal proposal for 15-months extension, Jan. 15, 1964, Princeton Univ., Princeton, N. J.

[13]Jahn, R. G. and von Jaskowsky, W. F., "Pulsed Electromagnetic Gas Acceleration," NASA NsG-306-63 progress report for the period 1 January 1964 to 30 June 1964, Aeron. Eng. Rept. No. 634c, July 1964, Princeton Univ., Princeton, N. J.

[14]Jahn, R. G., von Jaskowsky, W. F. and Casini, A. L., "Gas-triggered Pinch Discharge Switch," NASA NsG-306-63, Aerospace and Mechanical Sciences Tech. Note No. 101, July 1964, Princeton Univ., Princeton, N. J.

[15]Corr, J. M., "Double Probe Studies in an 8" Pinch Discharge," M.S.E. thesis, Sept. 1964, Princeton Univ., Princeton, N. J.

[16]Jahn, R. G. and von Jaskowsky, W. F., "Exhaust of a Pinched Plasma From an Axial Orifice," A.I.A.A. Bulletin, Vol. 1, No. 10, Oct. 1964, p. 570.

[17]Jahn, R. G. and von Jaskowsky, W. F., "Current Distributions in Large-radius Pinch Discharges," A.I.A.A. Journal, Vol. 2, No. 10, Oct. 1964, pp. 1749-1753.

[18]Jahn, R. G., von Jaskowsky, W. F. and Casini, A. L., "Gas-triggered Pinch Discharge Switch", The Review of Scientific Instruments, Vol. 36, No. 1, Jan. 1964, pp. 101-102.

[19]Jahn, R. G. and von Jaskowsky, W. F., "Exhaust of a Pinched Plasma from an Axial Orifice," A.I.A.A. Paper 65-92, A.I.A.A. 2nd Aerospace Sciences Meeting, New York, N. Y., 25-27 Jan. 1964.

PROJECT REFERENCES

[20]Jahn, R. G. and von Jaskowsky, W. F., "Pulsed Electromagnetic Gas Acceleration," NASA NsG-306-63 progress report for the period 1 July 1964 to 31 December 1964, Aerospace and Mechanical Sciences Rept. No. 634d, Jan. 1965, Princeton Univ., Princeton, N. J.

[21]Wright, E. S., "The Design and Development of Rogowski Coil Probes for Measurement of Current Density Distribution in a Plasma Pinch," M.S.E. thesis, May 1965, Princeton Univ., Princeton, N. J.

[22]Jahn, R. G. and von Jaskowsky, W. F., "Pulsed Electromagnetic Gas Acceleration," NASA NsG-306-63 renewal proposal for 12-months extension, June 7, 1964, Princeton Univ., Princeton, N. J.

[23]Jahn, R. G. and Black, N. A., "On the Dynamic Efficiency of Pulsed Plasma Accelerators," A.I.A.A. Journal, Vol. 3, No. 6, June 1965, pp. 1209-1210.

[24]Black, N. A., "Linear Pinch Driven by a High-current Pulse-forming Network," A.I.A.A. Bulletin, Vol. 2, No. 6, June 1965, p. 309.

[25]Wright, E. S. and Jahn, R. G., "The Design and Development of Rogowski Coil Probes for Measurement of Current Density Distribution in a Plasma Pinch," NASA NsG-306-63, Aerospace and Mechanical Sciences Rept. No. 740, June 1965, Princeton Univ., Princeton, N. J.

[26]Rowell, G. A., "Cylindrical Shock Model of the Plasma Pinch," M.S.E. thesis, July 1965, Princeton Univ., Princeton, N. J.

[27]Black, N. A., "Linear Pinch Driven by a High-current Pulse-forming Network," A.I.A.A. Paper 65-336, A.I.A.A. 2nd Annual Meeting, San Francisco, Calif., 26-29 July 1965.

[28]Jahn, R. G. and von Jaskowsky, W. F., "Pulsed Electromagnetic Gas Acceleration," NASA NsG-306-63 progress report for the period 1 January 1965 to 30 June 1965, Aerospace and Mechanical Sciences Rept. No. 634e, July, 1965, Princeton Univ., Princeton, N. J.

[29]Jahn, R. G. and Ducati, A. C., "Design and Development of a Thermo-Ionic Electric Thrustor," 5QS 085-968 Interim Report, NASA Contract NASw-968, Aug. 1965, Giannini Scientific Corp., Santa Ana, Calif.

PROJECT REFERENCES

[30]Jahn, R. G., von Jaskowsky, W. F. and Burton, R. L., "Ejection of a Pinched Plasma From an Axial Orifice," A.I.A.A. Journal, Vol. 3, No. 10, Oct. 1965, pp. 1862-1866.

[31]Jahn, R. G. and Wright, E. S., "Miniature Rogowski Coil Probes for Direct Measurement of Current Density Distribution in Transient Plasmas," The Review of Scientific Instruments, Vol. 36, No. 12, Dec. 1965, pp. 1891-1892.

[32]Jahn, R. G. and von Jaskowsky, W. F., "Pulsed Electromagnetic Gas Acceleration," NASA NsG-306-63 progress report for the period 1 July 1965 to 31 December 1965, Aerospace and Mechanical Sciences Rept. No. 634f, Jan. 1966, Princeton Univ., Princeton, N. J.

[33]Burton, R. L. and Jahn, R. G., "Electric and Magnetic Field Distributions in a Propagating Current Sheet," A.I.A.A. Bulletin, Vol. 3, No. 1, Jan. 1966, p. 35.

[34]Rowell, G. A., Jahn, R. G. and von Jaskowsky, W. F., "Cylindrical Shock Model of the Plasma Pinch," NASA NsG-306-63, Aerospace and Mechanical Sciences Rept. No. 742, Feb. 1966, Princeton Univ., Princeton, N. J.

[35]Burton, R. L. and Jahn, R. G., "Electric and Magnetic Field Distributions in a Propagating Current Sheet," A.I.A.A. Paper 66-200, A.I.A.A. 5th Electric Propulsion Conference, San Diego, Calif., 7-9 Mar. 1966.

[36]Black, N. A., "Pulse-forming Networks for Propulsion Research," Proceedings of the 7th Symposium on Engineering Aspects of Magnetohydrodynamics, Princeton Univ., Princeton, N. J., Mar. 30-April 1, 1966, pp. 10-11.

[37]Jahn, R. G., "Electromagnetic Propulsion," Astronautics and Aeronautics, Vol. 4, No. 2, February, 1966, pp. 73-75.

[38]Black, N. A., "Dynamics of a Pinch Discharge Driven by a High-current Pulse-forming Network," Ph.D. thesis, May 1966, Princeton Univ., Princeton, N. J.

[39]Black, N. A. and Jahn, R. G., "Dynamics of a Pinch Discharge Driven by a High-current Pulse-forming Network," NASA NsG-306-63, Aerospace and Mechanical Sciences Rept. No. 778, May 1966, Princeton Univ., Princeton, N. J.

PROJECT REFERENCES

[40]Jahn, R. G., "Pulsed Plasma Propulsion," Proceedings of the 5th NASA Intercenter and Contractors Conference on Plasma Physics, Washington, D. C., 24-26 May 1966, pt. V, pp. 75-81.

[41]Jahn, R. G. and von Jaskowsky, W. F., "Pulsed Electromagnetic Gas Acceleration," NASA NsG-306-63 renewal proposal for 24-months extension, May 25, 1966, Princeton Univ., Princeton, N. J.

[42]Ducati, A. C., Jahn, R. G., Muehlberger, E. and Treat, R. P., "Design and Development of a Thermo-Ionic Electric Thrustor," FR-056-968 Final Report, NASA CR-54703, May 1966, Giannini Scientific Corp., Santa Ana, Calif.

[43]Jahn, R. G. and Clark, K. E., "A Large Dielectric Vacuum Facility," A.I.A.A. Journal, Vol. 4, No. 6, June 1966, p. 1135.

[44]John, R. R., Bennett, S. and Jahn, R. G., "Current Status of a Plasma Propulsion," A.I.A.A. Bulletin, Vol. 3, No. 5, May 1966, p. 264.

[45]John, R. R., Bennett, S. and Jahn, R. G., "Current Status of a Plasma Propulsion," A.I.A.A. Paper 66-565, A.I.A.A. 2nd Propulsion Joint Specialist Conference, Colorado Springs, Colo., 13-17 June 1966.

[46]Jahn, R. G. and von Jaskowsky, W. F., "Pulsed Electromagnetic Gas Acceleration," NASA NsG-306-63 progress report for the period 1 January 1966 to 30 June 1966, Aerospace and Mechanical Sciences Rept. No. 634g, July 1966, Princeton Univ., Princeton, N. J.

[47]Burton, R. L., "Structure of the Current Sheet in a Pinch Discharge," Ph.D. thesis, Sept. 1966, Princeton Univ., Princeton, N. J.

[48]Burton, R. L. and Jahn, R. G., "Structure of the Current Sheet in a Pinch Discharge," NASA NsG-306-63, Aerospace and Mechanical Sciences Rept. No. 783, Sept. 1966, Princeton Univ., Princeton, N. J.

[49]Jahn, R. G. and von Jaskowsky, W. F., "Pulsed Electromagnetic Gas Acceleration," NASA NsG-306-63 progress report for the period 1 July 1966 to 31 December 1966, Aerospace and Mechanical Sciences Rept. No. 634h, Jan. 1967, Princeton Univ., Princeton, N. J.

PROJECT REFERENCES

[50]Burton, R. L. and Jahn, R. G., "Structure of the Current Sheet in a Pinch Discharge," Bulletin of the American Physical Society, Vol. 12, Ser. II, Paper L1, May 1967, p. 848.

[51]Jahn, R. G., "Plasma Propulsion for Deep Space Flight," Bulletin of the American Physical Society, Vol. 12, Ser. II, Paper BC-1, May 1967, p. 646.

[52]Ellis, W. R., Jr., "An Investigation of Current Sheet Structure in a Cylindrical Z-Pinch," Ph.D. thesis, July 1967, Princeton Univ., Princeton, N. J.

[53]Ellis, W. R., Jr. and Jahn, R. G., "An Investigation of Current Sheet Structure in a Cylindrical Z-Pinch," NASA NsG-306-63, Aerospace and Mechanical Sciences Rept. No. 805, July 1967, Princeton Univ., Princeton, N. J.

[54]Jahn, R. G. and von Jaskowsky, W. F., "Pulsed Electromagnetic Gas Acceleration," NASA NsG-306-63 progress report for the period 1 January 1967 to 30 June 1967, Aerospace and Mechanical Sciences Rept. No. 634i, July 1967, Princeton Univ., Princeton, N. J.

[55]Clark, K. E. and Jahn, R. G., "The Magnetoplasmadynamic Arc," Astronautica Acta, Vol. 13, No. 4, 1967, pp. 315-325.

[56]Jahn, R. G., "The MPD Arc," NASA Contract NASw-1513, Aug. 1967, Giannini Scientific Corp., Santa Ana, Calif.

[57]Eckbreth, A. C., Clark, K. E. and Jahn, R. G., "Current Pattern Stabilization in Pulsed Plasma Accelerators," A.I.A.A. Bulletin, Vol. 4, No. 9, Sept. 1967, p. 433.

[58]Clark, K. E., Eckbreth, A. C. and Jahn, R. G., "Current Pattern Stabilization in Pulsed Plasma Accelerators," A.I.A.A. Paper 67-656, A.I.A.A. Electric Propulsion and Plasmadynamics Conference, Colorado Springs, Colo., 11-13 Sept. 1967.

[59]Jahn, R. G. and von Jaskowsky, W. F., "Pulsed Electromagnetic Gas Acceleration," NASA NsG-306-63 progress report for the period 1 July 1967 to 31 December 1967, Aerospace and Mechanical Sciences Rept. No. 634j, Jan. 1968, Princeton Univ., Princeton, N. J.

PROJECT REFERENCES

[60]Ducati, A. C., Jahn, R. G., Muehlberger, E. and Treat, R. P., "Exploratory Electromagnetic Thruster Research," TR 117-1513 Annual Report, NASA CR 62047, Feb. 1968, Giannini Scientific Corp., Santa Ana, Calif.

[61]Jahn, R. G., PHYSICS OF ELECTRIC PROPULSION, McGraw-Hill Book Company, New York, 1968.

[62]Burton, R. L. and Jahn, R. G., "Acceleration of Plasma by a Propagating Current Sheet," The Physics of Fluids, Vol. 11, No. 6, June 1968, pp. 1231-1237.

[63]Jahn, R. G. and von Jaskowsky, W. F., "Pulsed Electromagnetic Gas Acceleration," NASA NGR 31-001-005 step-funding renewal proposal for the period 1 October 1968 to 30 September 1971, June 1, 1968, Princeton Univ., Princeton, N. J.

[64]Jahn, R. G. and von Jaskowsky, W. F., "Pulsed Electromagnetic Gas Acceleration," NASA NsG-306/31-001-005 progress report for the period 1 January 1968 to 30 June 1968, Aerospace and Mechanical Sciences Rept. No. 634k, July 1968, Princeton Univ., Princeton, N. J.

[65]Wilbur, P. J., "Energy Transfer from a Pulse Network to a Propagating Current Sheet," Ph.D. thesis, Sept. 1968, Princeton Univ., Princeton, N. J.

[66]Wilbur, P. J. and Jahn, R. G., "Energy Transfer from a Pulse Network to a Propagating Current Sheet," NASA NGR 31-001-005, Aerospace and Mechanical Sciences Rept. No. 846, Sept. 1968, Princeton Univ., Princeton, N. J.

[67]Ducati, A. C., Jahn, R. G., Muehlberger, E. and Treat, R. P., "Exploratory Electromagnetic Thruster Research, Phase II," 2SS108-1513 Interim Report, NASA Contract NASw-1513, Oct. 1968, Giannini Scientific Corp., Santa Ana, Calif.

[68]Eckbreth, A. C., Clark, K. E. and Jahn, R. G., "Current Pattern Stabilization in Pulsed Plasma Accelerators," A.I.A.A. Journal, Vol. 6, No. 11, Nov. 1968, pp. 2125-2132.

PROJECT REFERENCES

[69]Eckbreth, A. C., "Current Pattern and Gas Flow Stabilization in Pulsed Plasma Accelerators," Ph.D. thesis, Dec. 1968, Princeton Univ., Princeton, N. J.

[70]Eckbreth, A. C. and Jahn, R. G., "Current Pattern and Gas Flow Stabilization in Pulsed Plasma Accelerators," NASA NGL 31-001-005, Aerospace and Mechanical Sciences Rept. No. 857, Dec. 1968, Princeton Univ., Princeton, N. J.

[71]York, T. M., "Pressure Distribution in the Structure of a Propagating Current Sheet," Ph.D. thesis, Dec. 1968, Princeton Univ., Princeton, N. J.

[72]York, T. M. and Jahn, R. G., "Pressure Distribution in the Structure of a Propagating Current Sheet," NASA NGL 31-001-005, Aerospace and Mechanical Sciences Rept. No. 853, Dec. 1968, Princeton Univ., Princeton, N. J.

[73]Eckbreth, A. C. and Jahn, R. G., "Current Pattern and Gas Flow Stabilization in Pulsed Plasma Accelerators," A.I.A.A. Bulletin, Vol. 5, No. 12, Dec. 1968, p. 730.

[74]Wilbur, P. J. and Jahn, R. G., "Energy Transfer From a Pulse Network to a Propagating Current Sheet," A.I.A.A. Bulletin, Vol. 5, No. 12, Dec. 1968, p. 730.

[75]Ellis, W. R. and Jahn, R. G., "Ion Density and Current Distributions in a Propagating Current Sheet, Determined by Microwave Reflection Technique," Rept. No. CLM-P-187, Dec. 1968, Culham Laboratory, Abingdon, Berkshire, Great Britain.

[76]Jahn, R. G. and von Jaskowsky, W. F., "Pulsed Electromagnetic Gas Acceleration," NASA NGL 31-001-005 progress report for the period 1 July 1968 to 31 December 1968, Aerospace and Mechanical Sciences Rept. No. 634, Jan. 1969, Princeton Univ., Princeton, N. J.

[77]Eckbreth, A. C. and Jahn, R. G., "Current Pattern and Gas Flow Stabilization in Pulsed Plasma Accelerators," A.I.A.A. Paper 69-112, A.I.A.A. 7th Aerospace Sciences Meeting, New York, N. Y., 20-22 Jan. 1969.

PROJECT REFERENCES

[78]Wilbur, P. J. and Jahn, R. G., "Energy Transfer From a Pulse Network to a Propagating Current Sheet," A.I.A.A. Paper 69-113, A.I.A.A. 7th Aerospace Sciences Meeting, New York, N. Y., 20-22 Jan. 1969.

[79]Ellis, W. R. and Jahn, R. G., "Ion Density and Current Distributions in a Propagating Current Sheet, Determined by Microwave Reflection Technique," Journal of Plasma Physics, Vol. 3, Pt. 2, 1969, pp. 189-213.

[80]York, T. M. and Jahn, R. G., "Pressure Distribution in the Structure of a Propagating Current Sheet," A.I.A.A. Bulletin, Vol. 6, No. 2, Feb. 1969, p. 75.

[81]Clark, K. E. and Jahn, R. G., "Quasi-steady Plasma Acceleration," A.I.A.A. Bulletin, Vol. 6, No. 2, Feb. 1969, p. 75.

[82]York, T. M. and Jahn, R. G., "Pressure Distribution in the Structure of a Propagating Current Sheet," A.I.A.A. Paper 69-264, A.I.A.A. 7th Electric Propulsion Conference, Williamsburg, Va., 3-5 Mar. 1969.

[83]Clark, K. E. and Jahn, R. G., "Quasi-steady Plasma Acceleration," A.I.A.A. Paper 69-267, A.I.A.A. 7th Electric Propulsion Conference, Williamsburg, Va., 3-5 Mar. 1969.

[84]Jahn, R. G. and Mickelsen, W. R., "Electric Propulsion Notebook," A.I.A.A. Professional Study Series, Williamsburg, Va., 1-2 Mar. 1969.

[85]Boyle, M. J., "Plasma Velocity Measurements with Elec.-tric Probes," B.S.E. thesis, April 1969, Princeton Univ., Princeton, N. J.

[86]Clark, K. E., "Quasi-steady Plasma Acceleration," Ph.D. thesis, May 1969, Princeton Univ., Princeton, N. J.

[87]Clark, K. E. and Jahn, R. G., "Quasi-steady Plasma Acceleration," NASA NGL 31-001-005, Aerospace and Mechanical Sciences Rept. No. 859, May 1969, Princeton Univ., Princeton, N. J.

PROJECT REFERENCES

[88]Boyle, M. J., "Plasma Velocity Measurements with Electric Probes," Paper No. 4 (Paper presented at the Northeastern Regional Student Conference, Princeton Univ., Princeton, N. J., 9-10 May 1969).

[89]Mickelsen, W. R. and Jahn, R. G., "Status of Electric Propulsion," A.I.A.A. Bulletin, Vol. 6, No. 6, June 1969, p. 257.

[90]Mickelsen, W. R. and Jahn, R. G., "Status of Electric Propulsion," A.I.A.A. Paper 69-497, A.I.A.A. 5th Propulsion Joint Specialist Conference, U. S. Air Force Academy, Colo., 9-13 June 1969.

[91]Ducati, A. C. and Jahn, R. G., "Electron Beam from a Magnetoplasmadynamic Arc," The Physics of Fluids, Vol. 12, No. 6, June 1969, pp. 1177-1181.

[92]Jahn, R. G. and von Jaskowsky, W. F., "Pulsed Electromagnetic Gas Acceleration," NASA NGL 31-001-005 progress report for the period 1 January 1969 to 30 June 1969, Aerospace and Mechanical Sciences Rept. No. 634m, July 1969, Princeton Univ., Princeton, N. J.

[93]Jahn, R. G. and von Jaskowsky, W. F., "Pulsed Electromagnetic Gas Acceleration," NASA NGR 31-001-005 step-funding renewal proposal for the period 1 October 1969 to 30 September 1970, July 1, 1969, Princeton Univ., Princeton, N. J.

[94]Jahn, R. G., Clark, K. E., Oberth, R. C. and Turchi, P. J., "Acceleration Patterns in Quasi-steady MPD Arcs," A.I.A.A. Bulletin, Vol. 6, No. 12, Dec. 1969, p. 701.

[95]Ducati, A. C. and Jahn, R. G., "Repetitively Pulsed, Quasi-steady Vacuum MPD Arc," A.I.A.A. Bulletin, Vol. 6, No. 12, Dec. 1969, p. 701.

[96]Jahn, R. G., von Jaskowsky, W. F. and Clark, K. E., "Pulsed Electromagnetic Gas Acceleration: Acceleration Processes in Quasi-steady Arcs," (Paper delivered at the 6th NASA Intercenter and Contractors Conference on Plasma Physics, NASA Langley Research Center, Hampton, Va., 8-10 Dec. 1969), pp. 8-15.

PROJECT REFERENCES

[97]Jahn, R. G., von Jaskowsky, W. F. and Clark, K. E., "Pulsed Electromagnetic Gas Acceleration," NASA NGL 31-001-005 progress report for the period 1 July 1969 to 31 December 1969, Aerospace and Mechanical Sciences Rept. No. 634n, Jan. 1970, Princeton Univ., Princeton, N. J.

[98]Eckbreth, A. C. and Jahn, R. G., "Current Pattern and Gas Flow Stabilization in Pulsed Plasma Accelerators," A.I.A.A. Journal, Vol. 8, No. 1, Jan. 1970, pp. 138-143.

[99]Jahn, R. G., Clark, K. E., Oberth, R. C. and Turchi, P. J., "Acceleration Patterns in Quasi-steady MPD Arcs," A.I.A.A. Paper 70-165, A.I.A.A. 8th Aerospace Sciences Meeting, New York, N. Y., 19-21 Jan. 1970.

[100]Ducati, A. C. and Jahn, R. G., "Repetitively Pulsed, Quasi-steady Vacuum MPD Arc," A.I.A.A. Paper 70-167, A.I.A.A. 8th Aerospace Sciences Meeting, New York, N. Y., 19-21 Jan. 1970.

[101]Wilbur, P. J. and Jahn, R. G., "Energy Transfer from a Pulse Network to a Propagating Current Sheet," A.I.A.A. Journal, Vol. 8, No. 1, Jan. 1970, pp. 144-149.

[102]Clark, K. E. and Jahn, R. G., "Quasi-steady Plasma Acceleration," A.I.A.A. Journal, Vol. 8, No. 2, Feb. 1970, pp. 216-220.

[103]York, T. M. and Jahn, R. G., "Pressure Distribution in the Structure of a Propagating Current Sheet," The Physics of Fluids, Vol. 13, No. 5, May 1970, pp. 1303-1309.

[104]Jahn, R. G., "Pulsed Electromagnetic Gas Acceleration," NASA NGL 31-001-005 step-funding renewal proposal for period 1 October 1970 to 30 September 1971, June 11, 1970, Princeton Univ., Princeton, N. J.

[105]Jahn, R. G., von Jaskowsky and Clark, K. E., "Pulsed Electromagnetic Gas Acceleration," NASA NGL 31-001-005, progress report for the period 1 January 1970 to 30 June 1970, Aerospace and Mechanical Sciences Rept. No. 634o, July 1970, Princeton Univ., Princeton, N. J.

PROJECT REFERENCES

[106]Turchi, P. J. and Jahn, R. G., "The Cathode Region of a Quasi-steady MPD Arcjet," A.I.A.A. Bulletin, Vol. 7, No. 9, Sept. 1970, p. 449.

[107]Clark, K. E., DiCapua, M. S., Jahn, R. G. and von Jaskowsky, W. F., "Quasi-steady Magnetoplasmadynamic Arc Characteristics," A.I.A.A. Bulletin, Vol. 7, No. 9, Sept. 1970, p. 449.

[108]Turchi, P. J. and Jahn, R. G., "The Cathode Region of a Quasi-steady MPD Arcjet," A.I.A.A. Paper 70-1094, A.I.A.A. 8th Electric Propulsion Conference, Stanford, Calif., 31 Aug.-2 Sept. 1970.

[109]Clark, K. E., DiCapua, M. S., Jahn, R. G. and von Jaskowsky, W. F., "Quasi-steady Magnetoplasmadynamic Arc Characteristics," A.I.A.A Paper 70-1095, A.I.A.A. 8th Electric Propulsion Conference, Stanford, Calif., 31 Aug.-2 Sept. 1970.

[110]Turchi, P. J., "The Cathode Region of a Quasi-steady Magnetoplasmadynamic Arcjet," Ph.D. thesis, Sept. 1970, Princeton Univ., Princeton, N. J.

[111]Turchi, P. J. and Jahn, R. G., "The Cathode Region of a Quasi-steady Magnetoplasmadynamic Arcjet," NASA NGL 31-001-005, Aerospace and Mechanical Sciences Rept. No. 940, Oct. 1970, Princeton Univ., Princeton, N. J.

[112]Oberth, R. C., "Anode Phenomena in High-Current Discharges," Ph.D. thesis, Dec. 1970, Princeton Univ., Princeton, N. J.

[113]Oberth, R. C. and Jahn, R. G., "Anode Phenomena in High-Current Discharges," NASA NGL 31-001-005, Aerospace and Mechanical Sciences Rept. No. 961, Dec. 1970, Princeton Univ., Princeton, N. J.

[114]Di Capua, M. S. and Jahn, R. G., "Voltage-Current Characteristics of Parallel-Plate Plasma Accelerators," A.I.A.A. Bulletin, Vol. 8, No. 1, Jan. 1971, p. 40.

[115]Oberth, R. C. and Jahn, R. G., "Anode Phenomena in High-Current Accelerators," A.I.A.A. Bulletin, Vol. 8, No. 1, Jan. 1971, p. 40.

[116]Di Capua, M. S. and Jahn, R. G., "Energy Deposition in Parallel-Plate Plasma Accelerators," A.I.A.A. Paper 71-197, A.I.A.A. 9th Aerospace Sciences Meeting, New York, N. Y., 25-27 Jan. 1971.

PROJECT REFERENCES

[117]Oberth, R. C. and Jahn, R. G., "Anode Phenomena in High-Current Accelerators," A.I.A.A. Paper 71-198, A.I.A.A. 9th Aerospace Sciences Meeting, New York, N. Y., 25-27 Jan. 1971.

[118]Jahn, R. G., Clark, K. E., Oberth, R. C. and Turchi, P. J., "Acceleration Patterns in Quasi-steady MPD Arcs," A.I.A.A. Journal, Vol. 9, No. 1, Jan. 1971, pp. 167-172.

[119]Jahn, R. G., von Jaskowsky, W. F. and Clark, K. E., "Pulsed Electromagnetic Gas Acceleration," NASA NGL 31-001-005, semi-annual report for period 1 July 1970 to 31 December 1970, Aerospace and Mechanical Sciences Rept. No. 634p, January 1971, Princeton University, Princeton, N. J.

[120]Jahn, R. G., von Jaskowsky, W. F. and Clark, K. E., "Pulsed Electromagnetic Gas Acceleration," NASA NGL 31-001-005 step-funding renewal proposal for the period 1 October 1971 to 30 September 1972, June 16, 1971, Princeton Univ., Princeton, N. J.

[121]Clark, K. E., Jahn, R. G. and von Jaskowsky, W. F., "Exhaust Characteristics of a Quasi-steady MPD Accelerator," DGLR Symposium on Electric Space Thruster System, Braunschweig, Germany, June 22-23, 1971, DLR Mitt. 71-21, Teil 1, pp. 81-100.

[122]Turchi, P. J. and Jahn, R. G., "Cathode Region of a Quasi-steady MPD Arcjet," A.I.A.A. Journal, Vol. 9, No. 7, July 1971, pp. 1372-1379.

[123]Jahn, R. G., von Jaskowsky, W. F. and Clark, K. E., "Pulsed Electromagnetic Gas Acceleration," NASA NGL 31-001-005, semi-annual report for period 1 January 1971 to 30 June 1971, Aerospace and Mechanical Sciences Dept. No. 634q, July 1971, Princeton University, Princeton, N. J.

[124]Cory, John S., "Mass,Momentum and Energy Flow from an MPD Accelerator," Ph.D. thesis, August 1971, Princeton University, Princeton, N. J.

PROJECT REFERENCES

[125]Cory, J. S. and Jahn, R. G., "Mass, Momentum and Energy Flow from an MPD Accelerator," NASA NGL 31-001-005, Aerospace and Mechanical Sciences Rept. No. 999, September 1971, Princeton University, Princeton, N. J.

[126]Jahn, R. G., von Jaskowsky, W. F. and Clark, K. E., "Quasi-steady Plasma Acceleration," International Symposium on Dynamics of Ionized Gases, University of Tokyo, September 1971.

[127]Di Capua, M. S., "Energy Deposition in the Parallel-Plate Plasma Accelerator," Ph.D. thesis, November 1971, Princeton University, Princeton, N. J.

[128]Di Capua, M. S. and Jahn, R. G., "Energy Deposition in Parallel-Plate Plasma Accelerators," NASA 31-001-005, Aerospace and Mechanical Sciences Rept. No. 1015, December 1971, Princeton University, Princeton, N. J.

[129]Parmentier, N., "Hollow Cathode, Quasi-steady MPD Arc," M.S.E. thesis, December 1971, Princeton University, Princeton, N. J.

[130]Parmentier, N. and Jahn, R. G., "Hollow Cathode, Quasi-steady MPD Arc," NASA NGL 31-001-005, Aerospace and Mechanical Sciences Rept. No. 1023, December 1971, Princeton University, Princeton, N. J.

[131]Jahn, R. G., von Jaskowsky, W. F. and Clark, K. E., "Pulsed Electromagnetic Gas Acceleration," NASA NGL 31-001-005, semi-annual report for period 1 July 1971 to 31 December 1971, Aerospace and Mechanical Sciences Report No. 634r, January 1972, Princeton University, Princeton, N. J.

[132]Oberth, R. C. and Jahn, R. G., "Anode Phenomena in High-Current Accelerators," A.I.A.A. Journal, Vol. 10, No. 1, January 1972, pp. 86-91.

[133]Clark, K. E., "Electric Propulsion," Astronautics and Aeronautics, Vol. 10, No. 2, February 1972, pp. 22-23.

[134]Hixon, T. L., "Near-Ultraviolet Spectroscopic Studies of a Quasi-Steady Magnetoplasmadynamic Arc,"B.A. thesis, April 1972, Princeton University, Princeton, N. J.

[135]Hixon, T. L., "Near-Ultraviolet Spectrographic Studies of AIII in an MPD Arc Discharge," Paper presented at the Northeastern Regional Student Conference, Rutgers University, New Brunswick, N. J., April 29, 1972.

PROJECT REFERENCES

[136]Clark, K. E., Jahn, R. G. and von Jaskowsky, W. F., "Distribution of Momentum and Propellant in a Quasi-Steady MPD Discharge," A.I.A.A. Bulletin, Vol. 9, No. 4, April 1972, p. 165.

[137]Bruckner, A. P. and Jahn, R. G., "Exhaust Plume Structure in a Quasi-steady MPD Arc," A.I.A.A. Bulletin, Vol. 9, No. 4, April 1972, p. 166.

[138]Clark, K. E., Jahn, R. G. and von Jaskowsky, W. F., "Measurements of Mass, Momentum and Energy Distributions in a Quasi-Steady MPD Discharge," A.I.A.A. Paper 72-497, A.I.A.A. 9th Electric Propulsion Conference, Bethesda, Md., 17-19 April 1972.

[139]Bruckner, A. P. and Jahn, R. G., "Exhaust Plume Structure in a Quasi-Steady MPD Arc," A.I.A.A. Paper 72-499, A.I.A.A. 9th Electric Propulsion Conference, Bethesda, Md., 17-19 April, 1972.

[140]Bruckner, A. P., "Spectroscopic Studies of the Exhaust Plume of a Quasi-steady MPD Accelerator," Ph.D. thesis, May 1972, Princeton University, Princeton, N. J.

[141]Bruckner, A. P. and Jahn, R. G., "Spectroscopic Studies of the Exhaust Plume of a Quasi-steady MPD Accelerator,"NASA NGL 31-001-005, Aerospace and Mechanical Sciences Rept. No. 1041, May, 1972, Princeton University, Princeton, N. J.

[142]Jahn, R. G., von Jaskowsky, W. F. and Clark, K. E., "Pulsed Electromagnetic Gas Acceleration," NASA NGL 31-001-005 step-funding renewal proposal for the period 1 October 1972 to 30 September 1973, June 1972, Princeton University, Princeton, N. J.

[143]Jahn, R. G., von Jaskowsky, W. F. and Clark, K. E., "Pulsed Electromagnetic Gas Acceleration," NASA NGL 31-001-005, semi-annual report for period 1 January 1972 to 30 June 1972, Aerospace and Mechanical Sciences Report No. 634s, July 1972, Princeton University, Princeton, N. J.

[144]Kelly, A. J. and Clark, K. E., "Plasma Propulsion Systems," Aerospace and Mechanical Sciences Rept. No. 1074, September 1973, Princeton University, Princeton, N. J.

[145]Greco, R. V., Bliss, J. R., Murch, C. K., Clark, K. E., and Kelly, A. J., "Resistojet and Plasma Propulsion System Technology," AIAA Paper 72-1124 (1972).

GENERAL REFERENCES

A-1 John, R. R., Bennett, S., and Connors, J. F., "Experimental Performance of a High Specific Impulse Arc Jet Engine," AIAA Paper 64-669 (1964).

A-2 Malliaris, A. C., John, R. R., Garrison, R. L. and Libby, D. R., "Quasi-Steady MPD Propulsion at High Power," Final Tech. Rept. AVSD-0146-71-44, NASA CR 111872, February 1971.

A-3 Schoeck, P. A., Eckert, E. R. G., and Wutzke, S. A., "An Investigation of the Anode Losses in Argon Arcs and their Reduction by Transpiration Cooling," Aeronautical Research Laboratory, Office of Aerospace Research, U. S. Air Force, Report ARL 62-341, April 1962.

A-4 Guman, W. J., "A Comparison of Quasi-Steady with Short-Pulse Discharge Thruster Operation," AIAA Paper 72-459 (1972).

A-5 Malliaris, A. C. and Libby, D. R., "Velocities of Neutral and Ionic Species in an MPD Flow," AIAA Paper 69-109, (1969).

A-6 Volluz, R. J., "Wind Tunnel Instrumentation and Operation," Handbook of Supersonic Aerodynamics, Section 20, NAVORD Report 1488 (Vol. 6), January 1961.

A-7 Paschen, F., Ann. d. Physik, 50, 901 (1916); Schuler, H., Z. Physik, 35, 323 (1926).

A-8 Byers, D. C., "Performance of Various Oxide Magazine Cathodes in Kaufman Thrusters," NASA TN D-5074 (1968).

A-9 Lidsky, L. M., Rothleder, S. D., Rose, D. J., Yoshikawa, A., Michelson, C., and Mackin, Jr., R. J., "Highly Ionized Hollow Cathode Discharge," Journal of Applied Physics, Vol. 33, No. 8, 1962.

GENERAL REFERENCES

A-10 Zel'dovich, Ya.B. and Raizer, Yu.P., Physics of Shock Waves and High-Temperature Hydrodynamic Phenomena, Vol. I & II, Academic Press, New York, 1966.

A-11 Hinnov, E., "Measurement of Recombination-Rate Coefficient of He^{++}," Phys. Rev., Vol. 147, No. 1, July 8, 1966, pp. 197-200.

Appendix A: Semi-annual Statement of Expenditures

PULSED ELECTROMAGNETIC GAS ACCELERATION
NASA NGL 31-001-005

1 July 1972 thru 31 December 1972

Direct Costs

I.	Salaries and Wages		
	A. Professional	$ 24,526	
	B. Students	6,500	
	C. Technicians	8,203	
	D. Supporting Staff	3,859	
			$ 43,088
II.	Employee Benefits (21% of IA,IC, ID)		7,683
III.	Equipment		-
IV.	Materials and Services		5,927
V.	Travel		413
VI.	Tuition		2,200
	Total Direct Costs		$ 59,311

Indirect Costs

VIII.	Overhead (75% of I)	32,316
	Total	$ 91,627